ADAKITIC VOLCANISM IN SOUTHERN BC DURING THE EARLY EOCENE: ISOTOPIC AND GEOCHEMICAL CONSTRAINTS FROM THE PRINCETON GROUP

by

Ryan Ben Ickert
B.Sc. (Honors) University of Alberta, 2003

THESIS SUBMITTED IN PARTIAL FULFILLMENT OF
THE REQUIREMENTS FOR THE DEGREE OF

MASTER OF SCIENCE

In the
Department
of
Earth Sciences

SIMON FRASER UNIVERSITY

Spring 2006

APPROVAL

Name: Ryan Ickert

Degree: Master of Science

Title of Thesis: ADAKITIC VOLCANISM IN SOUTHERN BC DURING THE EARLY EOCENE: ISOTOPIC AND GEOCHEMICAL CONSTRAINTS FROM THE PRINCETON GROUP

Examining Committee:

Chair: **Dr. H. Dan Gibson**
Assistant Professor, Department of Earth Sciences
Simon Fraser University

Dr. Derek J. Thorkelson
Senior Supervisor
Associate Professor, Department of Earth Sciences
Simon Fraser University

Dr. Dan D. Marshall
Committee Member
Associate Professor, Department of Earth Sciences
Simon Fraser University

Dr. J. Kelly Russell
Committee Member
Professor, Department of Earth and Ocean Sciences
University of British Columbia

Dr. James S. Scoates
Committee Member
Associate Professor, Department of Earth and Ocean Sciences
University of British Columbia

Dr. Dante Canil
External Examiner
Professor, School of Earth and Ocean Sciences
University of Victoria

Date Defended/Approved: Mar. 08/06

ABSTRACT

The Princeton Group is an assemblage of volcanic and clastic sedimentary rocks in south-central British Columbia, and is part of the Challis-Kamloops belt that stretches from central British Columbia to the northwestern USA. Volcanics were deposited largely as composite-volcanoes, and are composed of calc-alkaline basaltic-andesite, andesite, dacite, and rhyolite. $^{40}Ar/^{39}Ar$ dating indicates that magmatism occurred during the Early to Middle-Eocene, from 53-47 Ma. $^{143}Nd/^{144}Nd$ measurements indicate that the PG is primarily juvenile, with εNd_{50} = 1.2-6.4.

Princeton Group rocks geochemically resemble those of many rnodern continental arcs and have an "adakitic" signature that extends throughout their compositional range. This signature is not derived from melting of subducted oceanic crust, but from an already enriched "arc-like" source, hypothesized to be mafic dykes emplaced into the lithospheric mantle during Mesozoic magmatism. These dykes subsequently melted during lithospheric heating in the Eocene, probably caused by upwelling asthenosphere related to a slab-window or slab-tear.

ACKNOWLEDGEMENTS

Finally! A place in my thesis that I can get a word in without having to worry about pesky things like science, grammar, spelling, or the judgement of my supervisor. Not only do I have full editorial control, but it is the most enjoyable part: the one where I get to thank some of the people that helped me along the way.

I will start at the most obvious place, thank you to my senior supervisor Derek for enjoyable, endless, rambling talks about geology, discussions and advice about all things Princeton, not knocking me upside the head when he was informed that I wrecked my field truck, and most importantly for having the patience of a saint. Thank you Derek.

Jill Sutton was instrumental in helping me get through the last year of my thesis. She provided unflagging support and patience through all of the ups and downs in the last few months. I can't imagine having done it without you, thank you.

I would also like to acknowledge my three interesting, amusing, and patient lab-mates. In chronological order: Thanks to Julianne for always having a smile, helping me get started at SFU, and knowing more about the Tertiary igneous geology of the Canadian Cordillera than I could possibly ever hope to. Thanks to Christa for kindly listening to hours of my monologues, and for providing great assistance and good fun in the field (gin, shotguns, pickups and

all). Thanks to Dejan for providing superb field assistance, discussions of all matters scientific, and giving me a new perspective on guacamole.

I have had the opportunity to learn from a number of geologists at SFU and UBC who have, collectively, made my stay here enjoyable and have helped me improve as a scientist. These people include (but are not limited to) Dan Gibson, Kelly Russell, Dan Marshall and Greg Dipple. In a similar vein, my extended supervisory committee, Kelly Russell, James Scoates, and Dan Marshal, and the external examiner for my defense, Dante Canil, have made important and useful comments on an earlier draft of this thesis. Tom Ullrich provided valuable advice and superb technical assistance in the determination of the ^{40}Ar-^{39}Ar dates.

Brenda Gould facilitated access to reserve land, provided helpful advice on logging roads, and kindly permitted me to stay at her home during my field work.

I have also had the pleasure of making the acquaintance of a number of people in the department here at SFU and at UBC who have made my time more pleasurable. They include (but are not limited to) Scott, Tricia, Richard, Guang (Gabe), Majid, Kenna, Sarah B, Pat, Smudge, Gillian, Sarah G, and Glyn. A particularly big thank-you goes to Sarah M.

A different set of thank yous goes out to my friends and family in Edmonton, who always kept my feet on the ground. These people include Mom and Dad, my sisters Nadia and Carla, Ryan M., Scott J., Trevor, Sara, Steve C., and Mel B.

Casper, the golden retriever, not only kept my feet warm while I was writing at home but was also always able to keep my focus on the important things, like playing catch with a teddy bear or trying to bite the dot produced by a laser pointer.

There are numerous other people who contributed in a non-trivial way to the production of this thesis, including all the "behind the scenes" people that make everything run smoothly (Matt, Rodney, Tarja, Christine, Nedra, and Glenda) and all of the people whom I have cruelly forgotten. My sincere apologies to those I have missed.

I was supported by an NSERC post-graduate scholarship and a SFU entrance scholarship. Research costs were borne by an NSERC grant to Derek Thorkelson.

TABLE OF CONTENTS

LIST OF FIGURES

LIST OF TABLES

ADAKITIC VOLCANISM DURING THE EARLY EOCENE IN SOUTHERN BC: ISOTOPIC AND GEOCHEMICAL CONSTRAINTS FROM THE PRINCETON GROUP

Abstract

The Princeton Group is an assemblage of terrestrial volcanic and clastic sedimentary rocks in south-central British Columbia, and is part of the Challis-Kamloops belt that stretches from central British Columbia to the northwestern United States. The volcanic rocks were largely deposited as cinder cones and composite volcanoes, and are composed of basaltic andesite (olivine + clinopyroxene), andesite and dacite (hornblende + plagioclase + clinopyroxene), and rhyolite (biotite + quartz + K-feldspar), with calc-alkaline affinity. New $^{40}Ar/^{39}Ar$ dates on hornblende and groundmass separates, and whole rock indicate that magmatism took place during the Early to Middle Eocene, from 53-47 Ma. New neodymium isotopic measurements, in conjunction with previously published results, indicate that the Princeton Group has an εNd_{50} = 1.2-6.4 and therefore represents primarily juvenile additions to the continental crust.

The major and trace element abundances of Princeton Group rocks resemble those of many modern continental arcs. The compositions are notable, however, because they have an "adakitic" signature that extends throughout their entire compositional range, including high-Mg# basaltic andesite. Trace element modelling indicates that this signature was not derived from anatexis of normal

oceanic crust, but from an "arc-like" source enriched in large-ion lithophile elements. This source may have been basaltic dykes that were emplaced into the lithospheric mantle during Mesozoic arc magmatism and subsequently partially melted during an event of lithospheric heating in the Eocene. The heating may have been caused by upwelling asthenosphere related to a slab window or slab tear.

Introduction

The Princeton Group represents part of an intense, early Tertiary magmatic event that affected large areas of western North America (Fig. 1). In the interior of southern British Columbia and the northwestern United States, the magmatic event is preserved mainly as volcanic successions of the Challis-Kamloops belt (Souther 1991). This belt stretches ~1500 km from central BC, where it is 200 km wide, into Idaho and Wyoming where it broadens to over 500 km. Although the separate volcanic fields of the Challis-Kamloops belt have been the focus of numerous studies (Ewing 1981b; Ewing 1981a; Dudas 1991; Norman and Mertzman 1991; McKervey 1998; Morris et al. 2000; Dostal et al. 2001; Breitsprecher 2002; Feeley et al. 2002; Dostal et al. 2003; Feeley 2003; Feeley and Cosca 2003; Lindsay and Feeley 2003; Morris and Creaser 2003), consensus has not been reached on the relationship of igneous activity to plate tectonics (cf. Breitsprecher et al. 2003; Feeley 2003). Workers in different parts of the Challis-Kamloops belt have attributed volcanic activity to a variety of mechanisms including typical arc volcanism (Ewing 1980; Morris and Creaser 2003), rifting in a volcanic arc (Dostal et al. 2001; Dostal et al. 2005),

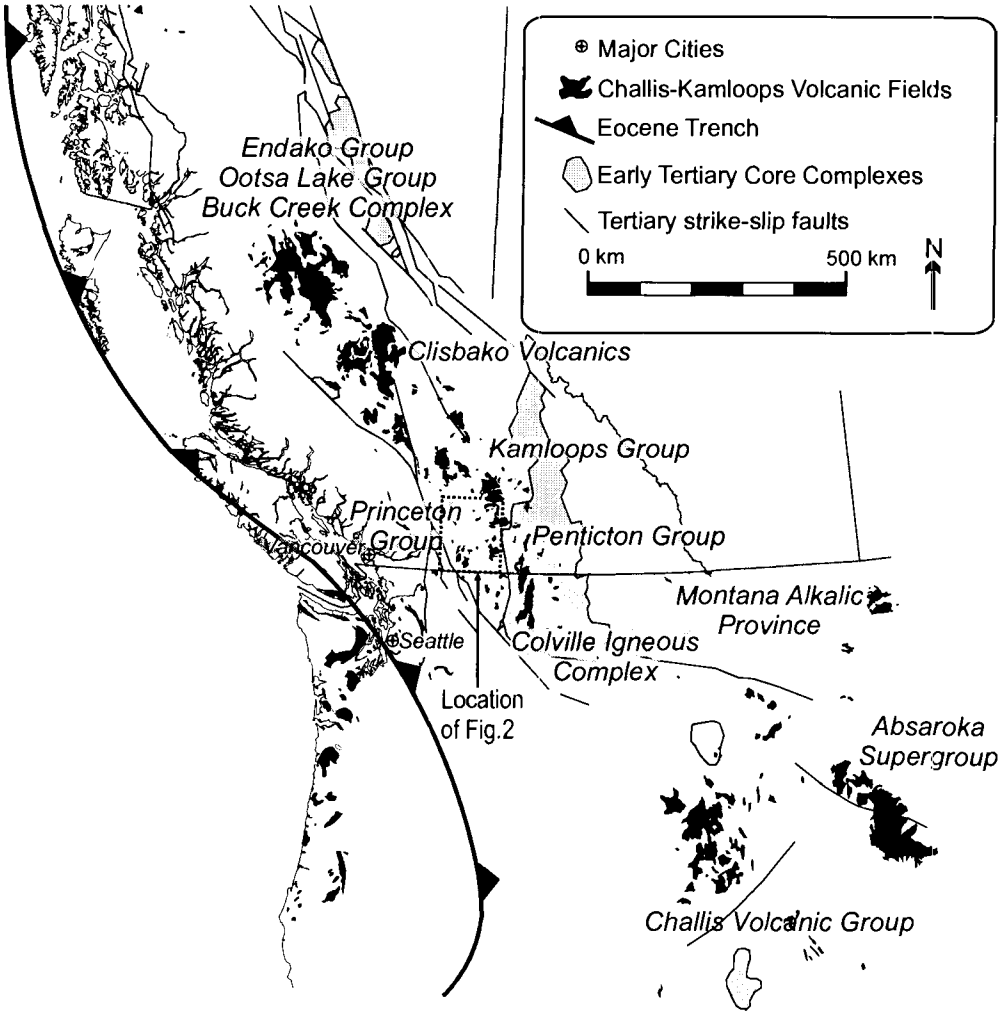

Figure 1: Map of Eocene volcanic fields in the Challis-Kamloops Belt and related geological features. After Burchfiel (1993), Dickinson (1991), Wheeler and McFeely (1991), and Breitsprecher (2002).

decompression melting (Dudas 1991; Norman and Mertzman 1991; Morris and Hooper 1997; Morris et al. 2000), and arc to intraplate processes related to a slab window (Thorkelson and Taylor 1989; Breitsprecher et al. 2003; Dostal et al. 2003; Haeussler et al. 2003). The differences in interpreted tectonic setting commonly diverge near the United States-Canada border, with arc processes commonly appealed to in the north, and intraplate processes typically invoked to the south.

The presence of adakites (Defant and Drummond 1990) and adakitic high Mg# andesites (Kelemen et al. 2003; Mg# = molar $100\times Mg/[Mg+Fe^{2+}]$) in the Princeton Group (Breitsprecher et al. 2003) raises important questions about the geodynamic setting of Southern BC during the Eocene. Adakites are an important class of intermediate to silicic composition lavas with high Sr/Y and La/Yb that are most often associated with the partial melting of garnet-bearing metabasalt, in particular the partial melting of young, hot subducted oceanic crust. High Mg# andesites are commonly associated with adakites and have similar trace element signatures, but are much more mafic. Controversy surrounds the interpretation of adakites (Garrison and Davidson 2003), as the geochemical signature is not unique to a single process or tectonic setting (Atherton and Petford 1993; Feeley and Hacker 1995; Xu et al. 2002). The Princeton Group is particularly interesting because the adakitic geochemical signature is present over a wide range of bulk compositions, from highly evolved rhyolite to primitive basaltic andesite. Evolved ($SiO_2 > 63$ wt.%, Mg# < 45) adakites are typically interpreted as melts of lower continental crust that have not

interacted with peridotite, whereas primitive (mafic) adakites are often inferred to have traversed the mantle after genesis by partial melting of subducted crust. The presence of both mafic and felsic magmas in the Princeton Group provides a unique opportunity to examine how adakitic magmas with greatly differing bulk compositions relate to one another, and to their geodynamic setting.

This paper presents results from a detailed examination of the Princeton Group, the most southwestern part of the Challis-Kamloops belt in Canada. Detailed field work and sampling were carried out near two well-exposed sections of Princeton Group at Agate Mountain and near Flat Top Mountain, both of which are southeast of Princeton, BC. These areas are composed of lavas, high-level intrusions, and pyroclastic rocks and are interpreted to be the eroded and uplifted remnants of larger volcanoes. Field, petrographic, geochronologic and geochemical data from these and other areas are provided, and are integrated with previous work. Together, they lead to a new tectono-magmatic model for Eocene magmatism in western North America and provide a new interpretation for the origin of their adakitic signature.

Geological Setting

The North American Cordilleran orogen is largely a product of accretion of pericratonic and allochthonous terranes, mainly of late-Paleozoic to Mesozoic age, to the western margin of Laurentia (Monger and Price 2002; Dickinson 2004). The Princeton Group is located in the Intermontane belt, which is comprised of supracrustal and intrusive rocks that were affected by Mesozoic compressional and Tertiary transtensional deformation (Monger 1985). The

exposed basement to the Princeton Group is composed largely of Mesozoic arc rocks and subordinate Paleozoic rocks (Monger 1989; Monger and McMillan 1989). Although many of these basement rocks appear to have an oceanic affinity and have juvenile Sr and Nd isotopic compositions (the term juvenile indicates a time integrated supra- or sub-chondritic Sm/Nd or Rb/Sr, respectively; Ghosh 1995), geophysical imaging indicates that rocks with affinity to ancestral North America may continue beneath the Princeton Group in the lower crust as a westward tapering wedge (Clowes et al. 1995).

The Princeton Group lies south of the Kamloops Group (Ewing 1981b; Ewing 1981a; Breitsprecher 2002) and west of the Penticton Group (Fig. 2; Church 1973). The Kamloops Group is a subduction-related volcanic arc-like assemblage of mafic, intermediate, and felsic volcanic rocks with subordinate intercalated non-marine sedimentary rocks (Ewing 1981b). The Penticton Group is similar to the Kamloops Group, but also contains alkaline, intraplate-like lavas near its base (Yellow Lake Member; Dostal et al. 2003). There are few precise age constraints on the Kamloops or Penticton groups, however, numerous K-Ar dates suggest that most of the volcanic activity took place from 54-45 Ma, with a culmination at 50-49 Ma. The Penticton Group may correlate with parts of the Klondike Mountain and the Sanpoil Volcanic formations of the Colville Igneous Complex in Washington (Church 1973; Morris et al. 2000; Dostal et al. 2003; McClaughry and Gaylord 2005).

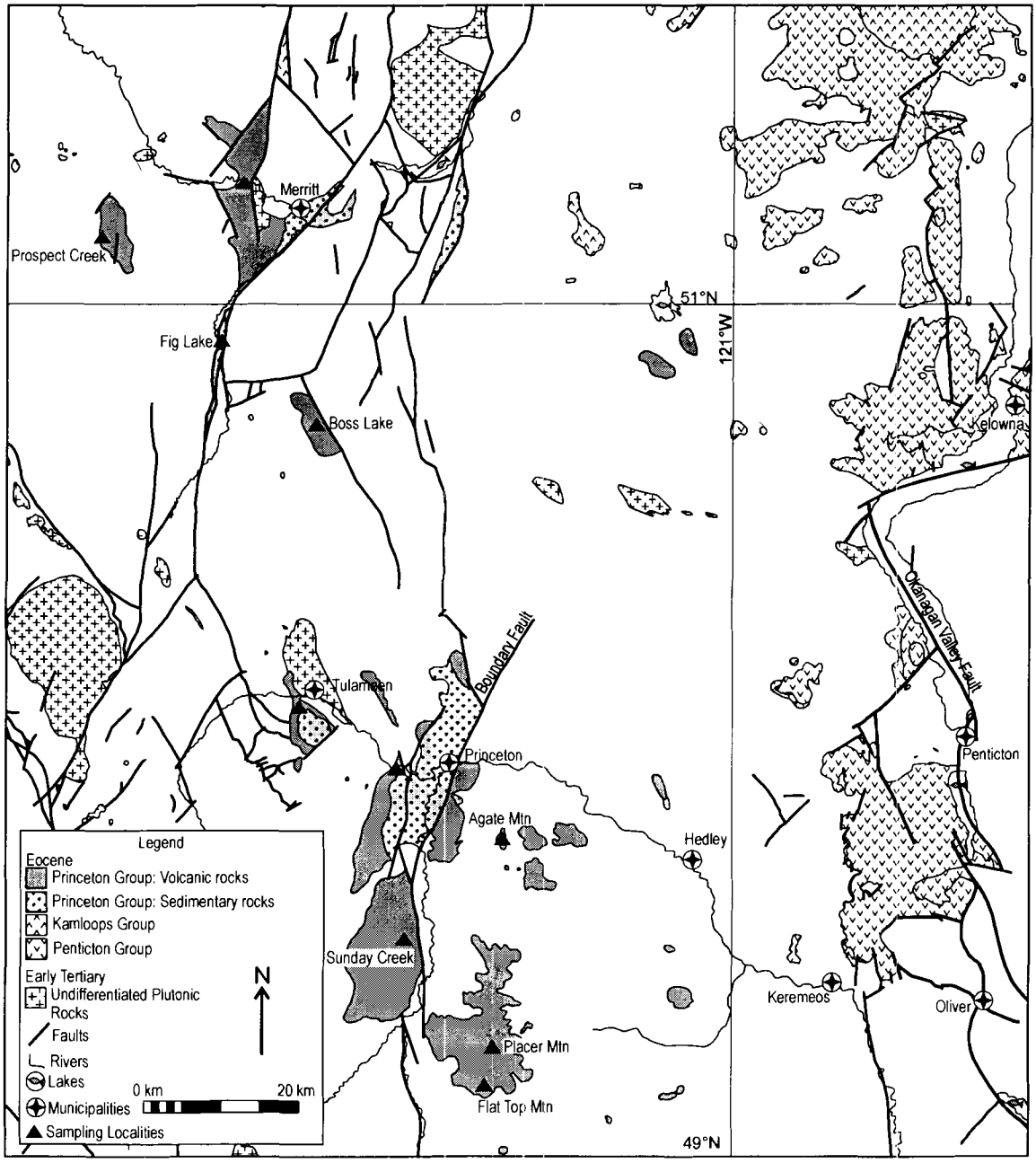

Figure 2: Map of the Princeton Group and related Eocene units and features. The approximate positions of important sampling locations (as discussed in text) are indicated by a triangle, but for accurate positions refer to co-ordinates given in the appendices. Features are adapted from Massey et al. (2005), Monger (1989), and Monger and McMillan (1989).

Princeton Group Volcanism and Sedimentation

Stratigraphic Definition and Nomenclature

The Princeton Group is an assemblage of volcanic and clastic sedimentary rocks exposed in a belt of discontinuous outliers that extends from the United States-Canada border north to Merritt BC, over a width of approximately 45 km (Fig. 2; Monger 1989; Monger and McMillan 1989). The volcanic rocks include tuff, breccia and lava that range in composition from basaltic andesite to rhyolite. Aphyric andesitic to dacitic sills have locally inflated stratigraphic sections by up to two times their original thickness. Epiclastic sedimentary rocks are dominated by conglomerate, sandstone, siltstone and coal (Williams and Ross 1979; McMechan 1983; Read 2000).

The stratigraphy of the Princeton Group (Rice 1947) was defined on the basis of detailed mapping near the town of Princeton (e.g. Camsell 1913; Rice 1947; Shaw 1952; McMechan 1983; Read 2000) and divided into two formations: a lower, primarily volcanic unit named the Cedar Formation (Camsell 1913) and an upper, sedimentary and volcanic succession named the Allenby Formation (Shaw 1952). Although the formations are well-defined near the town of Princeton, distinguishing them away from the type area is problematic for three reasons. First, there is no clear lithologic difference between the Cedar Formation and the volcanic part of the Allenby Formation. Hence, where only volcanic rocks crop out, correlation with either formation is possible. Second, the

lateral continuity of these formations has not been demonstrated, and it remains possible that the stratigraphic order and lithologic character in one location differ from those in another. Third, the lateral extent of the Princeton Group itself is unclear, because coeval volcanic and sedimentary rocks to the north and east have been called the Kamloops and Penticton groups, respectively, yet the criteria for separating those volcanics from the Princeton Group are not well established. Indeed, the separation of the three groups from one another is largely a result of a geographically-based historical usage of nomenclature rather than divisions based on geological character or superposition of one succession over another (Breitsprecher 2002). In this study, however, the geographical extent of the Princeton Group follows the traditional definition of Monger (1989) and Monger and McMillan (1989), and the volcanic rocks of the Cedar Formation are not differentiated from those in the Allenby Formation.

Structural Setting

Princeton Group magmatism occurred during an interval of widespread normal and dextral strike-slip faulting in British Columbia, Washington, and Idaho (Fig. 2; Ewing 1980; Monger 1985; Parrish et al. 1988). Block faulting influenced the deposition and preservation of the volcanic and sedimentary rocks of the Princeton Group. South of Merritt, for example, transtensional faulting led to development of the Fig Lake graben within which >2 km of conglomerate and dacite are preserved (Fig. 1; Thorkelson 1989). Similar deposits are not found elsewhere in the Princeton Group, implying that the Fig Lake depositional system was a local, fault-bounded feature with negligible lateral continuity. Similarly,

McMechan (1983) interpreted the Eocene rocks around Princeton as deposits within an actively subsiding half-graben, termed the Princeton basin (Fig. 2). Read (2000) subsequently correlated sedimentary rocks and tephra from the Princeton basin to the nearby rocks at Tulameen, but not southward to the strata near Sunday Creek. Thus, the current distribution of Princeton Group outliers probably reflects the locations of original, variably restricted depositional centres, many of which were fault-controlled. Subsequent post-depositional faulting appears to have modified these successions in size, shape, and relative elevation.

Not all of the Princeton Group successions, however, were strongly controlled by synvolcanic faulting. For example, the successions at Agate Mountain and Flat Top Mountain (Fig. 2), which were examined in detail for this study, appear to represent the growth of large stratovolcanoes or volcanic fields.

Agate Mountain

A 135 m-thick section is exposed in the west-facing cliff-face of Agate Mountain, approximately 12 km southeast of Princeton (Fig. 3). The section consists of flat-lying lava flows, tephra and sills with basaltic andesite to andesite compositions. The basal contact of the unit is not exposed, but is probably no more than 70 m below the base of the section, based on subjacent exposures of basement. The top of the section is the present erosional land surface; therefore, the original maximum thickness is unknown. About half of the section is tephra, most of which is a coarse red-weathering pyroclastic breccia composed

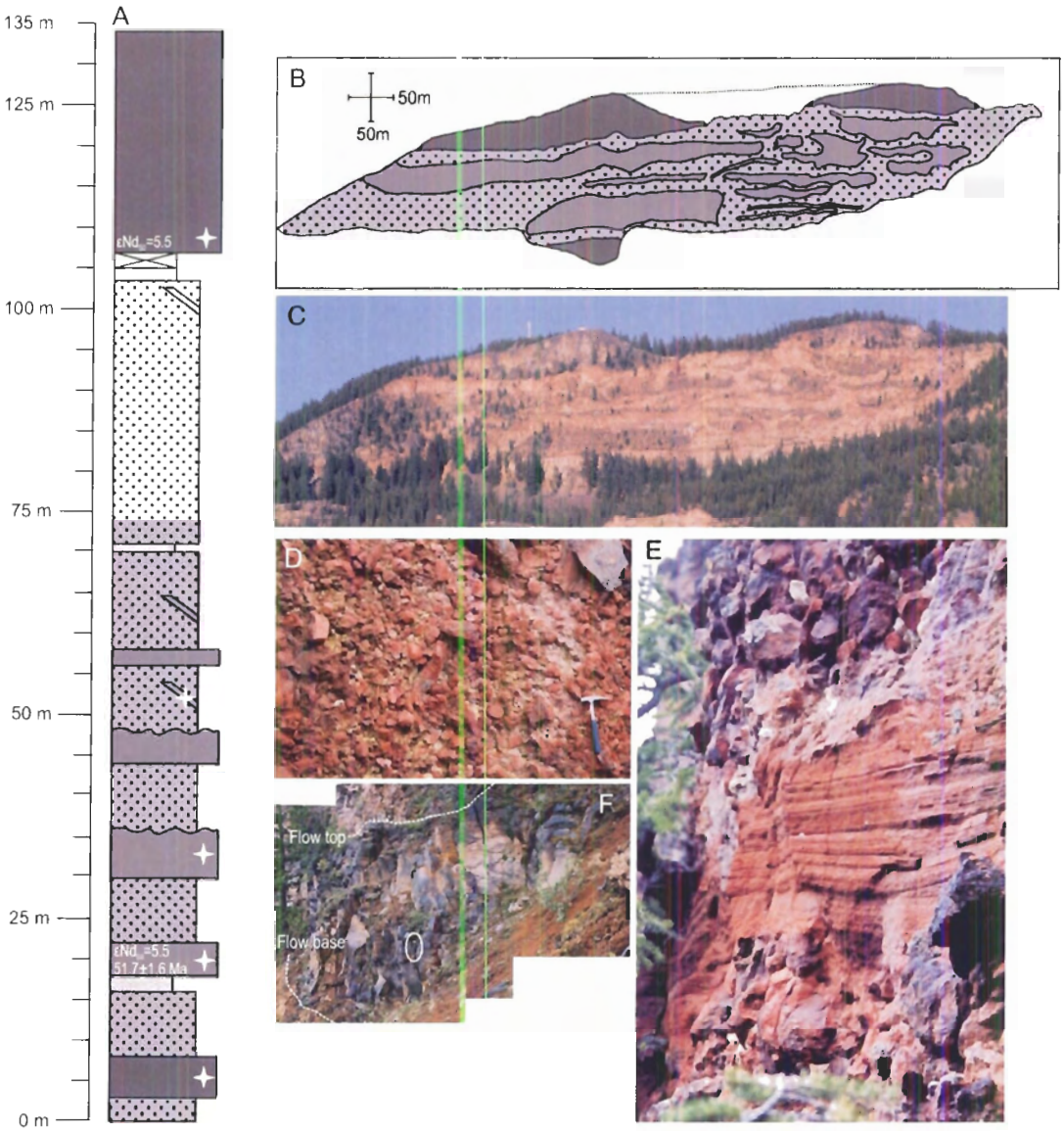

Figure 3: Stratigraphy and geology of Agate Mountain, see Fig. 2 for location. A) Stratigraphic section from Agate Mountain. The locations of samples for geochemistry, Nd isotopic analysis and ^{40}Ar-^{39}Ar geochronology are displayed. B,C) Photograph and interpretive sketch of prominent west-facing cliff at Agate Mountain. D) Blocks of scoriaceous andesite of the coarse tephra facies. Hammer for scale. E) Red weathering well bedded lapillistone/tuff between accumulations of scoria. The bed in the centre is approximately 75 cm thick. F) Basaltic andesite lava flow. Hammer (circled) for scale.

of scoriaceous to dense bombs and lesser lapilli. This coarse material is poorly to moderately well-sorted and poorly stratified and is commonly cemented by yellow clay, and locally by chalcedony. Subordinate, finer-grained tephra occurs in three horizons of metre-scale, well sorted, red-weathering, planar bedded layers of lapillistone and tuff. Lava flows occupy 13% of the section and are concentrated near the bottom. They are generally dark grey weathering, 5-7 m thick, and have thin, rubbly flow-tops. Vesicles, where present, are commonly lined, but not filled, with a green secondary mineral. The sills are more silicic than the flows (see geochemistry section, below), occupy 20-40% of the section and range up to 30 m thick. They are mostly concordant with the stratigraphic layering and range from tabular to lensoidal, but some have irregular shapes and are locally discordant. Both the lavas and the sills are sparsely porphyritic. The lavas have a phenocryst assemblage of olivine + pyroxene + magnetite, with olivine predominant, and a nearly holocrystalline groundmass of plagioclase + clinopyroxene + magnetite. The sills have an assemblage of pyroxene + plagioclase + olivine with a hypocrystalline groundmass of plagioclase + clinopyroxene + magnetite.

The Agate Mountain exposure is interpreted as a section through the lower part of a stratovolcano that was subsequently inflated by the injection of sills. The scoria-rich breccias are interpreted to be the deposits of strombolian-style eruptions from a nearby vent that were subsequently reworked by grain avalanching (e.g., McGetchin et al. 1974; Vesperman and Schmincke 2000; Riedel et al. 2003; Parfitt 2004; Valentine et al. 2005). The well-bedded tuffs and

lapillistones are interpreted to be fallout deposits from occasional, sustained eruptive columns (e.g. Riedel et al. 2003; Valentine et al. 2005). Based on their chemical and petrographic characteristics (below), the lavas are interpreted to be effusions of separate batches from the same parental magma that periodically poured down flanks of the cone. The sills represent chemically more evolved, more viscous magmas that were injected into the section, probably after the volcano had grown and the Agate Mountain section was buried beneath a greater thickness of volcanic strata.

Flat Top Mountain

Approximately 200 m of tephra and trachyandesite (below) are exposed on a south-east facing cliff two km east of Flat Top Mountain in one of the southernmost exposures of the Princeton Group, near the United States-Canada border (Fig. 4). Here, the Princeton Group dips shallowly (<15°) to the northwest. The top of the section is the current level of erosion and the base is not exposed. Several small faults obscure stratigraphic relationships near basement exposures, so it is not currently known how far the Princeton Group extends below the measured section.

Tephra, including very coarse pyroclastic breccia, tuff and lapilli-tuff, makes up the basal 75 m of the section. Clasts in pyroclastic breccia are dominated by altered aphyric to sparsely porphyritic andesite (similar to exposed coherent volcanic rock) with lesser vesicular clasts. The breccia is poorly sorted and composed of blocks ranging in size from >1 m to 10 cm. Tuff and lapilli-tuff

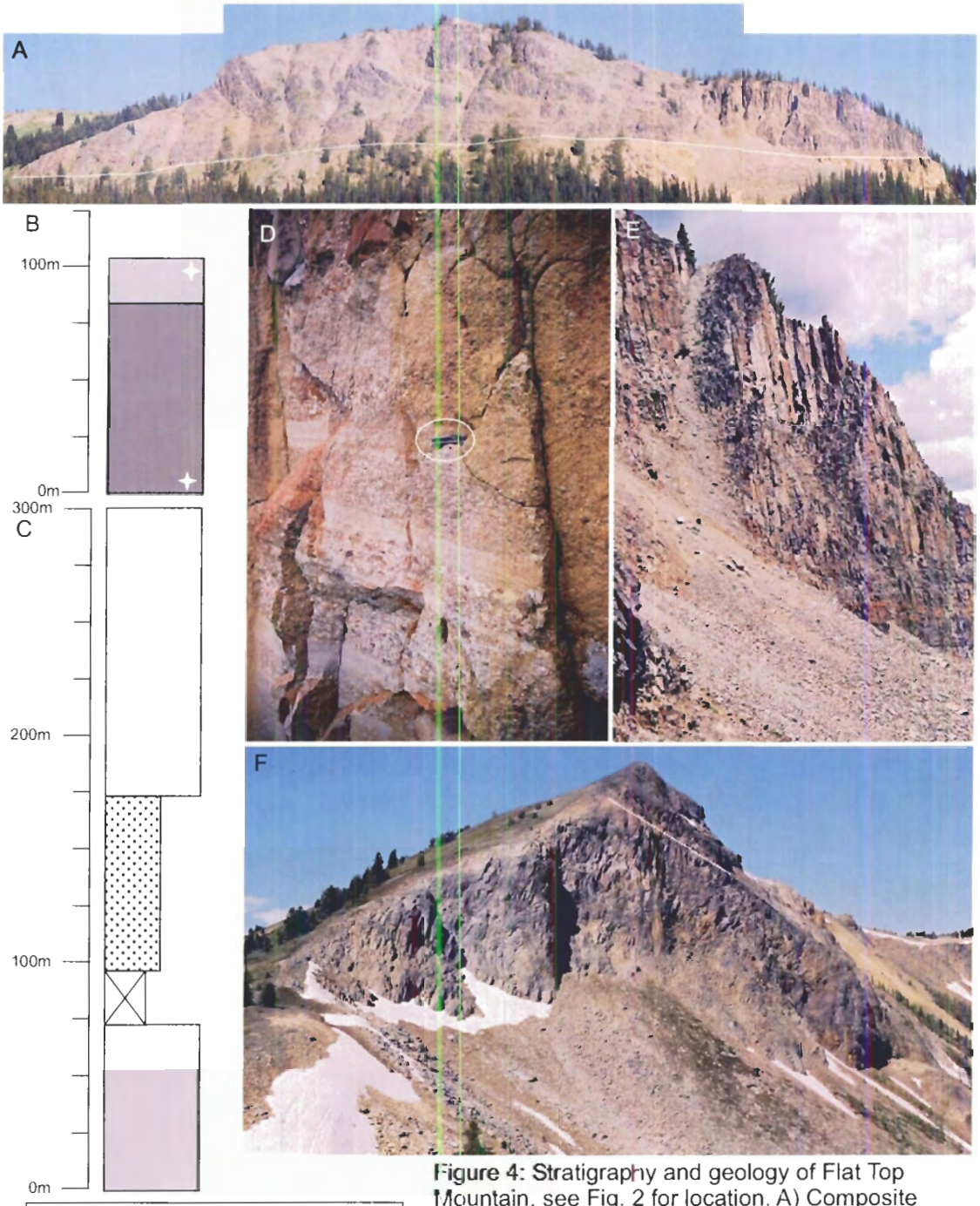

Figure 4: Stratigraphy and geology of Flat Top Mountain, see Fig. 2 for location. A) Composite photograph of prominent high-level clinopyroxene trachyandesite sill (above white line) and underlying tephra near Flat Top Mountain. C,D) Stratigraphic sections from Flat Top Mtn. (for photos see 4A,F). D) Interbedded lapillistone and tuff near Flat-Top Mtn. Folding knife (circled) for scale. E) Close-up of cliff section in A and D, height of cliff approximately 60 m. F) High level sill (above white line) capping hornblende plagioclase dacite dome.

are well-bedded, well-sorted and composed of ash or angular fragments of andesite, similar to that of the pyroclastic breccia, although the finer material is typically more heavily altered, making it difficult to determine the protolith in some cases.

Overlying the tephra is a 125 m-thick, concordant body of clinopyroxene trachyandesite that extends over an area of at least 1 km^2. The trachyandesite has crude vertical columnar joints, and is pervasively fractured, although the host rock is not significantly altered. The unit displays crude horizontal layering that is defined by sets of columnar joints that are separated by horizontal bands of more fractured rock, or by subtle changes in weathering colour and resistance to weathering. The unit is interpreted as either a sill or thick flow that may have been inflated by sill-like injections of magma prior to complete crystallization (cf. Self et al. 1996).

Other exposures in the vicinity of the Flat Top section include (a) thick (>75 m) units of columnar-jointed, highly porphyritic hornblende-plagioclase dacite containing hornblende gabbro xenoliths and (b) smaller bodies of weakly porphyritic plagioclase-hornblende dacite. Both unit types appear to extend over 3 km and are interpreted as volcanic domes or cryptodomes

The volcanic rocks at and near Flat Top Mountain are most likely the remnants of a composite volcano. The coarse pyroclastic breccia is interpreted as the product of collapse and minor reworking of the andesite-dominated volcanic flanks. The well-bedded lapilli-tuff and tuff are interpreted as fall-out

deposits resulting from nearby strombolian to plinian eruptions from a nearby vent. The proximity to basement rocks and the abundance of high-level intrusive rocks suggests that uplift has exposed the roots of the volcanic centre, and that later faulting has disrupted continuity between outcrops and the relationship to basement rocks. Similar exposures of massive or heavily fractured to columnar jointed andesite occur to the north around Placer Mountain, suggesting that the volcano or volcanic field extended at least 10 km northward.

Geochronology

Three samples of hornblende, one whole rock sample and one groundmass sample were dated by the $^{40}Ar/^{39}Ar$ laser fusion technique at the Pacific Centre for Isotopic and Geochemical Research, Department of Earth and Ocean Sciences at the University of British Columbia, Canada (Table 1). The three hornblende separates yielded dates of 52±1 Ma, 49±1 Ma, and 50.3±0.9 Ma, the groundmass separate yielded a date of 52±2 Ma, and the whole rock yielded a date of 50.2±0.4 Ma (all errors are at 2σ). Representative age spectra and an inverse isochron are presented in Fig. 5 and the analytical methods and sample descriptions are presented in Appendix 1. A compilation of available isotopic age determinations for the Princeton Group is presented in Table 2.

Discussion

The new $^{40}Ar/^{39}Ar$ geochronological results presented here, in conjunction with other recent $^{40}Ar/^{39}Ar$ (Villeneuve and Mathewes 2005) and U-Pb results (Archibald and Mortensen unpublished; Friedman and Thorkelson unpublished),

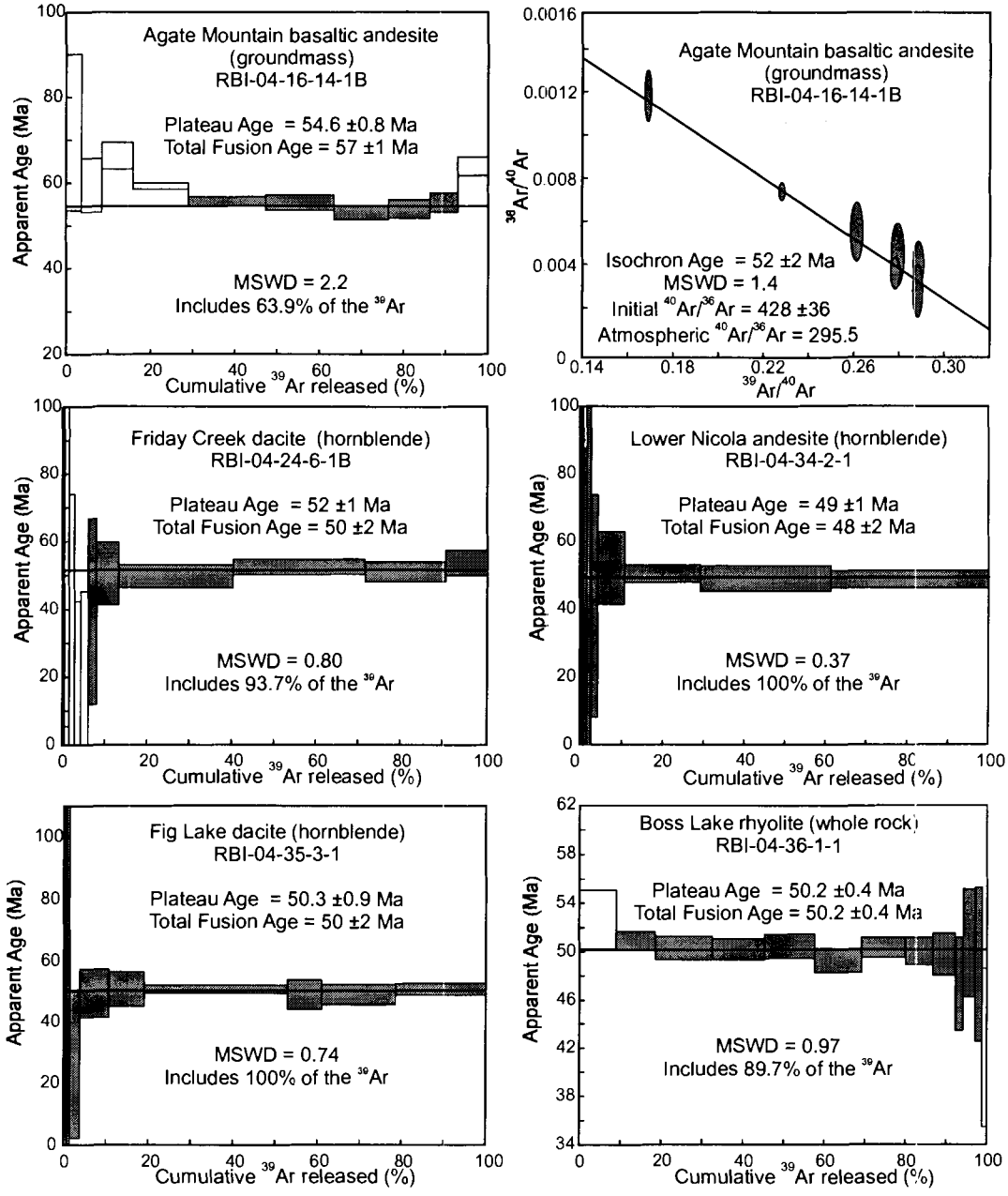

Figure 5: $^{40}Ar/^{39}Ar$ degassing spectra of five Princeton Group samples. The data was processed and plotted using Isoplot 3.09 (Ludwig 2003). The date determined from the plateau is the interpreted cooling age (the cooling age is likely identical to the eruption age) for all samples except for RBI-04-16-14-1B, for which the date determined by the inverse isochron method is the interpreted cooling age. The shaded release steps in the degassing spectra are the ones used in the plateau calculation. All uncertainties are reported at 2σ confidence limits.

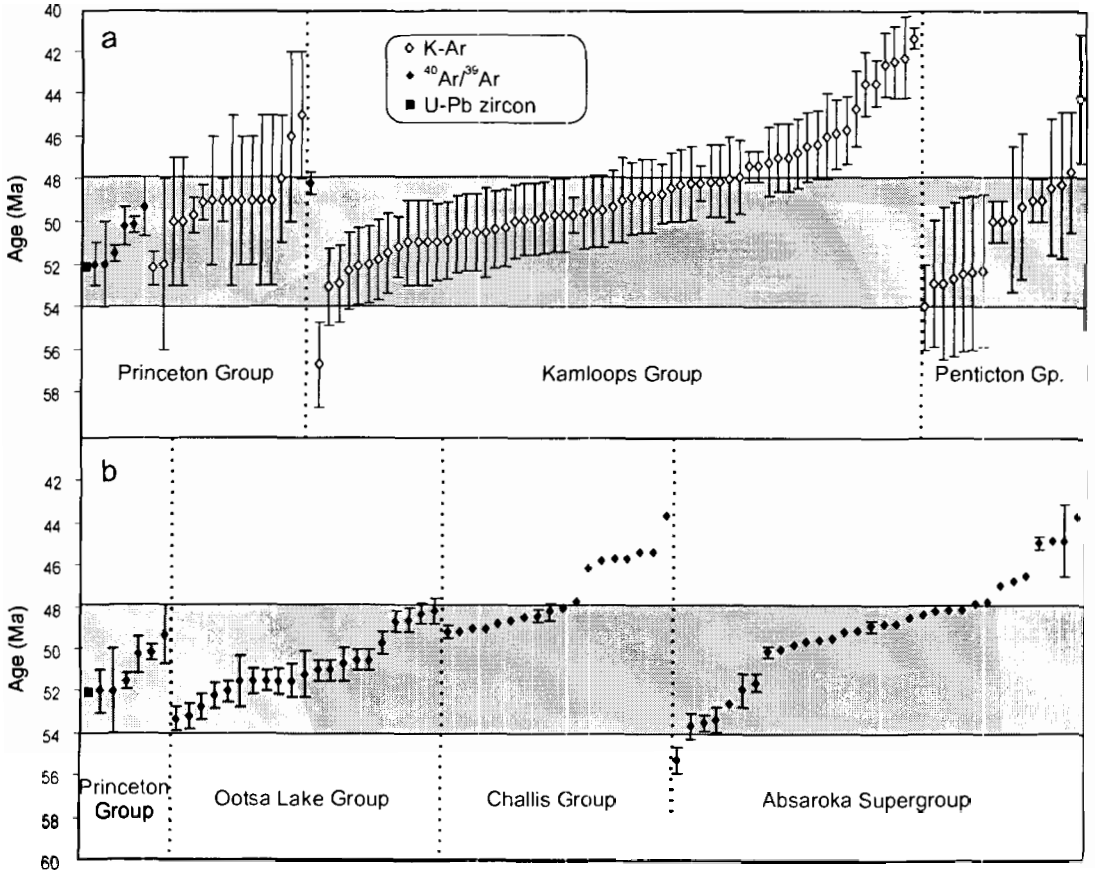

Figure 6: Compilation of select geochronological information the Challis-Kamloops belt. Error bars represent uncertainties at 2σ, where error bars are not present the uncertainties are smaller than the symbol. A) Graphical representation of all available geochronological information for volcanic rocks of the Princeton Group, Kamloops Group, and Penticton Group in south central British Columbia. The grey band represents duration of volcanic activity in the Princeton Group, as determined in this study. B) Representation of precise geochronology for the Princeton Group (K-Ar dates excluded), and volcanic fields of the Challis-Kamloops belt to the north (Ootsa Lake Group) and to the south (Challis Group and Absaroka Supergroup). Note the substantial synchronicity. Dates are compiled from Church 1979; Church and Suesser 1983; Mathews 1989; Hunt and Roddick 1990; Carlson et al. 1991; Berger and Snee 1992; Bardoux 1993; Janecke and Snee 1993; Wooden and Box 1996; Janecke et al. 1997; Hiza 1999; Grainger et al. 2001; Breitsprecher 2002; Feeley et al. 2002; Dostal et al. 2003; Feeley and Cosca 2003; and Church unpublished.

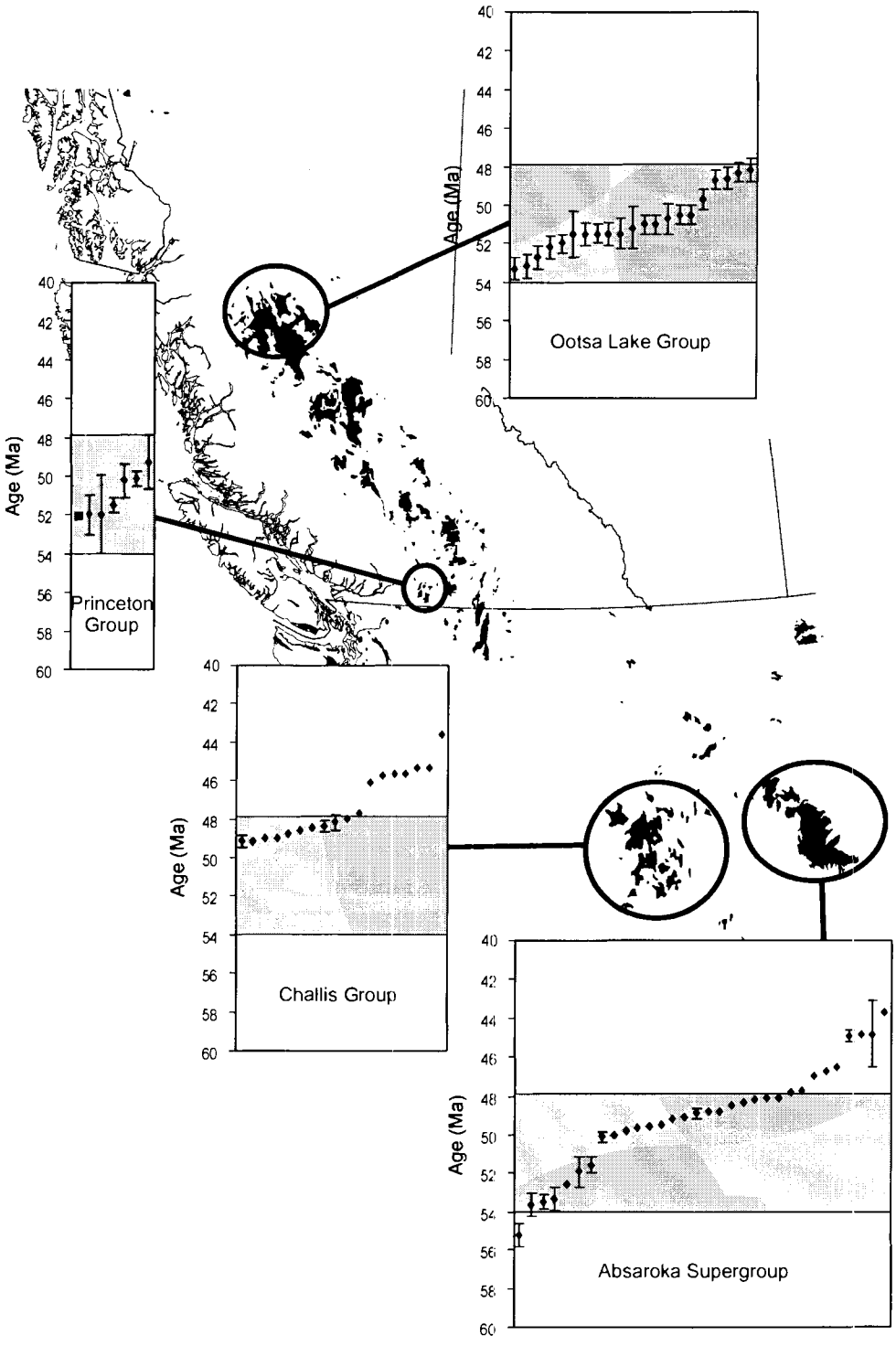

Figure 7: Compilation of recent ^{40}Ar-^{39}Ar and U-Pb dates from different volcanic belts in the Challis-Kamloops belt.

tightly constrain the duration of volcanic activity in the Princeton Group to 53-47 Ma. This 6 Ma duration of volcanic activity is similar to, but more smaller than the range provided by previous work (Fig. 6). From the available data, there does not appear to be significant spatial diachroneity or time-composition relations such as a mafic-to-felsic transition, for example.

The geochronological data results for the Kamloops Group (with a single exception, entirely composed of K-Ar analyses; compiled in Breitsprecher 2002) is of variable quality, but imply that the duration of volcanic activity was mainly in the range 53-46 Ma. A similar range of 54-47 Ma is suggested by results from the Penticton Group (Church 1979; Church and Suesser 1983; Mathews 1989; Hunt and Roddick 1990; Bardoux 1993; Dostal et al. 2003; Church unpublished), and the related Colville Igneous Complex (Carlson et al. 1991; Berger and Snee 1992; Wooden and Box 1996). Collectively, these data suggest that Eocene volcanism in southern BC was active during an interval lasting <10 Ma.

The interval of volcanism in central and northern British Columbia is similar to that in southern British Columbia (Fig. 6, Fig. 7). Grainger et al. (2001) studied the geochronology and local stratigraphic correlations of the Ootsa Lake Group in north-central BC. They determined an identical duration of volcanic activity of 53-47 Ma, and suggested that the age of most other volcanic units in north-central British Colombia (e.g. the Endako Group, Buck Creek Formation, and Newman Volcanics) fall into the same age bracket. Sparse geochronological results from small volcanic fields near the BC-Yukon border (Bennett Lake and

Mount Skukum Volcanic Complexes; Morris and Creaser 2003) suggest a slightly older history of 56-53 Ma.

To the south, precise $^{40}Ar/^{39}Ar$ age determinations from the Challis Volcanic Field have been provided by Janecke and Snee (1993) and Janecke et al. (1997; Fig. 6, Fig 7). These results suggest that intermediate composition volcanic activity took place from 49-48 Ma, followed by a pulse of explosive rhyolitic (possibly bimodal) volcanic activity from 46-45 Ma. The total duration of activity overlaps with the youngest volcanism in southern British Columbia, but continues later into the Eocene. One of the largest volcanic fields, the Absaroka Supergroup, has recently been the focus of a number of geochronological investigations (Hiza 1999; Feeley et al. 2002; Feeley and Cosca 2003). Volcanic activity was apparently the most protracted in the Absarokas, lasting ~10 Ma from 45-55 Ma and overlapping with volcanic activity in both BC and the Challis Field.

Petrography

Mineral assemblages generally correlate with bulk composition. Rocks with less than 60 wt. % SiO_2 generally have a phenocryst assemblage of clinopyroxene ± olivine ± orthopyroxene ± magnetite, lack plagioclase phenocrysts, and have a groundmass assemblage of plagioclase + clinopyroxene + magnetite and minor devitrified glass. Rocks with SiO_2 contents from 60-70 wt. % are typically either strongly porphyritic (with as much as 50 vol. % phenocrysts) and have a phenocryst assemblage of plagioclase + hornblende

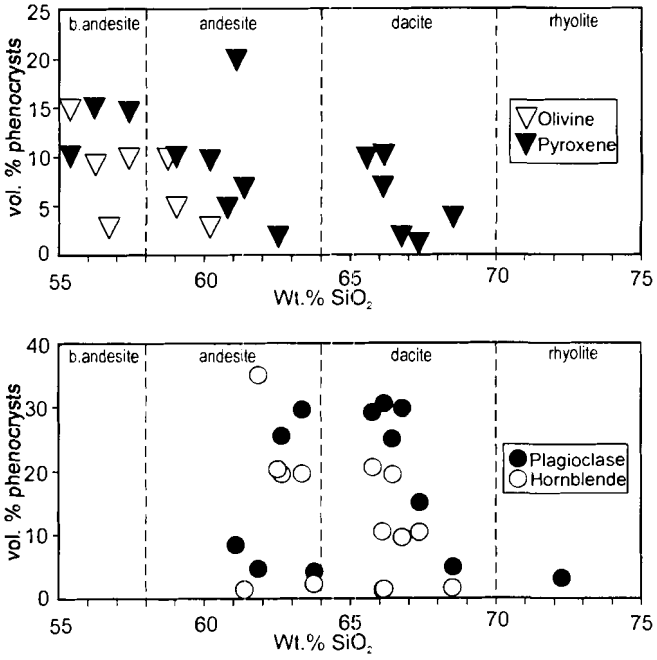

Figure 8: Modal phenocryst abundances for volcanic rocks in the Princeton Group, expressed as volume percent of the total rock. All abundances estimated visually. Orthopyroxene (opx) and clinopyroxene (cpx) are represented together, although generally cpx>>opx.

+ magnetite, or are only weakly porphyritic and have a phenocryst assemblage of plagioclase + clinopyroxene + magnetite (Fig. 8). Some dacites contain very small quantities of quartz and/or biotite phenocrysts. Trace amounts of clinopyroxene and hornblende are common in both hornblende-dominant and clinopyroxene-dominant rocks, respectively. In these more silicic samples, apatite and zircon are common trace minerals and the groundmass is composed of varying amounts of devitrified glass with microlites of plagioclase ± clinopyroxene ± magnetite. The only rhyolite sampled in this study (72 wt. % SiO_2) is weakly porphyritic and has small phenocrysts of K-feldspar, plagioclase, quartz, and biotite with a groundmass of devitrified glass and plagioclase microlites.

The phenocrysts have a wide range in textures. Olivine and pyroxene are typically subhedral, however, some pyroxenes have visible cores, and range from individual grains to glomerocrysts. In one unit the orthopyroxene phenocrysts are strongly embayed. Plagioclase is commonly oscillatory zoned, and sieve-textured, and locally has visible cores or intra-grain evidence for a resorption event in its history. Multiple plagioclase populations are common, as defined on the basis of texture, within a single sample. Hornblende is typically euhedral and optically unzoned, although in some flows the crystals have thick opacite (fine-grained Fe-Ti oxides) rims, which in many cases completely reduces smaller grains to silhouettes of fine-grained opaque minerals. It is unclear as to how much of this rim is due to late subsolidus alteration of the rocks and how much (if any) represents hornblende breakdown during changes in

conditions of magma storage or eruption (e.g. Rutherford and Devine 2003). In rare cases, individual crystals were in a clear reaction relationship with the melt. In one case, a quartz crystal reacted with the melt to form clinopyroxene, and in another, orthopyroxene reacted with the groundmass to form hornblende. These instances are rare and it is unclear to what extent they controlled the chemical evolution of the magma.

Xenoliths of coarse-grained crystalline rock are locally abundant, particularly in some of the strongly porphyritic dacites. Most are less than 1 cm in diameter but range up to 3 cm. A small proportion of these xenoliths appear to be accidental crustal fragments and include foliated granitoid rocks. The majority of the xenoliths, however, have a massive, plutonic igneous texture and a mineral assemblage of plagioclase + hornblende + magnetite, identical to the host dacite or andesite. The hornblende is typically euhedral and the magnetite is commonly embayed. Both are enclosed by large, commonly oikocrystic, plagioclase that is unzoned except for narrow rims at their margins. In places, the groundmass projects far into individual xenoliths into cavities bounded by euhedral crystal faces, and probably represents original magmatic porosity. Smaller xenoliths (<0.75 cm) with an identical mineral assemblage typically have different textures, which include those with equal-sized hornblende and plagioclase, and those comprised entirely of hornblende. These xenoliths are probably cognate with respect to the host rock. Phenocrysts of plagioclase in the host andesite/dacite are not simply disaggregated xenolithic grains as they commonly have complex zoning patterns, whereas the xenolithic crystals do not.

Geochemistry and Neodymium Isotopes

Analytical Techniques and Uncertainties

Twenty-six rock samples were selected for chemical analysis and a subset of seven was selected for Nd isotopic analysis. Samples that were free of secondary minerals and amygdules were selected and chipped clean of weathered surfaces in the field. Seven of the chemical samples were from Agate Mountain, eleven samples were from the region at and around Flat Top Mountain and Placer Mountain, two were from the Sunday Creek region (which complement the four previously published by Breitsprecher 2002), and the remaining six samples were from other localities to the north and northwest. The samples for Nd isotopic analysis were selected to represent a broad geographic and compositional range.

Major element and trace element concentrations were analyzed at commercial laboratories, (ACTLABS [n=25] and ALS Chemex [n=1]) and are reported in Table 3, where all major element oxides are normalized to 100% on an anhydrous basis. Major elements and select trace elements were determined by fusion ICP-OES (inductively coupled plasma optical emission spectroscopy) and all other trace elements, including the lanthanides, were determined by ICP-MS (inductively coupled plasma mass-spectrometry) or INAA (instrumental neutron activation analysis). Nearly all uncertainties are <10 % (relative) and most are <3% (Table 3). Relative uncertainties for Tl, Ge, Ta, Cs, Bi, Lu, Pb, and Mo are >10%. Concentrations of elements and oxides (including K_2O, Ba and Sr) do not correlate with loss-on-ignition (LOI), strongly suggesting that low-

temperature alteration has not significantly affected the chemistry of these samples.

Neodymium isotopic compositions were determined at the Pacific Centre for Isotopic and Geochemical Research, Department of Earth and Ocean Sciences, University of British Columbia, and are reported in Table 4. The analyses were carried out by conventional thermal ionization mass-spectrometry (TIMS) on a Finnigan Triton mass spectrometer, following the methodology of Weis et al. (2005). The average $^{143}Nd/^{144}Nd$ of the La Jolla standard run during the analytical session was 0.511853±6 (n=11).

Results

Major Elements

Volcanic rocks from the Princeton Group exhibit a wide and continuous range in major element chemistry (Fig. 9). The SiO_2 contents range from 55-72 wt. % and MgO contents range from 0.62-9.50 wt. %. On a total-alkali vs. SiO_2 diagram (Fig. 9; Le Maitre 2002) the rocks are classified as basaltic andesite, basaltic trachyandesite, andesite, trachyandesite, dacite and rhyolite. Andesite and dacite predominate. All samples are subalkaline (Irvine and Baragar 1971), most are medium-K, and four samples are high-K (Fig. 9; Le Maitre 2002). The whole suite exhibits relatively constant and low FeO/MgO, similar to that associated with calc-alkaline suites, although two samples from the Sunday Creek area (out of six from the suite) have significantly lower MgO contents than the others from the area and appear to be tholeiitic (Fig. 9; Miyashiro 1974).

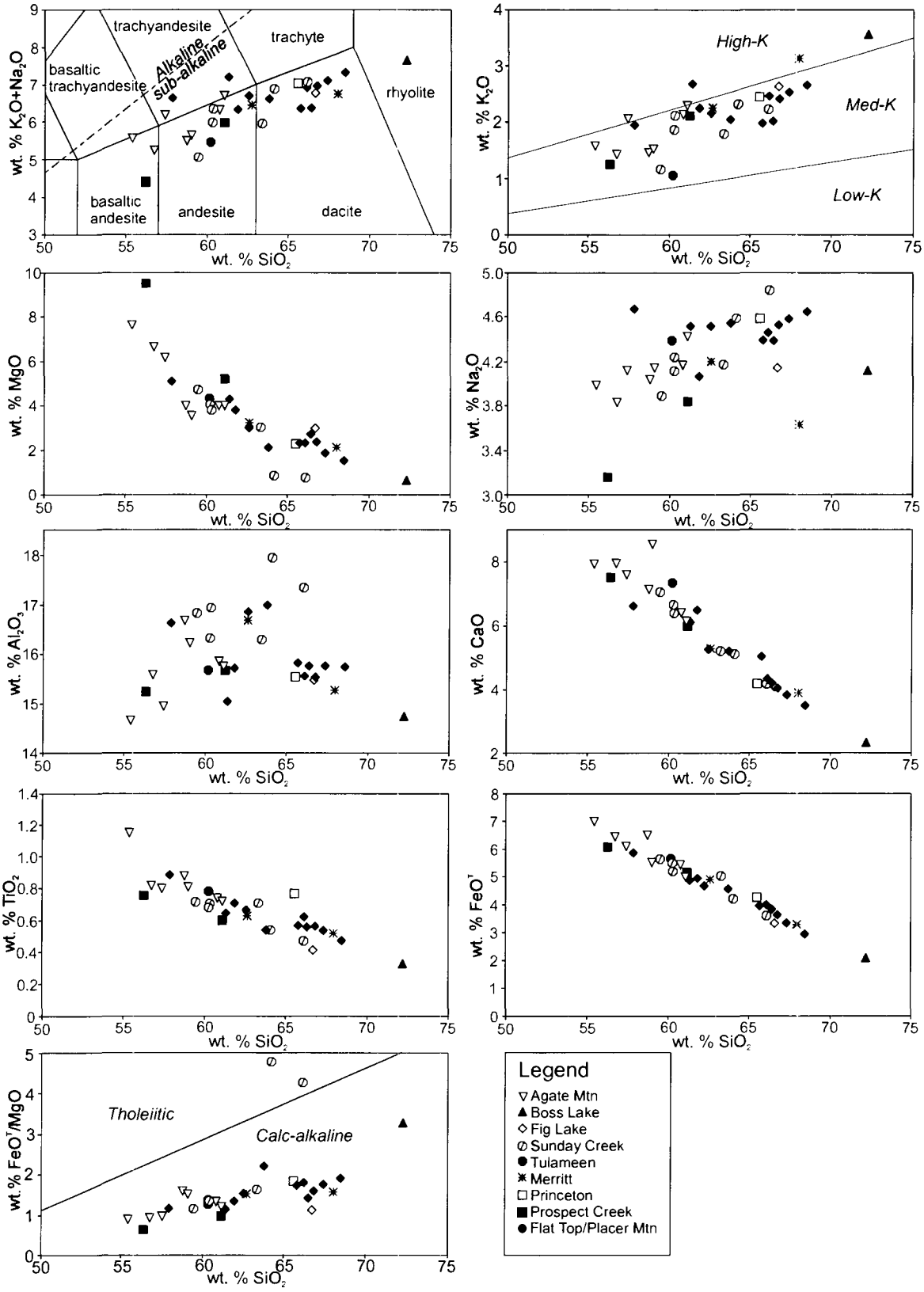

Figure 9: SiO_2 variation (Harker) diagrams for major element oxides. Total alkali vs. silica (TAS) diagram in top left after Le Maitre (2002) and SiO_2 vs. FeO^T/MgO diagram after Miyashiro (1974). The uncertainties on analyses at 2σ are typically smaller than the symbols.

They form a calc-alkalic to calcic suite (variation in the alkali-lime index is due to scatter in Na_2O and K_2O) according to the definition of Peacock (1931).

Some major oxides that partition strongly into or are essential constituents of mafic minerals (including MnO, MgO, and FeO) have strong negative correlations with SiO_2 content. Additionally, TiO_2, which is incompatible in olivine and clinopyroxene (but moderately compatible in hornblende and very compatible in magnetite), also has a strong negative correlation with SiO_2. No obvious inflections in the patterns are present. Other major elements (e.g., K_2O, Na_2O, and Al_2O_3) correlate poorly with SiO_2, both within individual suites and within the Princeton Group as a whole.

The Mg# (molar $Mg/(Mg+Fe^{2+})\cdot 100$); FeO recalculated based on $Fe_2O_3/FeO=0.3$; Gill 1981) of the Princeton Group volcanic rocks are unusually high for calc-alkaline volcanic suites. The Mg# varies from 92-27 with the vast majority greater than 50. Correspondingly, these rocks are in Fe-Mg equilibrium with olivine of a high forsterite content (calculated after Roeder and Emslie 1970), ranging from Fo_{89} to Fo_{61} (excluding a very high MgO sample that has accumulated orthopyroxene) although most are in Fe-Mg equilibrium with olivine of Fo_{89} to Fo_{80}. If calculations are performed assuming all Fe as Fe^{2+}, however, the equilibrium forsterite content in olivine decreases by 3-6 mol%.

Trace Elements

Multi-element diagrams (normalized to normal mid-ocean ridge basalt: NMORB, Sun and McDonough 1989) of volcanic rocks from the Princeton Group have broadly similar patterns to average upper continental crust and modern

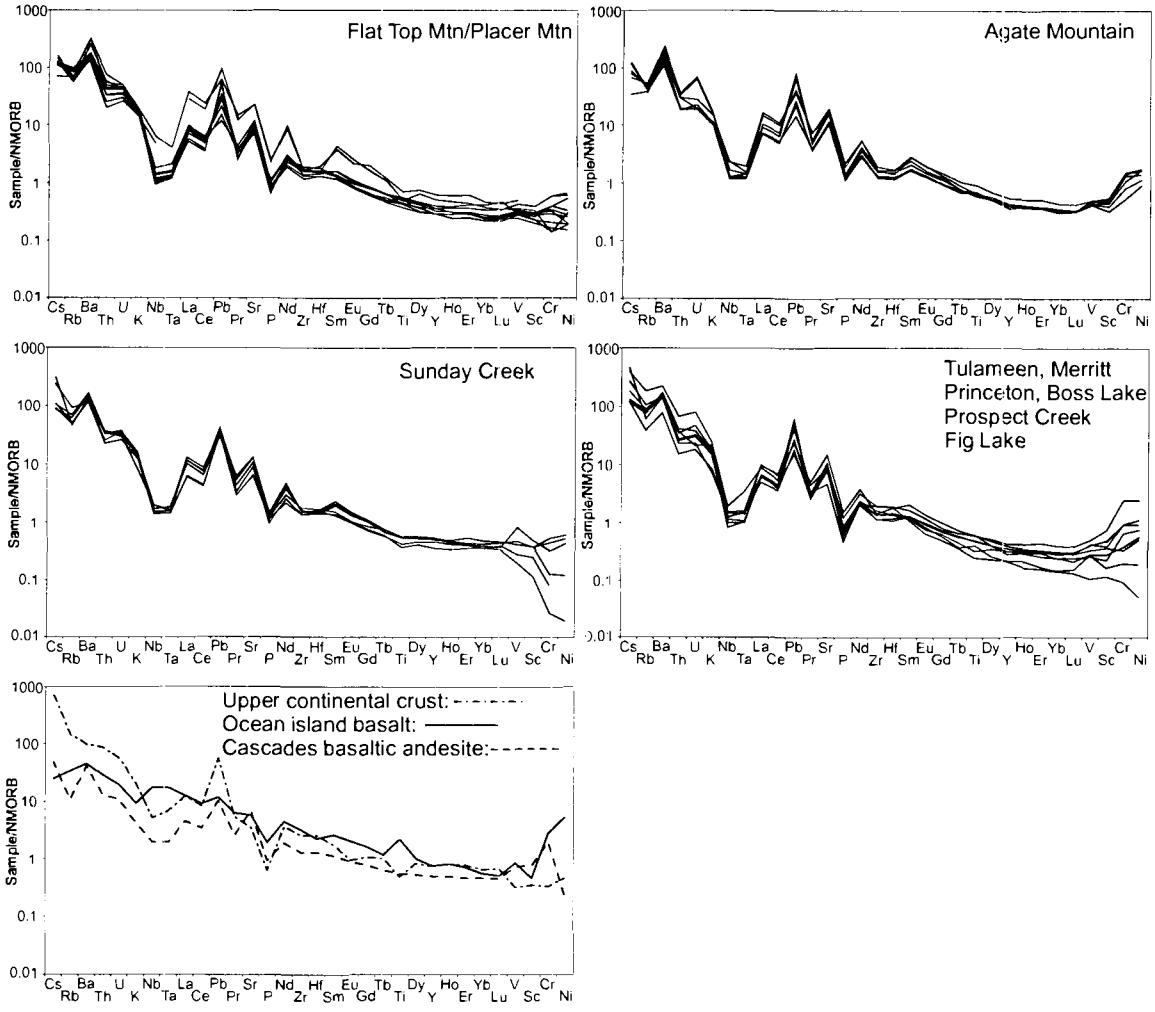

Figure 10: NMORB (Normal Mid-Ocean Ridge Basalt; Sun and McDonough 1989) normalized trace element diagrams. For reference, the upper continental crust composition of Rudnick and Gao (2003), a typical EM-1 ocean-island basalt from Pitcairn Island (sample 49DS-1 of Eisele et al. 2002; Hofmann 2003), and a basaltic andesite from Mount Shasta (sample 82-94a of Grove et al. 2002; Ta calculated assuming a chondritic Nb/Ta of 17.6). See Fig. 2 for locations.

subduction-related volcanic rocks (Fig. 10). These features include positive anomalies (defined as the measure of the value of the ratio of adjacent elements on the diagram relative to NMORB) in Pb and Sr, and negative anomalies in Nb, Ta, Hf, Zr, and Ti. These features are present all rocks from basalts to rhyolites.

The trace elements that are compatible in mafic phases (e.g., Ni, Cr, V, and Sc) have strong negative correlations with SiO_2 and generally have positive correlations with each other. For example, Ni concentrations range from relatively high values of ~175 ppm in olivine-bearing rocks from Agate Mountain, to <50 ppm in silicic andesites and dacites from elsewhere in the Princeton Group. Most trends have inflections at about 60 wt. % SiO_2, correlating with changes in phenocryst mineral assemblages from olivine and clinopyroxene dominated rocks to plagioclase and hornblende bearing rocks.

Many incompatible trace elements, including the high-field strength elements (HFSE; e.g., Zr, Hf, Nb, Ta), actinides (Th, U), and rare earth elements (La to Lu) correlate poorly with SiO_2. The large ion-lithophile elements Sr and Rb show weak negative and positive correlations respectively with SiO_2 and Ba have no correlation with SiO_2. The abundances of most HFSE are relatively low and constant at only about 1-2 times that of normal mid-ocean ridge basalt (NMORB; Sun and McDonough 1989), but concentrations of actinides, light rare earth elements (LREE), and LILE are highly elevated resulting in suprachondritic La/Nb, U/Nb, and Ba/Nb, common features in both average upper continental crust (Rudnick and Gao 2003) and subduction-related magmas (Gill 1981; Pearce and Peate 1995). The concentrations of heavy rare earth elements

(HREE) are particularly low and relatively constant at about 0.2-0.5 times NMORB, resulting in relatively high ratios of light to heavy REE (La/Yb = 9-82).

Adakite and high-Mg# Andesite

The Princeton Group contains abundant adakite and high-Mg# andesite. Adakites are defined as rocks with SiO_2 >56 wt.%, Al_2O_3 >15 wt.%, Na_2O >3.5 wt. %, Sr >400 ppm, Y <18 ppm, Sr/Y > 40, Yb < 1.9 ppm, and La/Yb > 20 (Defant and Kepezhinskas 2001). High-Mg# andesites (also referred to as high-Mg andesites) are defined as rocks with SiO_2 > 54 wt. % and Mg# > 56 (Kelemen et al. 2003) and, although by definition they are not necessarily equivalent to adakites, are commonly adakitic or associated with adakites. Including those already identified by Breitsprecher et al. (2003), nearly half of all rocks analyzed in the Princeton Group are adakites and three-quarters are high-Mg# andesites. Three quarters of the adakites are also high-Mg# andesites.

Adakite and related high-Mg# andesite are intriguing classes of volcanic rock that are associated with controversial topics such as slab-melting in subduction zones (Defant and Drummond 1990), crustal differentiation (Atherton and Petford 1993) and crustal growth (Kelemen 1995), and Archean plate tectonics (Martin 1999). Adakite in the Princeton Group was previously linked to slab-melting (Breitsprecher et al. 2003; Thorkelson and Breitsprecher 2005), although that connection is challenged in this paper, and is discussed in detail, below.

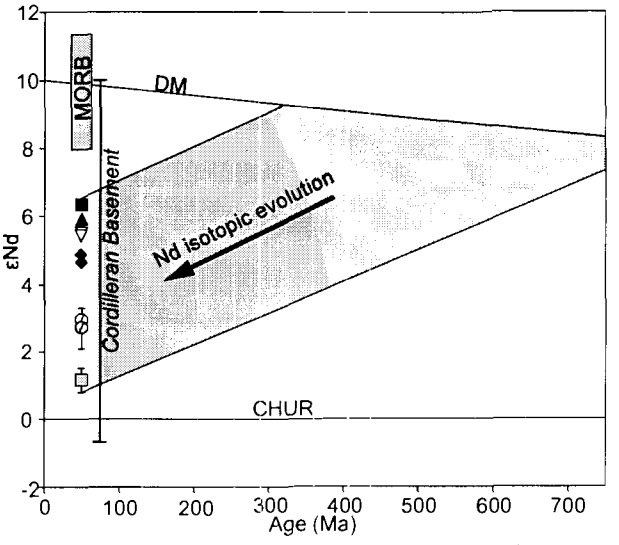

Figure 11: εNd vs. time diagram. Errors bars represent 2σ uncertainty, where error bars are absent the errors are smaller than the symbols. Symbols are as in Fig. 9, however grey symbols are data from Ghosh (1995). MORB field is the 2σ distribution for NMORB from the East Pacific Rise (http://www.petdb.org/). The Cordilleran Basement bracket is the 2σ distribution for basement rocks to the Princeton Group (Ghosh 1995; Smith and Thorkelson 2001). DM curve is from Goldstein et al. (1984). The field labeled Nd isotopic evolution is based on projecting the Nd isotopic compositions of Princeon Group rocks back in time assuming they had a present day Sm/Nd.

Neodymium Isotopes

Seven new Nd isotopic analyses of whole rocks were determined for the Princeton Group (Fig. 11; Table 4). Two previous Nd isotopic compositions were provided by Ghosh (1995), although without accompanying major or trace element analyses. The total range in εNd at 50Ma (εNd_{50})ranges from 1.2 to 6.4. Correlations of εNd_{50} with major element abundances or trace element ratios are not evident: For example, the lowest εNd_{50} values (1.2-2.9) occur in Sunday Creek dacites with low Ni concentrations and Mg#, but the Boss Lake rhyolite has a relatively high εNd_{50} of 5.9, greater than a primitive olivine-bearing basaltic andesite at Agate Mountain (εNd_{50} = 5.5). In addition, where multiple analyses are available from the same suite (Agate Mountain and Flat Top Mountain, two analyses each) the εNd_{50} are identical within uncertainty, suggesting little variation in the degree of contamination within individual centres.

The Nd isotopic compositions are all more radiogenic than the bulk earth, similar to the source of most oceanic basalts. Although the relatively high εNd_{50} values rule out a significant contribution from typical ancient continental crust or derivative sedimentary rocks, they do not rule out contributions from juvenile continental rocks with short crustal residence times. For example, the range in εNd_{50} of the exposed Mesozoic basement to the Princeton Group (from Ghosh 1995; Smith and Thorkelson 2002; n=45) completely overlaps with that of the Princeton Group. They do, however, differ significantly from some alkaline rocks near the base of the nearby Penticton Group, the Yellow Lake Member, which

has a range of εNd_{50} from −4 to −6 (Dostal et al. 2003). Depleted mantle model ages representing the minimum time of extraction from the mantle (assuming a uniform composition mantle source) range from 350-750 Ma.

Compositional Variation in the Princeton Group: Crystallization, Assimilation, and Source Heterogeneities

The large compositional variations in the Princeton Group can be explained mainly by fractional crystallization, with subordinate assimilation of crustal material and magma mixing. Basaltic andesites and andesites, when compared to andesites and dacites, have higher concentrations of Ni, Sc and Cr, as well as higher MgO, FeO, and CaO. Mineral assemblages are dominated by olivine and clinopyroxene in these rocks (Fig. 8) and fractional crystallization of these minerals can account for the strongly negative trends on Harker diagrams. Furthermore, the co-variations between these elements change in concert with changes in the phenocryst assemblages. For example, as a function of SiO_2, Ni concentrations drop rapidly (from >170ppm to <70ppm) while olivine and clinopyroxene dominate the phenocryst assemblages. However, at about 60 wt. % SiO_2, when plagioclase and hornblende dominate the assemblages, the drop is less pronounced and the trend is more scattered. This change in trend can be attributed to the higher compatibility of Ni in olivine and clinopyroxene, compared to hornblende and plagioclase.

Quantitative modelling, by calculating Rayleigh fractional crystallization paths using the observed phenocryst assemblages, demonstrates that fractional crystallization is likely to have been the dominant process by which Princeton

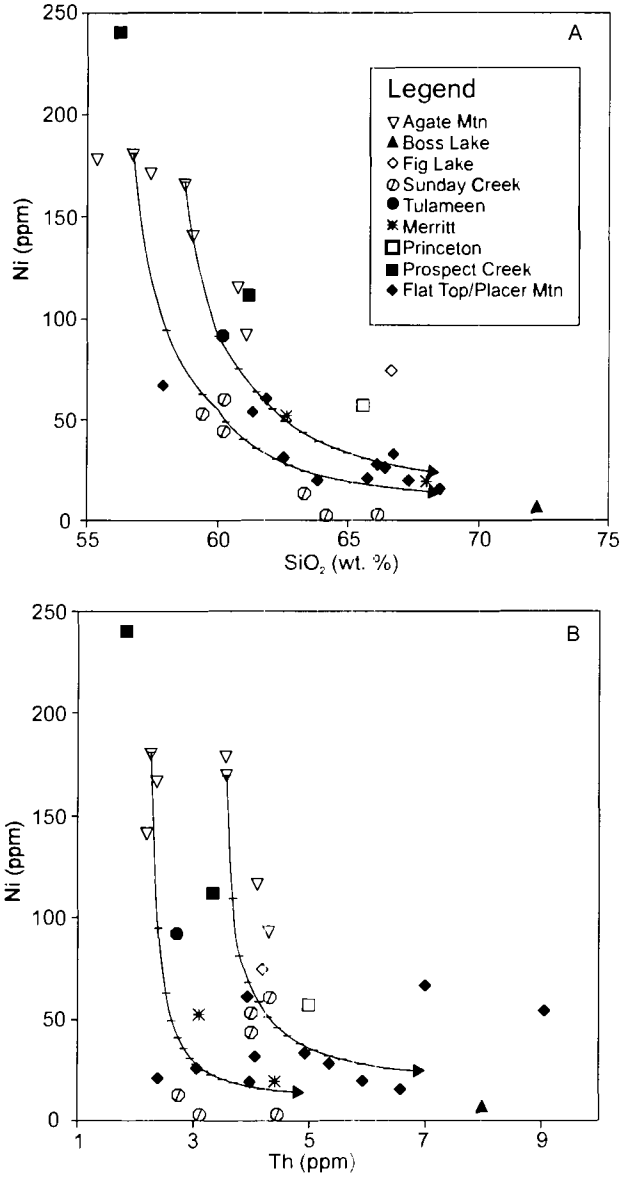

Figure 12: Raleigh-type fractional crystallization modelling. The two lines represent modelled liquid lines of descent from two different parental compositions (RBI-04-16-14-1; RBI-04-15-13-1). Each model has two stages. Olivine + clinopyroxene + magnetite are fractionated until the magma is at 60 wt. % SiO2, then hornblende + plagioclase + apatite + zircon + magnetite are fractionated. Tic marks represent 2% crystallization increments. Errors at 2σ are smaller than the symbols.

Group rocks are related (Fig. 12). The modelling calculates the changing abundances of Ni and SiO_2 by fractionation of observed phenocryst assemblages, where the fractionating assemblage varies with bulk composition (e.g., Fig. 8). The two curves in Fig. 12a show the results of fractional crystallization starting from two different primitive (olivine phyric, Mg# > 60) Princeton Group magmas. Other compatible elements have inflections similar to those in Fig. 12a that also correlate with changes in phenocryst assemblages. Strontium concentrations, for example, vary widely in the plagioclase-free mafic rocks but steadily decreases once plagioclase becomes a major fractionating phase because Sr is compatible in plagioclase.

Variations in incompatible element abundances (e.g., some LILE, REE, HFSE, actinides) are also generally consistent with fractional crystallization but the models are heavily dependant on the choice of parental magmas. Variations as a function of SiO_2 or compatible elements are generally scattered or show a weak increase (e.g., Th in Fig. 12b). These trends are understandable because incompatible element concentrations increase modestly as a result of low degrees of fractional crystallization (e.g., an increase by only a factor of ~1.4 at 30% crystallization). The strong dependency of incompatible element abundances in evolved magmas on the abundances in primitive magmas is illustrated quantitatively in Fig. 12b. Here, two fractional crystallization paths (calculated in the same way as those in Fig. 12a) have been calculated for Ni and Th from two different primitive lavas, each with a different Th content. In the calculated liquid-lines-of-descent, the large, primary, differences in Th contents

are maintained over a large degree of fractional crystallization. Therefore, the scattered trends in incompatible element ratios against indices of differentiation, such as SiO_2 or Ni, can be understood as heterogeneity in the parental magmas, either as a function of source heterogeneity or as degree of melting in the source area.

Petrographic and isotopic evidence is also consistent with fractional crystallization as a dominant process in differentiation. The common presence of hornblende-gabbro xenoliths, interpreted as fragments of coeval plutonic rocks, is evidence that the magmas had partly crystallized prior to eruption. In addition, at Flat Top Mountain and Agate Mountain, where the Nd isotopic compositions of multiple samples are available, different units have identical isotopic compositions within error suggesting a negligible role for open-system processes such as assimilation and mixing.

Petrographic evidence suggests that magma mixing and assimilation of crustal material may account for some of the chemical variability in the Princeton Group volcanic rocks. For example, multiple textural populations of plagioclase are clear evidence for the mixing of different magmas. Similarly, the presence of accidental xenoliths and xenocrysts in reaction relationships with the host magma indicate assimilation of crustal rock. However, the typically non-linear chemical trends on some variation diagrams (such as Ni vs. SiO_2) indicate that magma mixing is likely to have played a minor role in magma differentiation, as mixing should produce linear trends on all variation diagrams. Assimilation with fractional crystallization (AFC; De Paolo 1981b) produces trends similar to

fractional crystallization, especially at low ratios of mass assimilated to mass fractionated. AFC modelling predicts that the most chemically evolved rocks should have the most "crustal" or unradiogenic Nd isotopic signature. Although this characteristic is evident in highly differentiated dacite from Sunday Creek (Mg# = 32-35; εNd_{50} = 2.7-2.9; Ghosh 1995; this study) it is not true for the highly evolved rhyolite from Boss Lake (Mg# = 41; εNd_{50} = 5.9). The importance of assimilation relative to fractional crystallization, therefore, remains uncertain.

Heterogeneity of the highest Mg#, or most "primitive" magmas of the Princeton Group is an important factor in the variability of trace element abundances. Primitive magma heterogeneity is evident from mafic rocks (Mg# > 65) which display ranges in many trace element abundances that are nearly as high as those in the more evolved rocks. The variability in primitive rock compositions are therefore likely mantle-derived, rather than a consequence of crustal assimilation and fractionation. The adakitic character of the Princeton Group is, therefore, a primary feature rather than one generated by crustal-level processes such as assimilation, fractional crystallization or magma mixing. Constraints on the origins of primitive rocks in the Princeton Group are explored in more detail below.

Discussion

Adakite and High-Mg# Andesite: Review of Petrogenetic and Tectonic Significance

Adakites were originally defined on the basis of rocks with compositions that were similar to theoretically and experimentally predicted compositions of

melts of subducted oceanic crust (Kay 1978; Defant and Drummond 1990; Drummond and Defant 1990). The major element definition is provided by high pressure and temperature experiments on the partial melting of amphibolite-grade metamorphosed basalt (Beard and Lofgren 1991; Rapp et al. 1991; Rushmer 1991; Sen and Dunn 1994; Wolf and Wyllie 1994; Rapp and Watson 1995; Lopez and Castro 2001). Broad distinguishing characteristics include SiO_2>56 wt. % and "trondhjemitic" affinities (high Na/K, Barker 1979), which serve to distinguish amphibolite melts from peridotite melts (which typically have SiO_2<50%), and melts of pelites (which are "granitic," i.e., higher in K_2O). The adakitic trace element signature is defined by a high Sr, Sr/Y, La/Yb, and low Y and Yb, consistent with the *presence* of garnet (to account for low Y, Yb and high La/Yb values) and the *absence* of plagioclase (to account for the high Sr contents and Sr/Y and the absence of an Eu anomaly) in the same rock. The Mg#, and Ni and Cr contents of pure slab melts should be low (e.g., Mg# < 40; (Sen and Dunn 1994; Rapp and Watson 1995). However, the observed abundances in rocks interpreted to be, at least in part, slab-melts are much higher. The high Mg# and compatible element contents of putative slab-melts are typically attributed to reaction between ascending silicic melts and mantle peridotite after partial melting of subducted crust (Kay 1978; Rapp et al. 1999).

Based on experimental work (see above studies), residual solids from low to moderate degree partial melt of an amphibolite at pressures of about 10-15 kbar typically include amphibole, plagioclase, garnet, clinopyroxene and rutile. At higher pressures and higher degrees of partial melting the residual assemblages

would be dominated by an eclogitic (clinopyroxene, garnet, and rutile) assemblage. Arguments based on the trace element systematics of Sr, discussed above, indicate that plagioclase cannot be a residual phase, which places constraints on the minimum degree of partial melting at 10-15 kbar. Plagioclase is a ubiquitous phase in experiments during the initial stages (low degrees) of anatexis; therefore, if the trace element signature is to be compatible with the partial melting of garnet-amphibolite, melt extraction must not occur until at least 20% melting has occurred (Sen and Dunn 1994). This value is similar to the estimates of the rheological critical melt percentage for the extraction of felsic silicate liquids from a solid source, suggesting that >20% is a mechanically realistic value (Petford 2003). Alternatively, the destabilization of plagioclase at high-pressures and fluid-saturated conditions may account for its absence (Poli 1993). However, fluid-saturation is probably rare in subducted lithosphere at amphibolite grade, and partial melting under these conditions will generate a small degree of rhyolitic, peraluminous, fluid-saturated melt, unlike that associated with adakites (Clemens and Vielzeuf 1987; Beard and Lofgren 1991; Yardley and Valley 1997).

Other work has demonstrated that adakitic magmas can be generated by means other than slab melting. Atherton and Petford (1993) identified adakites in the Cordillera Blanca batholith of Peru that they interpreted to be the result of melting of underplated basalt at the base of continental crust. Feeley and Hacker (1995) studied a Quaternary stratovolcano in the Central Volcanic Zone of the Andes and concluded that adakites at this volcanic centre were derived though

the interaction of basaltic magmas with garnet-bearing rocks at the base of the crust, followed by low pressure fractional crystallization to produce andesites and dacites. Other hypotheses on the origin of specific adakites include delamination of basaltic crust (Xu et al. 2002; Gao et al. 2004), subduction erosion (Kay and Kay 2002), and remelting of arc-basalt trapped and solidified in the upper mantle (Macpherson and Hall 2002).

Adakites in the Princeton Group: Petrogenesis of Primitive Magmas

The least evolved high Mg# andesites in the Princeton Group best record information on the nature of the mantle source area and the melt regime as they have been least modified by processes such as crystal fractionation or assimilation of crustal material. The most primitive suite of volcanic rocks in the Princeton Group are the olivine + clinopyroxene + opaque basaltic andesites and andesites exposed at and within a few km of Agate Mountain (a lone sample from Prospect Creek has a higher MgO at 9.2% but has little stratigraphic context and will not be considered in further detail). Three of these samples are in Fe-Mg equilibrium with Fo_{88-89} olivine (Roeder and Emslie 1970), a composition near to that of typical mantle olivine ($\geq Fo_{90}$). Although they are not adakites *sensu-stricto* (because of slightly lower SiO_2 or Al_2O_3 than permitted in the definition) they have "adakitic" trace element signatures such as fractionated REE (La/Yb = 16-34), fractionated HREE (Gd/Yb = 3.2-4.6) and high Sr/Y (90-145). In addition they have very high LILE contents, including Ba > 690 ppm and Sr > 935 pm.

Two hypotheses are explored below using trace element modelling. One is the mainstream adakite hypothesis, i.e., that the adakitic high Mg# andesites

formed by the melting of subducted and metamorphosed oceanic crust and evolved by melt-rock reaction with mantle peridotite. For this model, an average NMORB from the East Pacific Rise (determined using the PETDB compilation; http://www.petdb.org) is used as the composition of the subducted slab. This model fails to reproduce the trace element abundances observed in the Princeton Group. The second hypothesis is that they were generated by melting of metabasalt with arc-like (rather than MORB-like) trace element abundances. For this model, arc basalts from the Cretaceous Spences Bridge Group (Smith and Thorkelson 2002) and Triassic Nicola Group (Mortimer 1987) were selected. Both the Nicola and Spences Bridge groups occur in the same region as the Princeton Group.

Trace Element Modelling

The model concentrations of Ba, Th, Nb, La, Sr, Zr, Sm, Gd, Y, and Yb were calculated at 15-25% batch partial melting, with 49.5% garnet and clinopyroxene and 1% rutile, with and without the addition of small amounts (<5%) of plagioclase and hornblende, followed by reaction with peridotite. The modes were estimated from the experimental studies of Rapp and Watson (1995) and Sen and Dunn (1994). The chemical evolution of silicic melts in the mantle by peridotite-melt reaction is still poorly understood, but has a minor effect on the trace element ratios of the melt, for example Sr/Y, La/Yb, or La/Ba (Rapp et al. 1999). The reactions are dominated by dissolution of olivine with precipitation of orthopyroxene and possibly garnet, but since the incompatible trace element ratios (such as Sr/Y or La/Ba) are not affected by this process

(Rapp et al. 1999), the only effect of melt-peridotite interaction is to concentrate or dilute incompatible trace elements. The amount of dilution (primarily by olivine assimilation) required to bring an amphibolite-melt to Fe-Mg equilibrium with mantle olivine (~Fo_{90}) is 10-15% (e.g., Stern and Kilian 1996).

Internally consistent sets of mineral/melt partition coefficients at relevant pressures, temperatures, and compositions are used. Partitioning data for hydrous, tonalitic melts at 18 kb and 1000-1040°C, (Barth et al. 2002), have been used for garnet and clinopyroxene with the exception of the Th partition coefficient, which was taken from Klemme et al. (2002). Partition coefficients for hornblende were from the 2-5 kb, 900-945°C experiments of Hilyard et al. (2000) on hydrous, dacitic melts with the exception of Ba from Brenan et al. (1995) and Th, estimated from the GERM database (Geochemical Earth Reference Model; http://www.earthref.org/). Rutile partition coefficients are currently poorly understood, but those from Foley et al. (2000) compare well with those of Xiong et al. (2005) and are used herein. Plagioclase partition coefficients were calculated by the method of Wood and Blundy (2003) using An_{60} and 950°C with the exception of Nb, which was estimated from the GERM database and Th, which was estimated to be the same as U (Wood and Blundy 2003).

Results of Trace Element Modelling

Using the trace element concentrations of NMORB as the magma source composition yields a model composition that poorly matches those of high Mg# andesites in the Princeton Group (Fig. 13). In particular, the model melt has abundances of the LILE and LREE, and ratios of La/Yb and Sr/Y, which are well

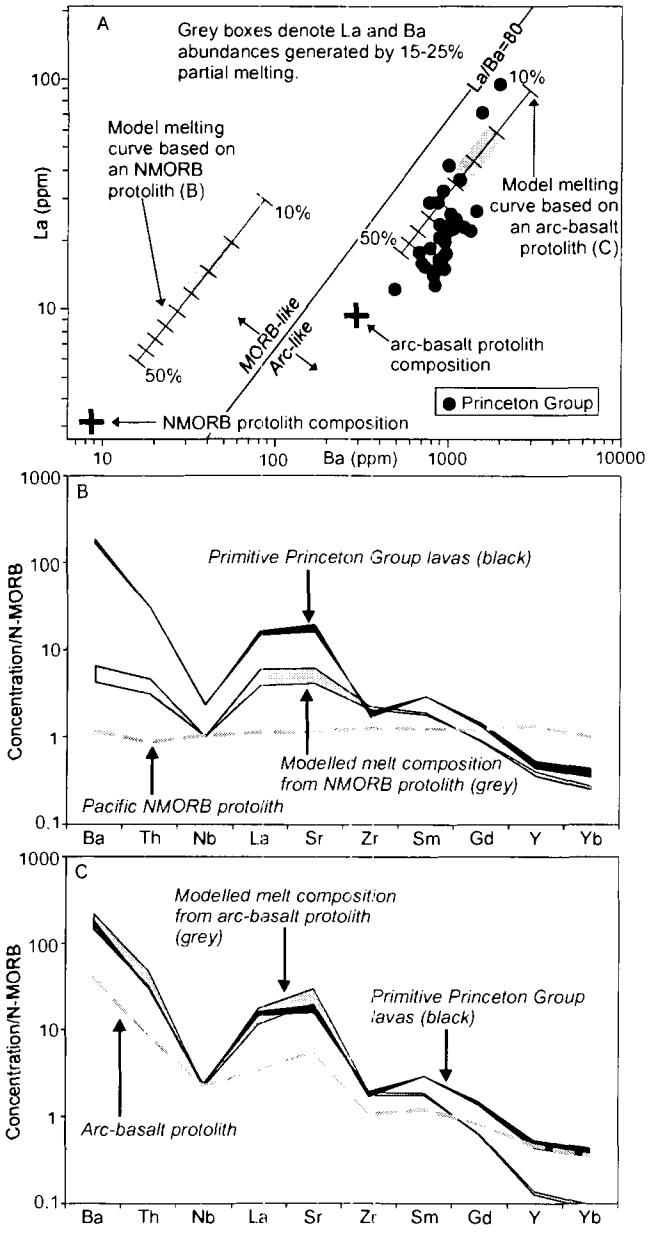

Fig. 13: The results of modeling trace element behavior during partial melting of garnet-amphibolite in the upper mantle. Two different model melt composition were calculated for two different starting compositions, one resembling Pacific NMORB and the other resembling an arc basalt. The results of both models are depicted here. A) Ba vs. La diagram illustrating that an NMORB starting composition poorly reproduces both the Ba and La abundances and the Ba-La ratio (all samples from the Princeton Group are depicted), whereas an arc-like starting composition provides a much better fit to the data. Barium and La abundances are poorly fractionated during partial melting and Ba-La ratios largely retain the value of their source. Line dividing arc-like La/Ba from MORB-like La/Ba from Gill (1981). Tics are 5% partial melting. B) The results of the model using a Pacific NMORB starting composition. The starting composition is dashed and the preferred range of modeled values are in grey. For comparison, the range of values in two adakitic, primitive, Princeton Group lavas are shown. C) The results of the model using an arc-basalt starting composition. NMORB normalizing values from Sun and McDonough (1989).

below those of the Princeton andesites, although they approximately match the Princeton samples in Nb, Zr, Y and Yb. Model Ba concentrations are an order of magnitude lower than those in the high Mg# andesites. Much lower degrees of partial melting (<5%), using the same plagioclase-free restite raises the LILE and LREE to the appropriate (Princeton Group) levels. This situation is unlikely, however, because at such small melt fractions plagioclase is likely to be present in the restite, and even a small amount of residual plagioclase (<5%) leads to a low Sr abundance (420-630 ppm) and Sr/Y ratio (30-50) in the melt, i.e., much less than those in the Princeton Group. The modelled melt composition is insensitive to modest changes in the abundances of residual clinopyroxene and garnet, (for example by changing garnet or clinopyroxene to as much as 75% of the total mode) and the addition of small amounts of hornblende (up to 15%). It is, however, sensitive to changes in the amount of rutile present, with greater percentages of rutile in the restite lowering the abundances of Nb in the model melt.

Using Spences Bridge Group arc basalt as the composition of the magma source provides a much better fit to most of the observed trace element abundances. The resultant melts match the Princeton Group andesites in all modelled elements, except for the HREE and Y, which are much lower in the modelled compositions (~0.3 ppm Yb in the model vs. ~ 1 ppm Yb in the observed rocks). Numerically, the discrepancy is the result of low concentrations of the HREE in the Spences Bridge Group (relative to many arc basalts), which may have been caused by interaction of Spences Bridge Group basalt with

garnet at the base of the crust, or mixing with slab-anatectic melts (cf. Smith and Thorkelson 2002). The modelled HREE concentrations are extremely low compared to typical crustal rocks but comparable to those in mantle peridotite (Rudnick and Gao 2003; Canil 2004). Such low concentrations are highly susceptible to change, either during ascent through the mantle, or by very small degrees of contamination from the crust. Consequently, the cause of the mismatch in HREE between PG values and those of the model is unknown. Using an averaged Triassic basalt from the Nicola Group (Mortimer 1987) as the magma source also yields a melt composition that closely matches the Princeton Group. The fit is slightly better in the HREE, but slightly poorer in the LILE, relative to the Spences Bridge Group model. Using either of the Mesozoic arc basalts yields a better overall fit than by using an NMORB source.

The identification of arc basalt rather than NMORB as a source for adakite runs contrary to the findings of previous studies of adakite petrogenesis. In particular, the high La/Yb and Sr/Y in adakites appear to be inconsistent with anatexis of NMORB, and instead require a source already enriched in LILE. This finding is especially robust when high percentages of partial melting are invoked (i.e., >20% melting), a condition which is required if the restite is to be plagioclase-free – a tenet of adakite petrogenesis (Martin 1999).

Petrogenesis

The trace element modelling and phase relations place important constraints on the origin of primitive, adakitic high Mg# andesites in the Princeton Group. The compositions of these rocks are consistent with a two-stage

process: 1) Partial melting of basaltic rocks with primitive arc-like trace element compositions at depths of approximately 30-80 km (e.g., Fig. 14) and, 2) reaction of the amphibolite-derived melt with peridotite, leading to elevation of Mg# and compatible element concentrations, and possibly enrichment in HREE (Fig. 15). This process can only occur where melting of arc meta-basalt occurs in the mantle environment.

A number of mechanisms are capable of introducing arc basalt into the mantle. Delamination (Kay and Kay 1993) or convective "dripping" (Jull and Kelemen 2001) of mafic, garnet-bearing, high density crustal rocks into the mantle have been proposed by Gao et al. (2004) and Xu et al. (2002) for the generation of adakites in China. In these models, the heating of the detached crustal blocks leads to adakite melt generation; the melts become increasingly mafic by reaction with mantle peridotite during their ascent. This scenario, however, may be unlikely for genesis of the Princeton Group because it seems to require wholesale removal of lithospheric mantle along with the lower crust (Kay and Kay 1993; Lustrino 2005). This is incompatible with studies of mantle xenoliths which identify that ancient lithospheric mantle is preserved through the Canadian Cordillera until at least late-Tertiary time (Peslier et al. 2000). Jull and Kelemen (2001), however, have calculated that convective instabilities between the crust and lithospheric mantle are possible and could result in foundering of lower crust without the loss of lithospheric mantle. If so, this hypothesis is difficult to rule out.

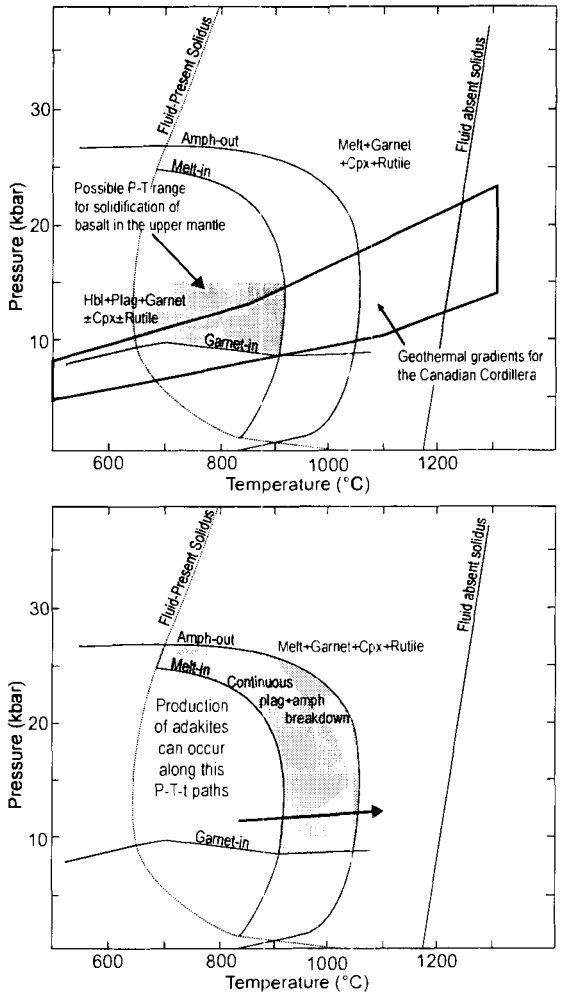

Figure 14: Depiction of important phase relations in the generation of adakites in the lithospheric mantle. Phase relationships are after Vielzeuf and Schmidt (2001), with additions to the hornblende-out curve after Rapp (1995) and Sen and Dunn (1994). A) Region of stability of solid basalt (amphibolite) in P-T space for the upper mantle. The shaded areas are the geothermal gradients for the crust and upper mantle of high-heat flow orogens (after Lewis et al. 2003, as discussed in text). B) Possible P-T-t path that would form adakitic magmas from amphibolite in the upper mantle (arrow).

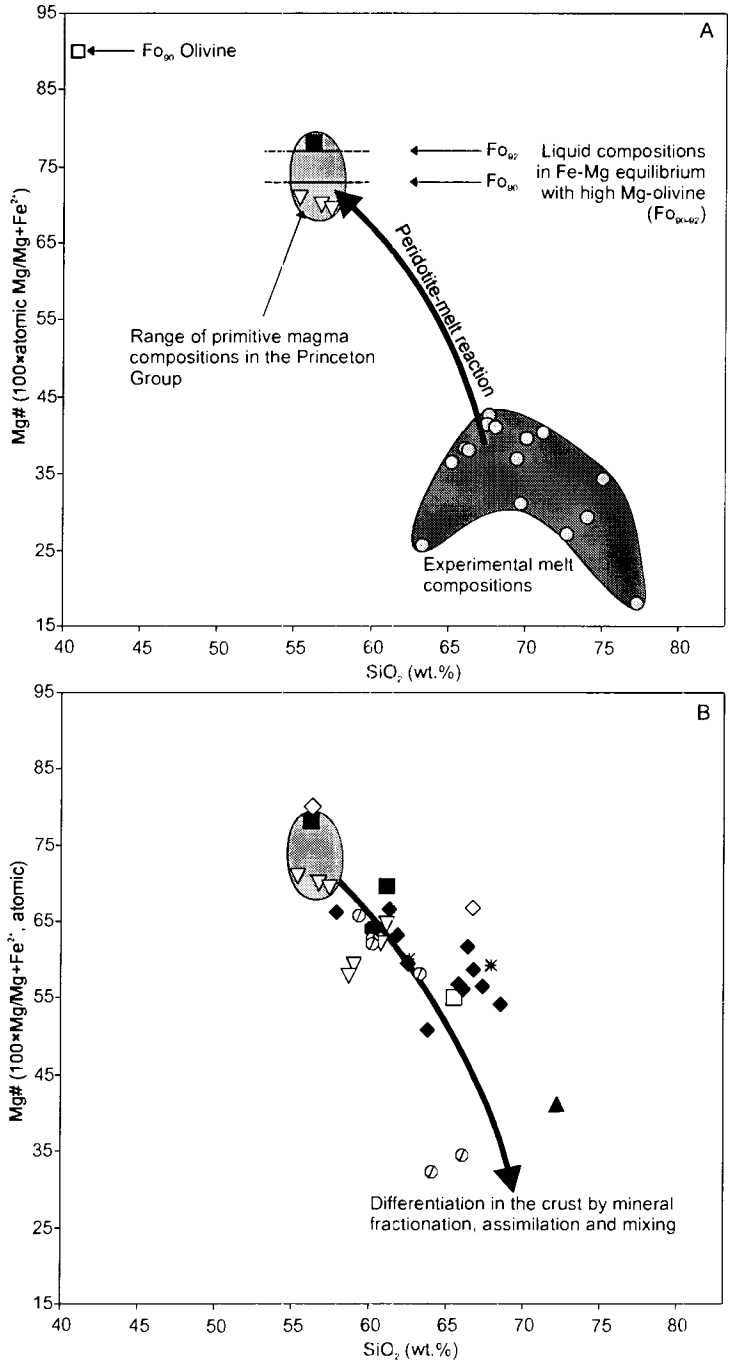

Figure 15: Diagram illustrating the chemical evolution of a silicic partial melt in the mantle. A) A partial melt of garnet amphibolite interacts with peridotite, dissolving olivine and precipitating a small amount of pyroxene (e.g., Rapp et al. 1999; Stern and Kilian 1996). The primary effect is to increase the Mg# of the melt and increase concentrations of compatible elements (e.g., Ni and Cr). The maximum Mg# that the melt can likely reach is defined by Mg-Fe equilibria between high-Mg, mantle olivine and melt (e.g., Roeder and Emslie 1970), shown by horizontal lines. B) Subsequent differentiation of the primitive, mantle equilibrated magma in the crust leads to more evolved compositions of andesite and dacite seen in the Princeton Group. Experimental compositions from Rapp and Watson (1995) and Sen and Dunn (1994).

A second mechanism is subduction erosion (Kay and Kay 2002; von Huene et al. 2004) in which a subducting slab drags ancient arc volcanic rocks from the forearc (for example, rocks presently preserved on Vancouver Island and the Queen Charlotte Islands) into the subduction zone. As proposed by Kay and Kay (2002), these blocks would be dragged by corner flow along with the subducted slab into deeper and hotter parts of the mantle, where they would melt. In this model, however, the melting of entrained blocks would likely be accompanied by partial melting of oceanic crust (with MORB composition), for which there is no geochemical evidence.

In a third mechanism, arc-basalt was emplaced into the lithospheric mantle as dikes and sills during previous intervals of arc magmatism (e.g., Macpherson and Hall 2002; Melcher and Meisel 2004), and that these intrusions were then partially melted during re-heating of the lithospheric mantle in the Eocene. Such intrusions could have originally been emplaced as feeder dykes to the Nicola and Spences Bridge groups. This scenario requires that the temperature of the lithospheric mantle in the Mesozoic was below the wet basalt solidus so that the mafic dykes would completely solidify. The temperature of the lithosphere was probably no hotter than that proposed by Lewis et al. (2003; see also Harder and Russell, in press) for the modern Canadian Cordillera, which is considered to be representative of hot orogenic belts throughout the world (Hyndman et al. 2005). Using their geothermal gradients and a wet basalt solidus of approximately 900 °C (Fig. 14), the temperature of the lithospheric mantle would be cold enough to induce crystallization in dykes of arc basalt at

depths <45 km (Fig. 14). Subsequent heating of the lithospheric mantle would cause partial melting of these dykes, yielding adakitic magmas. These melts would react with the surrounding peridotite and would become increasingly mafic, with higher Mg#, Ni and Cr, and rise into the crust as adakitic high-Mg# andesites (Fig. 16).

The melting of intrusions of LILE- and LREE-enriched arc-basalt that were previously emplaced into the lithospheric mantle is the preferred hypothesis for generating primitive andesites in the Princeton Group. It is difficult to exclude subduction erosion and delamination for the Princeton Group itself, but neither mechanism can explain volcanic activity throughout the entire belt, where a similar age, style, and chemistry of volcanic activity imply a broadly similar trigger. This conclusion is consistent with those of a number of workers who, largely on isotopic grounds, identified the melting of enriched lithospheric mantle in the central and southernmost parts of the Challis-Kamloops belt. These volcanic fields include the Penticton Group (Dostal et al. 2003), the Colville Igneous Complex (Morris et al. 2000), the Challis Group (McKervey 1998), the Absaroka Supergroup (Feeley 2003), the Buck Creek Complex (Dostal et al. 2001), and the Montana Alkalic Province (Dudas 1991). The origin of coeval volcanic rocks to the north, including the Buck Creek Complex, the Endako Group, the Ootsa Lake Group, and the Clisbako volcanics is less clear, although Dostal et al. (2001) suggested that volcanic activity in the Buck Creek complex could have involved anatexis of lithospheric mantle (Fig. 1).

Tectonic Setting of the Princeton Group

Asthenospheric upwelling has been proposed by a number of workers as a trigger for anatexis of lithospheric mantle in the Challis-Kamloops belt, and is herein regarded as the most likely cause of Princeton Group magmatism. The cause of the upwelling is uncertain, but two plate tectonic mechanisms have been proposed. In one, the asthenosphere welled up through a slab window emanating from a ridge-trench intersection somewhere along the Oregon – British Columbia coast (Thorkelson and Taylor 1989; Breitsprecher et al. 2003; Haeussler et al. 2003). A slab window is a slab-free region underneath an overriding plate that develops as a consequence of a ridge-trench intersection (Dickinson and Snyder 1979; Thorkelson 1996; Sisson et al. 2003). The presence of an Eocene slab window underneath British Columbia and the northwestern United States would replace cool, subducted oceanic lithosphere and the refrigerated mantle wedge with hot, sub-slab asthenosphere (Thorkelson 1996; Johnston and Thorkelson 1997). Magnetic anomalies preserved on the sea-floor in the Gulf of Alaska provide evidence for two oceanic plates, the Farallon and the Kula, subducting underneath North America during the early Tertiary. In addition, a growing wealth of onshore geological data seems to require the presence of at least one additional plate in the north Pacific region in the early Tertiary, i.e., the Resurrection plate of Haeussler et al. (2003). Madsen et al. (in press) further demonstrated the need for the Resurrection plate, but argued for its eventual separation into two sub-plates, the more northern of which they named the Eshamy plate. Thus, the most recent plate models show a complex pattern of slab windows among the subducted slabs of the Farallon,

Kula, Resurrection and possibly Eshamy plates beneath the northern Cordillera during the early Tertiary. These complex patterns would have had a large influence of the thermal state of the upper mantle beneath western North America at the time, and contributed to widespread lithospheric heating.

Other workers have proposed an alternative, that magmatism was triggered by breaking off of low-angle or "flat" subducted oceanic lithosphere of the Farallon plate (Humphreys 1995; McKervey 1998; Feeley 2003). Foundering of the broken part of the slab would permit influx of hot asthenosphere, triggering melting in the lithospheric mantle. This model accounts well for the late Tertiary "sweep" of magmatism across the United States (Humphreys 1995), although it has not been explicitly applied to magmatic activity to the north, in Canada. If slab break-off were the cause of the lithospheric heating, then it would have had to occur nearly simultaneously for an along-strike distance of >1000 km, i.e., from beneath the western United States through central British Columbia, implying the existence of a single subducted slab at that time, or the fortuitous tearing-away of more than one plate. As noted earlier, offshore and onshore geological records suggest that at least two additional plates were subducting beneath the region, and that continuity of a single slab beneath that stretch of the Cordillera in Eocene time is unlikely. The preferred tectonic and magmatic processes are illustrated in Fig. 16.

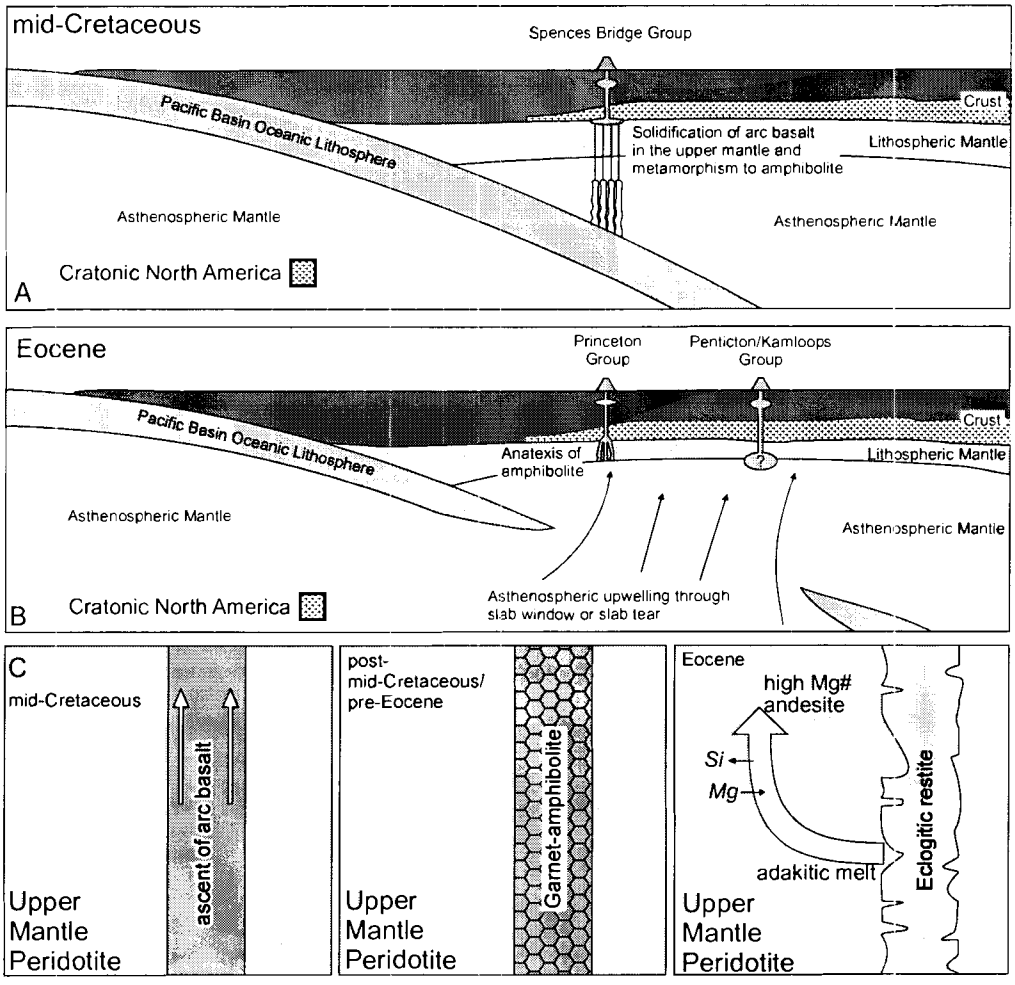

Figure 16: Diagram illustrating the preferred mechanism for the genesis of the Princeton Group and related Challis-Kamloops volcanic fields. A) Arc volcanism in the Mesozoic (Spences Bridge Group represented in this case) emplaces arc basalt in the upper mantle. Dikes from previous episodes of magmatism, for example the Triassic Nicola Group, may already have been emplaced. B) Upwelling of asthenosphere, either through a slab window or a slab tear, heats the lithospheric mantle. In the case of the Princeton Group, heterogeneities of Mesozoic arc basalt in the lithospheric mantle are partially melted, and the resultant adakitic magmas interact with mantle peridotite to form high-Mg# andesite with adakitic trace element signature. Elsewhere in the Challis-Kamloops field, heating is more extensive and along with lithospheric mantle, melting of the asthenosphere is also likely. The approximate location of cratonic North American crust is from Clowes et al. (1995). C) Schematic diagram of the evolution of a hypothetical basaltic dike from inception as a feeder to a Mesozoic arc, to solidifying into amphibolite, to partial melting and reacting with ambient peridotite during the Eocene thermal event.

Conclusions

The Princeton Group of south-central British Columbia is part of the Eocene Challis-Kamloops magmatic belt which extends from northern British Columbia to the western United States. The group consists of calc-alkaline volcanic and terrestrial sedimentary rocks that were deposited in a regime of dextral transtension. The volcanic rocks accumulated as cinder cones and stratovolcanoes, partly within extensional basins. New geochronological results indicate that they were erupted from approximately 53-47 Ma, similar to the interval of magmatism in other Challis-Kamloops successions.

Princeton Group lavas range from basaltic andesite to rhyolite, and differentiated by fractional crystallization with subordinate magma mixing and assimilation. Most have unusually primitive characteristics for rocks with SiO_2> 55 wt. % (including high Mg#, Ni and Cr contents) and are classified as high-Mg# andesites. An adakitic geochemical signature is present at the full range of rock compositions, including the high-Mg# andesites. Major and trace element abundances of the most primitive lavas are consistent with genesis by high-pressure anatexis of metabasalt with arc-like trace element systematics, followed by reaction with mantle peridotite. Melting of a subducted slab with an NMORB composition (a commonly invoked method of producing adakite) is incapable of producing the observed high LILE abundances in the Princeton Group. As well, anatexis of lower crustal rocks of the North American plate is not viable because

the resulting melts would be unable to react with mantle peridotite, and would therefore remain more felsic than the high Mg# andesites of the Princeton Group.

The most likely scenario for the origin of the primitive Princeton Group rocks involves Eocene heating of North American lithospheric mantle containing dykes of arc basalt which were emplaced during an earlier event of arc magmatism. At least two pre-Eocene events of arc magmatism in the area, represented by the Triassic Nicola Group and the Cretaceous Spences Bridge Group, could have contributed to this intrusive event. The most likely cause of lithospheric heating is the upwelling of hot asthenosphere, probably through a geometrically complex set of slab windows that developed as a result of microplate formation along the western margin of North America during the early Tertiary (e.g., Haeussler et al. 2003; Madsen et al. in press). Alternatively, upwelling may have been induced through the break-off and foundering of low-angle subducted lithosphere, or by a combination of the two processes.

Tables

Table 1: Compilation of isotopic dates for the Princeton Group

Age	Method	Material	Location	Lat (N)	Long (W)	Reference
49 ± 3	K-Ar	Hbl	Tulameen	49.50	120.77	C83
52.2 ± 0.8	K-Ar	Bt	Nicola River	50.17	121.05	HR87
49 ± 1	K-Ar	Hbl	North of Flat-Top Mtn.	49.12	120.46	HR87
49.1 ± 0.8	K-Ar	WR	Prospect Creek	50.08	121.15	HR87
49.7 ± 0.8	K-Ar	WR	Cathederal Ridge	49.05	120.21	HR87
49 ± 4	K-Ar	Bt	Tulameen	49.46	120.53	M64
45 ± 3	K-Ar	WR	Placer Creek	49.15	120.53	MaUP
48 ± 3	K-Ar	WR	Placer Creek	49.15	120.53	MaUP
49 ± 3	K-Ar	WR	Placer Creek	49.15	120.54	MaUP
50 ± 3	K-Ar	Bt	Nicola River	50.20	121.03	McUP
49 ± 3	K-Ar	Hbl	Nicola River	50.20	121.03	McUP
50 ± 3	K-Ar	Hbl	North of Merritt	50.23	120.94	McUP
52 ± 4	K-Ar	Hbl	North of Merritt	50.22	120.88	McUP
46 ± 4	K-Ar	Bt	North of Princeton	49.57	120.50	R00
49 ± 4	K-Ar	WR	North of Princeton	49.59	120.48	R00
49 ± 4	K-Ar	WR	Kingsvale	49.96	120.92	TH89
51.5 ± 0.4	$^{40}Ar/^{39}Ar$	Sa	Quilchina	50.13	120.51	VM05
52.08 ± 0.12	U-Pb	Zrc	Princeton	49.46	120.51	AMUP
48	K-Ar	Bt	Tulameen	49.48	120.75	HB67
51	K-Ar	Bt	Princeton	49.40	120.53	HB67
50	K-Ar	Plag	Princeton	49.40	120.53	HB67
51	K-Ar	Plag	Sunday Creek	49.23	120.55	HB67
49	K-Ar	Hbl	Sunday Creek	49.23	120.55	HB67
53	K-Ar	Hbl	Sunday Creek	49.22	120.55	HB67
48	K-Ar	Kfs	Sunday Creek	49.23	120.57	HB67
51	K-Ar	Kfs	Sunday Creek	49.23	120.57	HB67

Notes: C83 = Church (1983); HR87 = Hunt and Roddick (1987); M64 = Mathews (1964); MaUp = W.H. Mathews (unpublished data); WcUP = W.J. McMillan (unpublished data); R00 = Read (2000); TH89 = Thorkelson (1989); VM05 = Villeneuve and Mathewes (2005); AMUP = Archibald and Mortensen (unpublished data); HB67 = Hills and Baadsgaard (1967)

Unpublished data of W.H. Mathews and W.J. McMillan are compiled in Breitsprecher and Mortensen (2004) from lab sheets at the Geochronology Facility in the Department of Earth and Ocean Sciences, University of British Columbia.

All uncertainties reported at 2 σ confidence limits.

Where appropriate, dates have been recalculated using the decay constants of Steiger and Jager (1977).

Abbreviations: Hbl = hornblende; Bt = biotite; WR = whole rock; Sa = sanidine; Zrc = zircon; Plag = plagioclase; Kfs = K-feldspar

Table 2: $^{40}Ar/^{39}Ar$ results for volcanic rocks from the Princeton Group

				Plateau				Inverse Isochron			Total Fusion
Sample ID	Location	Rock type	Material	Date (Ma)	MSWD	Probability	^{39}Ar in plateau	Date (Ma)	MSWD	$^{40}Ar/^{36}Ar_i$	Date (Ma)
RBI-04-16-14-1B	Agate Mtn.	basaltic-andesite	Gm	54.6 ± 0.8	2.2	0.07	64%	*52 ± 2	1.4	428 ± 36	57 ± 1
RBI-04-24-6-1B	Friday Creek	dacite	Hbl	*52 ± 1	0.8	0.55	94%	53 ± 3	0.82	285 ± 28	50 ± 2
RBI-04-34-2-1	Lower Nicola	andesite	Hbl	*49 ± 1	0.37	0.95	100%	50 ± 2	0.35	291 ± 12	48 ± 2
RBI-04-35-3-1	Fig Lake	dacite	Hbl	*50.3 ± 0.9	0.74	0.69	100%	50 ± 1	0.79	297 ± 8	50 ± 2
RBI-04-36-1-1	Boss Lake	rhyolite	WR	*50.2 ± 0.4	0.97	0.47	90%	50 ± 1	1.02	307 ± 26	50.2 ± 0.4

Notes: All uncertainties at 2σ confidence limits.

Abbreviations: Gm = groundmass; Hbl = hornblende; WR = whole rock

** interpreted as best estimate of crystallization age*

Table 3: Major element oxide (wt.%) and trace element (ppm) concentrations of volcanic rocks from the Princeton Group

Sample	*RBI-04 15-10-1*	*RBI-04 15-12-1*	*RBI-04 15-13-1*	*RBI-04 16-14-1*	*RBI-04 16-17-1*	*RBI-04 12-1-1*	*RBI-04 17-3-1*	*RBI-04 36-1-1*	*RBI-04 23-3-1*	*RBI-04 24-6-1*	*RBI-04 25-1-1*	*RBI-04 34-2-1*	*RBI-04 39-1-1*	*RBI-04 37-5-1*
Locality	*AgM*	*AgM*	*AgM*	*AgM*	*AgM*	*AgM*	*AgM*	*BL*	*SC*	*SC*	*Tul*	*Mer*	*Pr*	*PC*
Rock-type	*t. and*	*and*	*and*	*b. and*	*and*	*t. and*	*b.t. and*	*rhy*	*dac*	*dac*	*and*	*and*	*dac*	*and*
SiO_2	61.09	59.04	58.74	56.74	60.80	57.41	55.39	72.27	66.10	63.35	60.20	62.65	65.55	61.08
Al_2O_3	15.78	16.24	16.68	15.61	15.87	14.95	14.68	14.73	17.36	16.28	15.69	16.68	15.55	15.69
FeO^T	5.02	5.55	6.58	6.46	5.47	6.16	7.05	2.00	3.60	5.04	5.65	4.87	4.25	5.15
MnO	0.07	0.23	0.13	0.11	0.06	0.10	0.11	0.03	0.04	0.06	0.10	0.05	0.05	0.09
MgO	4.09	3.60	4.00	6.70	4.00	6.22	7.62	0.62	0.84	3.08	4.43	3.22	2.29	5.22
CaO	6.14	8.56	7.13	7.98	6.41	7.62	7.94	2.31	4.22	5.23	7.36	5.28	4.23	6.01
Na_2O	4.43	4.15	4.05	3.86	4.18	4.13	4.00	4.09	4.85	4.18	4.39	4.20	4.58	3.84
K_2O	2.31	1.55	1.48	1.44	2.17	2.08	1.61	3.53	2.23	1.79	1.05	2.23	2.44	2.12
TiO_2	0.73	0.81	0.88	0.82	0.75	0.81	1.15	0.31	0.47	0.71	0.77	0.63	0.77	0.60
P_2O_5	0.34	0.27	0.32	0.27	0.29	0.53	0.45	0.11	0.29	0.27	0.35	0.20	0.28	0.19
LOI	0.96	3.26	3.69	1.92	2.10	1.40	2.23	0.70	2.62	2.88	2.55	2.97	2.13	1.45
Total	99.23	99.63	98.78	99.59	99.09	98.54	98.88	99.84	99.14	98.86	99.27	99.07	98.65	99.47
Cu	25	53	44	48	36	101	61	53	11	26	56	46	69	65
Ni	93	141	167	181	117	171	179	5	2	12	92	52	58	112
Pb	24	8	4	7	20	12	11	15	9	10	7	8	12	5
Ba	1468	960	800	690	1242	1168	1033	1402	1045	746	900	877	1073	872
Sr	1731	969	1022	985	1455	1742	1419	411	980	588	1312	867	787	802
Zr	125	101	97	93	117	125	144	141	128	98	106	84	144	100
	11	11	12	11	10	12	15	6	10	14	11	9	8	10
V	124	144	155	146	130	134	152	32	61	124	126	100	84	122
Co	21.8	28.6	33.0	35.8	23.7	30.5	35.3	6.8	10.1	20.4	30.6	19.4	17.3	29.8
Cr	146	376	419	405	226	302	423	26	7	35	250	91	105	255
Mo	15	9	14	9	13	22	17	bd	16	10	10	bd	bd	bd

Table 3: Major element oxide (wt.%) and trace element (ppm) concentrations of volcanic rocks from the Princeton Group continued

Sample	RBI-04 37-8-2	RBI-04 19-3-1	RBI-04 20-3-2	RBI-04 21-2-1	RBI-04 21-3-1	RBI-04 22-1-1	RBI-04 30-2-1	RBI-04 31-1-1	RBI-04 31-1-2	RBI-04 32-2-1	DM-04 18-1-1	RBI-05 02-2-1	
Locality	PC	FT/P	FT/P	FT/P	FT/P	FT/P	FT/P	FT/P	FT/P	FT/P	FT/P	FT/P	
Rock-type	b.and	and	dac	dac	and	dac	t.and	dac	dac	dac	dac	t.and	2σ error
SiO_2	56.23	62.55	66.15	63.75	61.85	66.77	61.37	68.50	66.42	67.35	65.76	57.84	0.4
Al_2O_3	15.25	16.85	15.54	16.99	15.69	15.51	15.01	15.72	15.75	15.78	15.82	16.60	0.1
FeO^T	6.08	4.64	3.96	4.55	4.94	3.65	4.84	2.88	3.81	3.31	3.94	5.83	0.04
MnO	0.11	0.08	0.05	0.08	0.09	0.07	0.08	0.02	0.04	0.04	0.07	0.06	0.001
MgO	9.50	3.00	2.22	2.07	3.74	2.27	4.27	1.49	2.70	1.88	2.27	5.03	0.04
CaO	7.54	5.28	4.32	5.17	6.45	4.06	6.07	3.47	4.19	3.83	5.03	6.56	0.06
Na_2O	3.14	4.52	4.45	4.54	4.05	4.52	4.51	4.65	4.38	4.58	4.38	4.67	0.04
K_2O	1.24	2.16	2.46	2.04	2.23	2.41	2.68	2.65	2.00	2.52	1.96	1.95	0.02
TiO_2	0.75	0.66	0.62	0.53	0.70	0.56	0.63	0.47	0.54	0.53	0.56	0.89	0.01
P_2O_5	0.16	0.25	0.24	0.27	0.26	0.17	0.54	0.15	0.18	0.18	0.21	0.58	0.06
LOI	1.89	1.98	1.83	1.11	3.41	1.35	1.43	1.47	2.20	1.29	2.55	1.82	-
Total	98.65	98.79	99.90	99.02	99.74	99.43	99.14	100.33	99.68	99.58	99.03	99.86	-
Cu	71	36	61	15	45	56	11	53	31	48	24	35	2
Ni	239	31	28	19	60	33	53	15	25	19	20	66	2
Pb	5	3	8	bd	10	4	18	6	bd	bd	16	28	4
Ba	485	1123	1081	967	892	976	1974	1106	829	1025	849	1585	14
Sr	704	1053	675	910	794	629	1991	651	680	670	754	2020	9
Zr	85	120	125	118	102	116	122	137	96	142	86	123	4
Y	12	10	9	11	10	8	14	8	8	8	10	17.2	0.8
V	150	106	95	85	125	85	99	71	85	82	90	144	2
Co	47.1	18.9	15.3	13.5	23.2	15.1	22.4	11.1	16.3	13.8	13.5	20.7	1
Cr	663	38	93	38	157	107	106	45	78	56	88	160	4
Mo	2	bd	7	10	14	7	30	5	8	12	bd	bd	6

Table 3: Major element oxide (wt.%) and trace element (ppm) concentrations of volcanic rocks from the Princeton Group continued

Sample	RBI-04 15-10-1	RBI-04 15-12-1	RBI-04 15-13-1	RBI-04 16-14-1	RBI-04 16-17-1	RBI-04 12-1-1	RBI-04 17-3-1	RBI-04 36-1-1	RBI-04 23-3-1	RBI-04 24-6-1	RBI-04 25-1-1	RBI-04 34-2-1	RBI-04 39-1-1	RBI-04 37-5-1
Locality	AgM	AgM	AgM	AgM	AgM	AgM	AgM	BL	SC	SC	Tul	Mer	Pr	PC
Rock-type	t. and	and	and	b. and	and	t. and	b.t. and	rhy	dac	dac	and	and	dac	and
Sc	13.1	19.4	20.5	20.5	15.8	18.1	21.9	4.7	4.6	15.2	15.5	14.5	11.2	19.4
Nb	3.9	3.0	3.0	2.8	3.1	5.6	5.4	4.4	4.0	3.3	3.3	1.9	3.5	2.3
Cs	0.5	0.9	0.8	0.2	0.6	0.6	bd	2.8	0.7	0.8	3.3	0.9	0.8	0.9
La	26.2	17.3	18.4	17.7	22.8	36.5	41.0	21.8	25.9	15.4	23.6	14.9	24.5	16.5
Ce	55.7	37.0	40.2	38.3	49.0	76.2	83.7	40.4	49.6	31.8	52.0	30.9	49.1	33.9
Pr	7.35	4.88	5.22	5.00	6.42	9.83	10.2	4.36	5.83	3.92	6.56	3.93	5.80	4.24
Nd	30.6	20.8	22.5	21.3	26.8	40.0	40.0	15.5	22.1	16.1	27.3	16.5	22.8	16.9
Sm	6.49	4.39	4.77	4.53	5.62	7.52	7.60	2.86	3.96	3.60	5.33	3.44	4.30	3.43
Eu	1.65	1.27	1.35	1.30	1.51	1.98	1.97	0.647	1.06	1.04	1.39	0.938	1.20	0.974
Gd	4.44	3.37	3.47	3.45	4.09	4.87	5.42	1.81	2.75	3.08	3.65	2.56	2.95	2.57
Tb	0.52	0.45	0.50	0.47	0.52	0.60	0.70	0.24	0.39	0.50	0.49	0.38	0.44	0.39
Dy	2.34	2.23	2.24	2.28	2.23	2.54	3.03	1.07	1.88	2.57	2.19	1.82	1.83	1.83
Ho	0.38	0.41	0.40	0.39	0.39	0.42	0.52	0.17	0.34	0.50	0.36	0.32	0.30	0.33
Er	1.06	1.10	1.07	1.16	1.09	1.14	1.50	0.48	1.07	1.59	1.01	0.95	0.91	0.99
Tm	0.151	0.168	0.159	0.165	0.157	0.159	0.211	0.067	0.152	0.237	0.142	0.144	0.127	0.143
Yb	0.94	1.00	1.06	1.09	1.06	1.05	1.34	0.44	1.10	1.46	0.94	0.87	0.76	0.99
Lu	0.15	0.15	0.15	0.15	0.15	0.15	0.19	0.06	0.15	0.21	0.13	0.13	0.10	0.14
Hf	3.5	2.7	2.6	2.4	3.2	3.0	3.6	3.8	3.4	2.9	3.7	2.4	3.9	2.8
Ta	0.19	0.17	0.17	0.16	0.19	0.21	0.26	0.45	0.25	0.19	0.18	0.13	0.21	0.13
Th	4.30	2.20	2.35	2.27	4.11	3.63	3.56	8.01	4.46	2.74	2.74	3.10	4.97	3.31
U	3.27	1.06	0.92	0.89	3.02	1.32	0.93	3.71	1.57	1.24	1.10	1.42	1.77	1.52

Table 3: Major element oxide (wt.%) and trace element (ppm) concentrations of volcanic rocks from the Princeton Group continued

Sample	RBI-04 37-8-2	RBI-04 19-3-1	RBI-04 20-3-2	RBI-04 21-2-1	RBI-04 21-3-1	RBI-04 22-1-1	RBI-04 30-2-1	RBI-04 31-1-1	RBI-04 31-1-2	RBI-04 32-2-1	DM-04 18-1-1	RBI-05 02-2-1	
Locality	PC	FT/P	FT/P	FT/P	FT/P	FT/P	FT/P	FT/P	FT/P	FT/P	FT/P	FT/P	
Rock-type	b.and	and	dac	dac	and	dac	t.and	dac	dac	dac	dac	t.and	2σ error
Sc	29.9	13.0	11.7	9.2	15.3	10.2	11.9	7.8	11.1	8.8	12.1	nd	0.4
Nb	2.9	4.2	2.3	3.2	3.1	2.2	14.5	3.4	2.8	2.5	2.6	11	0.2
Cs	0.8	1.1	0.8	1.0	0.5	0.8	0.9	0.9	0.8	0.9	0.9	0.5	0.2
La	12.1	23.9	22.0	19.6	20.1	17.4	93.2	24.3	14.2	22.0	12.7	69.3	0.6
Ce	26.4	47.6	39.0	37.7	40.6	36.1	174	45.2	28.4	42.0	25.8	137	1.2
Pr	3.40	5.73	5.22	4.68	5.04	4.24	19.2	5.04	3.55	4.84	3.27	16	0.1
Nd	14.6	22.1	20.3	18.4	20.5	16.6	71.0	18.7	14.8	18.4	13.5	60.9	0.6
Sm	3.32	4.24	4.11	3.61	4.21	3.37	11.3	3.32	3.07	3.52	2.99	9.8	0.2
Eu	1.01	1.15	1.05	0.985	1.09	0.882	2.59	0.807	0.818	0.887	0.844	2.2	0.06
Gd	2.70	3.09	2.95	2.88	3.13	2.43	5.98	2.18	2.32	2.35	2.28	7.3	0.1
Tb	0.44	0.41	0.41	0.43	0.43	0.33	0.73	0.30	0.36	0.32	0.37	0.8	0.02
Dy	2.36	2.02	1.89	2.11	2.10	1.64	2.90	1.40	1.70	1.47	1.71	3.4	0.08
Ho	0.44	0.37	0.32	0.39	0.37	0.29	0.47	0.24	0.29	0.25	0.31	0.6	0.02
Er	1.32	1.07	0.93	1.23	1.09	0.86	1.31	0.73	0.87	0.75	0.91	1.8	0.04
Tm	0.192	0.153	0.135	0.193	0.168	0.123	0.181	0.105	0.127	0.109	0.130	0.2	0.004
Yb	1.22	1.02	0.84	1.25	1.04	0.72	1.14	0.67	0.77	0.67	0.85	1.4	0.04
Lu	0.18	0.16	0.13	0.21	0.16	0.11	0.16	0.11	0.11	0.10	0.12	0.20	0.06
Hf	2.2	3.2	3.3	3.1	3.0	3.2	3.3	3.7	2.7	3.7	2.6	4	0.1
Ta	0.19	0.28	0.16	0.21	0.20	0.16	0.53	0.21	0.18	0.16	0.18	bd	0.04
Th	1.82	4.08	5.36	3.98	3.93	4.94	9.07	6.56	3.05	5.96	2.37	7	0.08
U (ppm)	0.86	1.71	2.08	1.68	1.62	1.98	2.38	2.34	1.39	2.13	1.21	2	0.02

Abbreviations: AgM: Agate Mountain; BL=Boss Lake; SC=Sunday Creek; Tul=Tulameen; Mer=Merritt; Pr=Princeton; PC=Prospect Creek; FT/P=Flat Top Mountain and Placer Mountain; t.and=trachyandesite; and=andesite; b.and=basaltic andesite; b.t.and=basaltic trachyandesite; rhy=rhyolite; dac=dacite; nd=no data; bd=below detection

Notes: Major elements (wt.% oxides) are normalized to 100% on an anhydrous basis. Errors are presented as two standard deviations.

Table 4: Nd isotopic compositions for volcanic rocks of the Princeton Group

Sample	Unit	Rock Type	Sm/Nd	$^{143}Nd/^{144}Nd_m$	$^{147}Sm/^{144}Nd$	$^{143}Nd/^{144}Nd_{50}$	εNd_{50}	$F_{Sm/Nd}$	T_{DM}
RBI-04-15-10-1	Agate Mountain	Trachyandesite	0.212 ± 0.007	0.512896 ± 7	0.1284	0.512854 ± 4	5.5 ± 0.1	-0.35	453
RBI-04-16-14-1	Agate Mountain	Basaltic andesite	0.21 ± 0.01	0.512899 ± 10	0.1277	0.512857 ± 5	5.5 ± 0.2	-0.35	444
RBI-04-36-1-1	Boss Lake	Rhyolite	0.19 ± 0.01	0.5129140 ± 7	0.1131	0.512877 ± 2	5.9 ± 0.1	-0.42	358
RBI-04-23-3-1	Friday Creek	Dacite	0.18 ± 0.01	0.512760 ± 4	0.1094	0.512724 ± 2	2.9 ± 0.1	-0.44	569
RBI-04-37-8-2	Prospect Creek	Basaltic andesite	0.23 ± 0.02	0.512945 ± 6	0.1367	0.512900 ± 4	6.4 ± 0.1	-0.30	405
RBI-04-31-1-1	Flat-Top Mountain	Dacite	0.18 ± 0.01	0.512847 ± 8	0.1067	0.512812 ± 4	4.7 ± 0.2	-0.46	431
DM-04-18-1-1	Flat-Top Mountain	Dacite	0.22 ± 0.02	0.512867 ± 6	0.1344	0.512823 ± 4	4.9 ± 0.1	-0.32	542
DM-04-18-1-1*	Flat-Top Mountain	Dacite	0.22 ± 0.02	0.512875 ± 6	0.1343	0.512831 ± 4	5.0 ± 0.1	-0.32	527

Notes: All uncertainties reported at 2 σ. Sm-Nd ratio from Table 4. εNd_{50} is the per 10000 variation at 50 Ma from a chondritic reservoir with present-day $^{147}Sm/^{144}Nd = 0.1966$ and $^{143}Nd/^{144}Nd = 0.512638$. $F_{Sm/Nd}$ is the Sm/Nd fractionation relative to a chondritic reservoir. T_{DM} is the model age, in Ma for extraction from a depleted mantle-type reservoir using the model of Goldstein et al. (1984).

* = duplicate sample

Reference List

Amelin, Y. and Rotenberg, E., 2004. Sm-Nd systematics of chondrites. Earth and Planetary Science Letters, 223(3-4): 267-282.

Arndt, N. T. and Goldstein, S. L., 1987. Use and abuse of crust-formation ages. Geology, 15(10): 893-895.

Atherton, M. P. and Petford, N., 1993. Generation of sodium-rich magmas from newly underplated basaltic crust. Nature, 362(6416): 144-146.

Bardoux, 1993. The Okanagan Valley normal fault from Penticton to Enderby, south-central British Columbia. PhD Thesis, Carleton University, Ottawa, 292 pp.

Barker, F., 1979. Trondhjemite: definition, environment and hypotheses of origin. In: F. Barker (Editor), Trondhjemites, Dacites, and Related Rocks. Elsevier, New York, pp. 1-12.

Barth, M. G., Foley, S. F. and Horn, I., 2002. Partial melting in Archean subduction zones: constraints from experimentally determined trace element partition coefficients between eclogitic minerals and tonalitic melts under upper mantle conditions. Precambrian Research, 113(3-4): 323-340.

Beard, J. S. and Lofgren, G. E., 1991. Dehydration melting and water-saturated melting of basaltic and andesitic greenstones and amphibolites at 1, 3, and 6.9 kb. Journal of Petrology, 32(2): 365-401.

Bedard, J. H., 2005. Partitioning coefficients between olivine and silicate melts. Lithos, 83(3-4): 394-419.

Berger, B. R. and Snee, L. W., 1992. Thermochronological constraints on mylonite and detachment fault development, Kettle Highlands, northeastern Washington and southern British Columbia., Geological Society of America, Abstracts with Programs, pp. 65.

Breitsprecher, K., 2002. Volcanic stratigraphy, petrology and tectonic setting of the eastern margin of the Eocene Kamloops Group, south-central British Columbia. M.Sc. Thesis, Simon Fraser University, Burnaby, 221 pp.

Breitsprecher, K., Thorkelson, D. J., Groome, W. G. and Dostal, J., 2003. Geochemical confirmation of the Kula-Farallon slab window beneath the Pacific Northwest in Eocene time. Geology, 31(4): 351-354.

Brenan, J. M., Shaw, H. F., Ryerson, F. J. and Phinney, D. L., 1995. Experimental determination of trace-element partitioning between pargasite and a synthetic hydrous andesitic melt. Earth and Planetary Science Letters, 135(1-4): 1-11.

Burchfiel, B. C., 1993. Tectonostratigraphic map of the Cordileran orogenic belt: contimerinous United States. Geological Society of America.

Camsell, C., 1913. Geology and mineral deposits of the Tulameen District, B.C. Geological Survey of Canada Memoir 26, pp. 188.

Canil, D., 2004. Mildly incompatible elements in peridotites and the origins of mantle lithosphere. Lithos, 77(1-4): 375-393.

Carlson, D. H., Fleck, R., Moye, F. J. and Fox, K. F., 1991. Geology, geochemistry, and isotopic character of the Colville Igneous Complex, northeastern Washington. Journal of Geophysical Research-Solid Earth and Planets, 96(B8): 13313-13333.

Church, B. N., 1973. Geology of the White Lake Basin. In: Bulletin 61 Department of Mines and Petroleum Resources (Editor), pp. 115.

Church, B. N., 1979. Tertiary stratigraphy and resource potential in south-central British Columbia (82E, L). In: Mines and Petroleum Resources British Columbia Ministry of Energy, Geological Fieldwork 1978, Paper 1979-1 (Editor), pp. 7-15.

Church, B. N. and Suesser, U., 1983. Geology and magnetostratigraphy of Miocene basalts of the Okanagan Highlands, British Columbia (82L/2,3). In: Mines and Petroleum Resources British Columbia Ministry of Energy, Geological Fieldwork 1982, Paper 1983-1 (Editor), pp. 32-36.

Clemens, J. D. and Vielzeuf, D., 1987. Constraints on melting and magma production in the crust. Earth and Planetary Science Letters, 86(2-4): 287-306.

Clowes, R. M., Zelt, C. A., Amor, J. R. and Ellis, R. M., 1995. Lithospheric structure in the southern Canadian Cordillera from a network of seismic refraction lines. Canadian Journal of Earth Sciences, 32(10): 1485-&.

De Paolo, D. J., 1981a. Neodymium isotopes in the Colorado Front Range and crust-mantle evolution in the Proterozoic. Nature, 291(5812): 193-196.

De Paolo, D. J., 1981b. Trace-element and isotopic effects of combined wallrock assimilation and fractional crystallization. Earth and Planetary Science Letters, 53(2): 189-202.

Defant, M. J. and Kepezhinskas, P., 2001. Evidence suggests slab melting in arc magmas. EOS (Transactions, American Geophysical Union), 82: 65-69.

Defant, Marc J. and Drummond, Mark S., 1990. Derivation of some modern arc magmas by melting of young subducted lithosphere. Nature, 347(6294): 662-665.

Dickinson, W. R., 1991. Tectonic setting of faulted Tertiary strata associated with the Catalina core complex in southern Arizona; GSA Special paper 264. Geological Society of America, 106 pp.

Dickinson, W. R., 2004. Evolution of the North American Cordillera. Annual Review of Earth and Planetary Sciences, 32: 13-45.

Dickinson, W. R. and Snyder, W. S., 1979. Geometry of triple junctions related to San Andreas transform. Journal of Geophysical Research, 84(NB2): 561-572.

Dostal, J., Breitsprecher, K., Church, B. N., Thorkelson, D. and Hamilton, T. S., 2003. Eocene melting of Precambrian lithospheric mantle: Analcime-bearing volcanic rocks from the Challis-Kamloops belt of south central British Columbia. Journal of Volcanology and Geothermal Research, 126(3-4): 303-326.

Dostal, J., Church, B. N., Reynolds, P. H. and Hopkinson, L., 2001. Eocene volcanism in the Buck Creek basin, central British Columbia (Canada): transition from arc to extensional volcanism. Journal of Volcanology and Geothermal Research, 107(1-3): 149-170.

Dostal, J., Owen, J. V., Church, B. N. and Hamilton, T. S., 2005. Episodic volcanism in the Buck Creek complex (Central British Columbia, Canada): A history of magmatism and mantle evolution from the Jurassic to the early Tertiary. International Geology Review, 47(6): 551-572.

Drummond, M. S. and Defant, M. J., 1990. A model for trondhjemite-tonalite-dacite genesis and crustal growth via slab melting - Archean to modern comparisons. Journal of Geophysical Research, 95(B13): 21503-21521.

Dudas, F. O., 1991. Geochemistry of igneous rocks from the Crazy Mountains, Montana, and tectonic models for the Montana Alkalic Province. Journal of Geophysical Research, 96(B8): 13261-13277.

Eisele, Jurgen, Sharma, Mukul, Galer, Stephen J. G., Blichert-Toft, Janne, Devey, Colin W. and Hofmann, Albrecht W., 2002. The role of sediment recycling in EM-1 inferred from Os, Pb, Hf, Nd, Sr isotope and trace element systematics of the Pitcairn hotspot. Earth and Planetary Science Letters, 196-212(3-4): 197.

Ewing, Thomas E., 1980. Paleogene tectonic evolution of the Pacific Northwest. The Journal of Geology, 88(6): 619-638.

Ewing, Thomas E., 1981a. Petrology and geochemistry of the Kamloops Group, British Columbia. Canadian Journal of Earth Sciences, 18: 1478-1491.

Ewing, Thomas E., 1981b. Regional stratigraphy and structural setting of the Kamloops Group, south-central British Columbia. Canadian Journal of Earth Sciences, 18: 1464-1477.

Feeley, T. C., 2003. Origin and tectonic implications of across-strike geochemical variations in the Eocene Absaroka volcanic province, United States. Journal of Geology, 111(3): 329-346.

Feeley, T. C. and Cosca, M. A., 2003. Time vs. composition trends of magmatism at Sunlight volcano, Absaroka volcanic province, Wyoming. Geological Society of America Bulletin, 115(6): 714-728.

Feeley, T. C., Cosca, M. A. and Lindsay, C. R., 2002. Petrogenesis and implications of calc-alkaline cryptic hybrid magmas from Washburn volcano, Absaroka Volcanic Province, USA. Journal of Petrology, 43(4): 663-703.

Feeley, T. C. and Hacker, M. D., 1995. Intracrustal derivation of Na-rich andesitic and dacitic magmas - an example from Volcan Ollague, Andean Central Volcanic Zone. Journal of Geology, 103(2): 213-225.

Foley, S. F., Barth, M. G. and Jenner, G. A., 2000. Rutile/melt partition coefficients for trace elements and an assessment of the influence of rutile on the trace element characteristics of subduction zone magmas. Geochimica et Cosmochimica Acta, 64(5): 933-938.

Gao, S., Rudnick, R. L., Yuan, H. L., Liu, X. M., Liu, Y. S., Xu, W. L., Ling, W. L., Ayers, J., Wang, X. C. and Wang, Q. H., 2004. Recycling lower continental crust in the North China craton. Nature, 432(7019): 892-897.

Garrison, J. M. and Davidson, J. P., 2003. Dubious case for slab melting in the Northern volcanic zone of the Andes. Geology, 31(6): 565-568.

Ghosh, D. K., 1995. Nd-Sr isotopic constraints on the interactions of the Intermontane Superterrane with the western edge of North America in the southern Canadian Cordillera. Canadian Journal of Earth Sciences, 32(10): 1740-1758.

Gill, J., 1981. Orogenic andesites and plate tectonics. Springer, Berlin, 336 pp.

Goldstein, S. L., Onions, R. K. and Hamilton, P. J., 1984. A Sm-Nd isotopic study of atmospheric dusts and particulates from major river systems. Earth and Planetary Science Letters, 70(2): 221-236.

Grainger, N., 2000. Petrogenesis of Middle Jurassic to Miocene magmatism within the Nechako plateau, central British Columbia: Insight from petrography, geochemistry, geochronology and tracer isotope studies. M.Sc. Thesis, University of Alberta, 125 pp.

Grainger, N. C., Villeneuve, M. E., Heaman, L. M. and Anderson, R. G., 2001. New U-Pb and Ar/Ar isotopic age constraints on the timing of Eocene magmatism, Fort Fraser and Nechako River map areas, central British Columbia. Canadian Journal of Earth Sciences, 38(4): 679-696.

Grove, T. L., Parman, S. W., Bowring, S. A., Price, R. C. and Baker, M. B., 2002. The role of an H_2O-rich fluid component in the generation of primitive basaltic andesites and andesites from the Mt. Shasta region, N California. Contributions to Mineralogy and Petrology, 142(4): 375-396.

Haeussler, P. J., Bradley, D. C., Wells, R. E. and Miller, M. L., 2003. Life and death of the Resurrection plate: Evidence for its existence and subduction in the northeastern Pacific in Paleocene-Eocene time. Geological Society of America Bulletin, 115(7): 867-880.

Harder, Margaret and Russell, J. K., in press. Thermal state of the upper mantle beneath the Northern Cordilleran Volcanic Province (NCVP), British Columbia, Canada. Lithos.

Hills, L. V. and Baadsgaard, H., 1967. Potassium-argon dating of some Lower Tertiary strata in British Columbia. Bulletin of Canadian Petroleum Geology, 15: 138-149.

Hilyard, M., Nielsen, R. L., Beard, J. S., Patino Douce, Alberto E. and Blencoe, J., 2000. Experimental determination of the partitioning behavior of rare earth and high field strength elements between pargasitic amphibole and natural silicate melts. Geochimica et Cosmochimica Acta, 64(6): 1103-1120.

Hiza, Margaret, 1999. The geochemistry and geochronology of the Eocene Absaroka volcanic province, northern Wyoming and southwest Montana, United States of America. PhD Thesis, Oregon State University, 243 pp.

Hofmann, A. W., 2003. Sampling mantle heterogeneity through oceanic basalts: isotopes and trace elements. In: Roberta L. Rudnick (Editor), The Crust. Treatise on Geochemistry. Elsevier, pp. 64-101.

Humphreys, E. D., 1995. Post-Laramide removal of the Farallon slab, western United-States. Geology, 23(11): 987-990.

Hunt, P. A. and Roddick, J. C., 1990. A compilation of K-Ar ages: report 19. Radiogenic Age and Isotopic Studies: Report 3. Paper 87-2, Geological Survey of Canada Paper 89-2.

Hyndman, R. D., Currie, Claire A. and Mazzotti, Stephane P., 2005. Subduction zone backarcs mobile belts, and orogenic heat. GSA Today, 15(2): 4-10.

Irvine, T. N. and Baragar, W. R. A., 1971. Guide to chemical classification of common volcanic rocks. Canadian Journal of Earth Sciences, 8(5): 523-&.

Jacobsen, S. B. and Wasserburg, G. J., 1980. Sm-Nd isotopic evolution of chondrites. Earth and Planetary Science Letters, 50(1): 139-155.

Janecke, S. U., Hammond, B. F., Snee, L. W. and Geissman, J. W., 1997. Rapid extension in an Eocene volcanic arc: Structure and paleogeography of an intra-arc half graben in central Idaho. Geological Society of America Bulletin, 109(3): 253-267.

Janecke, S. U. and Snee, L. W., 1993. Timing and episodicity of Middle Eocene volcanism and onset of conglomerate deposition, Idaho. Journal of Geology, 101(5): 603-621.

Johnston, S. T. and Thorkelson, D. J., 1997. Cocos-Nazca slab window beneath Central America. Earth and Planetary Science Letters, 146(3-4): 465-474.

Jull, M. and Kelemen, P. B., 2001. On the conditions for lower crustal convective instability. Journal of Geophysical Research, 106(B4): 6423-6446.

Kay, R. W., 1978. Aleutian magnesian andesites: Melts from subducted Pacific Ocean crust. Journal of Volcanology and Geothermal Research, 4: 497-522.

Kay, R. W. and Kay, S. M., 1993. Delamination and delamination magmatism. Tectonophysics, 219(1-3): 177-189.

Kay, R. W. and Kay, S. M., 2002. Andean adakites: three ways to make them. Acta Petrologica Sinica, 18(3): 303-311.

Kelemen, P. B., 1995. Genesis of high Mg-number andesites and the continental-crust. Contributions to Mineralogy and Petrology, 120(1): 1-19.

Kelemen, P. B., Hanghoj, K. and Greene, A. R., 2003. One view of the geochemistry of subduction-related magmatic arcs, with an emphasis on primitive andesite and lower crust. In: Roberta L. Rudnick (Editor), The Crust. Treatise on Geochemistry. Elsevier, pp. 594-649.

Klemme, Stephan, Blundy, Jonathan D. and Wood, Bernard J., 2002. Experimental constraints on major and trace element partitioning during partial melting of eclogite. Geochimica et Cosmochimica Acta, 66(17): 3109-3123.

Le Maitre, R. W. (Editor), 2002. Igneous Rocks, A Classification and Glossary of Terms. Cambridge University Press, Cambridge, 236 pp.

Lewis, T. J., Hyndman, R. D. and Fluck, P., 2003. Heat flow, heat generation, and crustal temperatures in the northern Canadian Cordillera: Thermal control of tectonics. Journal of Geophysical Research, 108(B6).

Lindsay, C. R. and Feeley, T. C., 2003. Magmagenesis at the Eocene Electric Peak-Sepulcher Mountain complex, Absaroka Volcanic Province, USA. Lithos, 67(1-2): 53-76.

Lopez, S. and Castro, A., 2001. Determination of the fluid-absent solidus and supersolidus phase relationships of MORB-derived amphibolites in the range 4-14 kbar. American Mineralogist, 86(11-12): 1396-1403.

Ludwig, K. R., 2003. Isoplot 3.09 A Geochronological toolkit for Microsoft Excel., Berkeley Geochronology Center. Special Publication No. 4.

Lustrino, M., 2005. How the delamination and detachment of lower crust can influence basaltic magmatism. Earth-Science Reviews, 72(1-2): 21-38.

Macpherson, Colin G. and Hall, Robert, 2002. Timing and tectonic controls in the evolving orogen of SE Asia and the western Pacific and some implications for ore generation. In: D. J. Blundell, F. Neubauer and A. von Quadt (Editors), The Timing and Location of Major Ore Deposits in an Evolving Orogen. Geological Society, London, pp. 49-67.

Madsen, Julianne K., Thorkelson, Derek J., Friedman, R. M. and Marshall, Daniel D., in press. Cenozoic to Recent plate configurations in the Pacific Basin: Ridge subduction and slab window magmatism in western North America. Geosphere.

Martin, H., 1999. Adakitic magmas: modern analogues of Archaean granitoids. Lithos, 46(3): 411-429.

Massey, N. W. D., MacIntyre, D. G., Desjardins, P. J. and Cooney, R. T., 2005. Digital Geology Map of British Columbia, Open File 2005-2, DVD. In: B.C. Ministry of Energy and Mines (Editor).

Mathews, W. H., 1989. Neogene Chilcotin basalts in south-central British Columbia: geology, ages, and geomorphic history. Canadian Journal of Earth Sciences, 26: 969-982.

McClaughry, Jason D. and Gaylord, David R., 2005. Middle Eocene sedimentary and volcanic infilling of an evolving supradetachment basin: White Lake Basin, south-central British Columbia. Canadian Journal of Earth Sciences, 42(1): 49-66.

McGetchin, T. R., Settle, M. and Chouet, B. A., 1974. Cinder cone growth mmodeled after Northeast Crater, Mount-Etna, Sicily. Journal of Geophysical Research, 79(23): 3257-3272.

McKervey, John Antony, 1998. The petrogenesis of the Eocene Challis Volcanic Group, Idaho, western United States. PhD Thesis, Open University, Milton Keynes, 586 pp.

McMechan, R. D., 1983. Geology of the Princeton Basin. British Columbia. Ministry of Energy, Mines and Petroleum Resources; Paper 1983-3. British Columbia Ministry of Energy, Mines and Petroleum Resources, Victoria, 52 pp.

Melcher, F. and Meisel, T., 2004. A metamorphosed early Cambrian crust-mantle transition in the Eastern Alps, Austria. Journal of Petrology, 45(8): 1689-1723.

Miyashiro, A., 1974. Volcanic rock series in island arcs and active continental margins. American Journal of Science, 274(4): 321-355.

Monger, J., 1985. Structural evolution of the southwestern Intermontane belt, Ashcroft and Hope map areas, British Columbia. Current Research, Part A, Paper 85-1A: 349-358.

Monger, J., 1989. Geology, Hope, British Columbia. Geological Survey of Canada.

Monger, J. and McMillan, W. J., 1989. Geology, Ashcroft, British Columbia. Geological Survey of Canada.

Monger, J. and Price, R. A., 2002. The Canadian Cordillera: Geology and tectonic evolution. CSEG Recorder, 27: 17-36.

Morris, G. A. and Hooper, P. R., 1997. Petrogenesis of the Colville Igneous Complex, northeast Washington: Implications for Eocene tectonics in the northern US Cordillera. Geology, 25(9): 831-834.

Morris, G. A., Larson, P. B. and Hooper, P. R., 2000. 'Subduction style' magmatism in a nonsubduction setting: the Colville Igneous Complex, NE Washington State, USA. Journal of Petrology, 41(1): 43-67.

Morris, George A. and Creaser, Robert Andrew, 2003. Crustal recycling during subduction at the Eocene Cordilleran margin of North America: a petrogenetic study from the southwestern Yukon. Canadian Journal of Earth Sciences, 40(12): 1805-1821.

Mortimer, N., 1987. The Nicola Group: Late Triassic and Early Jurassic subduction-related volcanism in British Columbia. Canadian Journal of Earth Sciences, 24: 2521-2536.

Nagler, T. F. and Kramers, J. D., 1998. Nd isotopic evolution of the upper mantle during the Precambrian: models, data and the uncertainty of both. Precambrian Research, 91(3-4): 233-252.

Norman, M. D. and Mertzman, S. A., 1991. Petrogenesis of Challis volcanics from central and southwestern Idaho - Trace-element and Pb isotopic evidence. Journal of Geophysical Research, 96(B8): 13279-13293.

Parfitt, E. A., 2004. A discussion of the mechanisms of explosive basaltic eruptions. Journal of Volcanology and Geothermal Research, 134(1-2): 77-107.

Parrish, R. R., Carr, S. D. and Parkinson, D. L., 1988. Eocene extensional tectonics and geochronology of the southern Omineca Belt, British-Columbia and Washington. Tectonics, 7(2): 181-212.

Peacock, M. A., 1931. Classification of igneous rock series. Journal of Geology, 39: 54-67.

Pearce, J. A. and Peate, D. W., 1995. Tectonic implications of the composition of volcanic arc magmas. Annual Review of Earth and Planetary Sciences, 23: 251-285.

Peslier, A. H., Reisberg, L., Ludden, J. and Francis, D., 2000. Os isotopic systematics in mantle xenoliths; age constraints on the Canadian Cordillera lithosphere. Chemical Geology, 166(1-2): 85-101.

Petford, N., 2003. Rheology of granitic magmas during ascent and emplacement. Annual Review of Earth and Planetary Sciences, 31: 399-427.

Poli, S., 1993. The amphibolite-eclogite transformation - an experimental-study on basalt. American Journal of Science, 293(10): 1061-1107.

Rapp, R. P., 1995. Amphibole-out phase-boundary in partially melted metabasalt, its control over liquid fraction and composition, and source permeability. Journal of Geophysical Research, 100(B8): 15601-15610.

Rapp, R. P., Shimizu, N., Norman, M. D. and Applegate, G. S., 1999. Reaction between slab-derived melts and peridotite in the mantle wedge: experimental constraints at 3.8 GPa. Chemical Geology, 160(4): 335-356.

Rapp, R. P. and Watson, E. B., 1995. Dehydration melting of metabasalt at 8-32-Kbar - Implications for continental growth and crust-mantle recycling. Journal of Petrology, 36(4): 891-931.

Rapp, R. P., Watson, E. B. and Miller, C. F., 1991. Partial melting of amphibolite eclogite and the origin of Archean trondhjemites and tonalites. Precambrian Research, 51(1-4): 1-25.

Read, Peter B., 2000. Geology and Industrial Minerals of the Tertiary Basins, South-central British Columbia. British Columbia. Ministry of Energy, Mines and Petroleum Resources Geofile 2000-3. British Columbia. Ministry of Energy, Mines and Petroleum Resources, Victoria, 110 pp.

Renne, P. R., Swisher, C. C., Deino, A. L., Karner, D. B., Owens, T. L. and DePaolo, D. J., 1998. Intercalibration of standards, absolute ages and uncertainties in $^{40}Ar/^{39}Ar$ dating. Chemical Geology, 145(1-2): 117-152.

Rice, H. M. A., 1947. Geology and mineral deposits of the Princeton map-area, British Columbia. Geological Survey of Canada, Memoir, 243. Geological Survey of Canada, 136 pp.

Riedel, C., Ernst, G. G. J. and Riley, M., 2003. Controls on the growth and geometry of pyroclastic constructs. Journal of Volcanology and Geothermal Research, 127(1-2): 121-152.

Roeder, P. and Emslie, R., 1970. Olivine-liquid equilibrium. Contributions to Mineralogy and Petrology, 29: 275-289.

Rudnick, Roberta L. and Gao, Shan, 2003. Composition of the continental crust. In: Roberta L. Rudnick (Editor), The Crust. Treatise on Geochemistry. Elsevier, pp. 1-64.

Rushmer, T., 1991. Partial melting of 2 amphibolites - Contrasting experimental results under fluid-absent conditions. Contributions to Mineralogy and Petrology, 107(1): 41-59.

Rutherford, M. J. and Devine, J. D., 2003. Magmatic conditions and magma ascent as indicated by hornblende phase equilibria and reactions in the 1995-2002 Soufriere Hills magma. Journal of Petrology, 44(8): 1433-1454.

Self, S., Thordarson, T., Keszthelyi, L., Walker, G. P. L., Hon, K., Murphy, M. T., Long, P. and Finnemore, S., 1996. A new model for the emplacement of Columbia River Basalts as large, inflated pahoehoe lava flow fields. Geophysical Research Letters, 23(19): 2689-2692.

Sen, C. and Dunn, T., 1994. Dehydration melting of a basaltic composition amphibolite at 1.5 and 2.0 GPa - Implications for the origin of adakites. Contributions to Mineralogy and Petrology, 117(4): 394-409.

Shannon, R. D., 1976. Revised effective ionic-radii and systematic studies of interatomic distances in halides and chalcogenides. Acta Crystallographica Section A, 32(SEP1): 751-767.

Shaw, W. S., 1952. The Princeton Coalfield, B.C. Geological Survey of Canada Paper 52-12, pp. 28.

Sisson, Virginia B., Pavlis, Terry L., Roeske, Sarah M. and Thorkelson, Derek J., 2003. Introduction: An overview of ridge-trench interactions in modern and ancient settings. In: Virginia B. Sisson, Sarah M. Roeske and Terry L. Pavlis (Editors), Special Paper 371: Geology of a Transpressional Orogen Developed During Ridge-Trench Interaction Along the North Pacific Margin. Geological Society of America, Boulder, CO, pp. 1-18.

Smith, A. D. and Thorkelson, D., 2002. Geochemical and Nd-Sr-Pb isotopic evidence on the origin and geodynamic evolution of mid-Cretaceous continental arc volcanic rocks of the Spences Bridge Group, south-central British Columbia. Geological Journal, 37(2): 167-186.

Souther, J. G., 1991. Volcanic Regimes. In: H. Gabrielse, Yorath, C. J. (Editor), Geology of the Cordilleran Orogen in Canada. Geology of Canada. Geological Survey of Canada, pp. 457-490.

Stern, C. R. and Kilian, R., 1996. Role of the subducted slab, mantle wedge and continental crust in the generation of adakites from the Andean Austral volcanic zone. Contributions to Mineralogy and Petrology, 123(3): 263-281.

Sun, S. S. and McDonough, W. F., 1989. Chemical and isotopic systematics of oceanic basalts: implications for mantle composition and process. In: A. D. Saunders and M. J. Norry (Editors), Magmatism in the Ocean Basins. The Geological Society, pp. 313-345.

Thorkelson, D. J., 1989. Eocene sedimentation and volcanism in the Fig Lake Graben, southwestern British-Columbia. Canadian Journal of Earth Sciences, 26(7): 1368-1373.

Thorkelson, D. J., 1996. Subduction of diverging plates and the principles of slab window formation. Tectonophysics, 255(1-2): 47-63.

Thorkelson, D. J. and Taylor, R. P., 1989. Cordilleran slab windows. Geology, 17(9): 833-836.

Thorkelson, Derek J. and Breitsprecher, Katrin, 2005. Partial melting of slab window margins: genesis of adakitic and non-adakitic magmas. Lithos, 79(1-2): 25-41.

Valentine, Greg A., Krier, Don, Perry, Frank V. and Heiken, Grant, 2005. Scoria cone construction mechanisms, Lathorp Wells volcano, southern Nevada, USA. Geology, 33(8): 629-632.

Vesperman, D. and Schmincke, H. U., 2000. Scoria cones and tuff rings. In: H. Sigurdsson (Editor), Encyclopedia of Volcanoes. Academic Press, San Diego, California, pp. 683-694.

Vielzeuf, D. and Schmidt, M. W., 2001. Melting relations in hydrous systems revisited: application to metapelites, metagreywackes and metabasalts. Contributions to Mineralogy and Petrology, 141(3): 251-267.

Villeneuve, M. E. and Mathewes, R. W., 2005. An Early Eocene age for the Quilchena fossil locality, southern British Columbia. Geological Survey of Canada, Current Research, A4: 1-7.

von Huene, R., Ranero, C. R. and Vannucchi, P., 2004. Generic model of subduction erosion. Geology, 32(10): 913-916.

Weis, D., Kieffer, B., Maerschalk, C., Pretorius, W. and Barling, J., 2005. High-precision Pb-Sr-Nd-Hf isotopic characterization of USGS BHVO-1 and BHVO-2 reference materials. Geochemistry Geophysics Geosystems, 6. DOI:10.1029/2004GC000852

Wheeler, J. O. and McFeeley, P., 1991. Tectonic assemblage map of the Canadian Cordillera and adjacent parts of the United States of America. Map 1712A. Geological Survey of Canada.

Williams, V. E. and Ross, C. A., 1979. Depositional setting and coal petrology of Tulameen Coalfield, south-central British-Columbia. AAPG Bulletin-American Association of Petroleum Geologists, 63(11): 2058-2069.

Wolf, M. B. and Wyllie, P. J., 1994. Dehydration-melting of amphibolite at 10 Kbar - the effects of temperature and time. Contributions to Mineralogy and Petrology, 115(4): 369-383.

Wood, Bernard J. and Blundy, Jonathan D., 2003. Trace element partitioning under crustal and uppermost mantle conditions: The influence of ionic radius, cation charge, pressure, and temperature. In: Roberta L. Rudnick (Editor), The Crust. Treatise on Geochemistry. Elsevier, pp. 395-424.

Wooden, J. L. and Box, S. E., 1996. Contrasting inherited zircon populations in an Eocene vs. an early Cretaceous intrusive associated with the eastern Kettle Metamorphic core complex, NE Washington, Geological Society of America, Abstracts with Programs, pp. 444.

Xiong, X. L., Adam, J. and Green, T. H., 2005. Rutile stability and rutile/melt HFSE partitioning during partial melting of hydrous basalt: Implications for TTG genesis. Chemical Geology, 218-359(3-4): 339.

Xu, J. F., Shinjo, R., Defant, M. J., Wang, Q. A. and Rapp, R. P., 2002. Origin of Mesozoic adakitic intrusive rocks in the Ningzhen area of east China: Partial melting of delaminated lower continental crust? Geology, 30(12): 1111-1114.

Yardley, B. W. D. and Valley, J. W., 1997. The petrologic case for a dry lower crust. Journal of Geophysical Research, 102(B6): 12173-12185.

APPENDIX ONE: $^{40}AR/^{39}AR$ ANALYTICAL METHODS AND SAMPLE DESCRIPTIONS

$^{40}Ar/^{39}Ar$ Analytical Methods

Each sample was crushed and sieved to obtain fragments ranging in size from 0.125 to 0.600 mm. Crystals or rock fragments were hand-picked from the sieved fraction under ethanol with a binocular microscope. These separates were washed with deionized water, then placed in an ultrasonic bath for half an hour and finally air-dried at room temperature. Mineral separates were wrapped in aluminium foil and stacked in an irradiation capsule with similar-aged samples, neutron flux monitors (Fish Canyon Tuff sanidine, 28.03 Ma; Renne et al. 1998), optical grade CaF_2 and potassium glass. The samples were irradiated with cadmium shielding on April 25-27, 2005 at the McMaster Nuclear Reactor in Hamilton, Ontario, for 84 MWH, with a neutron flux of approximately 3.1016 neutrons/cm^2. Total fusion analyses (n=72) of 21 neutron flux monitor positions produced errors of <0.5% in the J value.

The samples were analyzed on June 2 and 3, 2005, at the Noble Gas Laboratory, Pacific Centre for Isotopic and Geochemical Research, University of British Columbia, Vancouver, BC, Canada. The mineral separates were step-heated at incrementally higher powers in the defocused beam of a 10W CO_2 laser (New Wave Research MIR10) until fused. The gas evolved from each step was analyzed by a VG5400 mass spectrometer equipped with an ion-counting

electron multiplier. All measurements were corrected for total system blank, mass spectrometer sensitivity, mass discrimination, and radioactive decay during and subsequent to irradiation, as well as interfering Ar from atmospheric contamination and the irradiation of Ca, Cl and K. Reactor induced correction factors are $(^{40}Ar/^{39}Ar)_K = 0.0302$, $(^{37}Ar/^{39}Ar)_{Ca} = 2242.27$, $(^{36}Ar/^{39}Ar)_{Ca} = 0.5326$, $Ca/K = 1.83(^{37}Ar_{Ca}/^{39}Ar_K)$.

The plateau and correlation ages were calculated using IsoPlot 3.09 (Ludwig 2003). Errors are quoted at the 2-sigma (95% confidence) level and are propagated from all sources except mass spectrometer sensitivity and age of the flux monitor. The best statistically-justified plateau and plateau age were picked based on the following criteria: 1) Three or more contiguous steps comprising more than 50% of the ^{39}Ar; 2) Probability of fit of the weighted mean age greater than 5%; 3) Slope of the error-weighted line through the plateau ages equals zero at 5% confidence; 4) Ages of the two outermost steps on a plateau are not significantly different from the weighted-mean plateau age (at 1.8σ six or more steps only); 5) Outermost two steps on either side of a plateau must not have nonzero slopes with the same sign (at 1.8σ nine or more steps only).

The presence of significant excess radiogenic Ar was identified in sample RBI-04-16-14-1B and as a result the crystallization age was determined from an inverse isochron (calculated using Isoplot 3.09). Analytical data is presented in Table 6.

Sample Descriptions

Agate Mountain Basaltic Andesite

Sample RBI-04-16-14-1 is a pyroxene olivine-phyric basaltic andesite lava flow from Agate Mountain (Fig. 2). The groundmass is holocrystalline, consisting of microlites of plagioclase + clinopyroxene + magnetite and small amounts of devitrified glass. Although the olivine is completely altered, the pyroxene phenocrysts and the groundmass are largely pristine. A groundmass separate yielded a plateau of 54.6±0.8 Ma, but an inverse isochron of the steps in the plateau shows imprecision in both the date and initial $^{36}Ar/^{40}Ar$, suggesting that excess radiogenic Ar is influencing the result. An inverse isochron of steps 3-9 yields a date of 51.7±1.6 Ma and a $^{36}Ar/^{40}Ar$ of 428±36 confirming the existence of excess Ar. The inverse isochron date of 51.7±1.6 Ma is interpreted as the crystallization age.

Sunday Creek Dacite

Sample RBI-04-24-6-1 is a strongly porphyritic plagioclase-hornblende dacite collected from a road-cut near Sunday Creek (Fig. 2). This sample is less than 5 km from the location where five samples were dated by Hills and Baadsgaard (1967). The hornblende crystals are green in plane-polarized light and commonly range in size from 0.15-1.5 mm. They have a thin opacite rim but are otherwise unaltered. A separate of hornblende crystals yielded a date of 52±1 Ma based on 6 contiguous plateaus containing 93.7 % of the ^{39}Ar and is interpreted as the igneous crystallization age. This date is in agreement with the 53 to 48 Ma range reported by Hills and Baadsgaard (1967).

Merritt Andesite

Sample RBI-04-34-2-1B is a strongly porphyritic plagioclase-hornblende dacite collected from an outcrop in the town of Lower Nicola, near Merritt (Fig. 2). The hornblende occupies ~20 vol. % of the rock and has a wide range in sizes, from <0.05 to 5 mm. They have a thin opacite rim but are otherwise unaltered. A separate of hornblende crystals yielded a date of 49±1 Ma based on 10 contiguous steps containing 100 % of the ^{39}Ar and is interpreted as the igneous crystallization age.

Fig Lake Dacite

Sample RBI-04-35-3-1 is a porphyritic hornblende-plagioclase dacite collected from an outcrop near Kingsvale, in the Fig Lake graben (Fig. 2; Thorkelson 1989). The whole rock geochemical analysis for the Princeton Group reported by Breitsprecher (2002) and the whole rock K-Ar date determined by Thorkelson (1989) are from the same outcrop. Hornblende crystals occupy ~10 vol. % of the rock, and range widely in size from 0.05 to 4 mm. Due to the development of thick opacite rims, many small grains are completely altered to fine grained Fe-Ti oxides, however larger grains are intact. A separate of hornblende yielded a date of 50.3±0.9 based on 11 contiguous heating steps containing 100% of the ^{39}Ar and is interpreted as the igneous crystallization age.

Boss Lake Rhyolite

Sample RBI-04-36-1-1 is an aphyric rhyolite collected near Boss Lake (Fig. 2). Small crystals of K-feldspar, plagioclase and quartz are abundant.

Biotite is too low in abundance and altered to yield a mineral separate. A separate of groundmass picked clean of phenocrysts yielded a date of 50.2±0.4 Ma based 11 contiguous heating steps containing 89.7% of the ^{39}Ar. This date is interpreted as the minimum age of crystallization; however, because it is consistent with other analysis it is probably close to the crystallization age.

Table 5: $^{40}Ar/^{39}Ar$ results for hornblende and groundmass separates, and a whole rock from the Princeton Group

RBI-04-24-6-1 Hornblende

J = 0.009701±0.000012

Laser Power (%)	$^{40}Ar/^{39}Ar$	$^{38}Ar/^{39}Ar$	$^{37}Ar/^{39}Ar$	$^{36}Ar/^{39}Ar$	Ca/K	Cl/K	%^{40}Ar atm	f ^{39}Ar	$^{40}Ar^*/^{39}Ar_K$	Age
2	153.119 ± 0.022	0.112 ± 0.097	0.716 ± 0.040	0.531 ± 0.037	2.676	0	100.77	0.71	-1.190 ± 4.858	-20.94 ± 86.01
2.2	35.665 ± 0.009	0.029 ± 0.266	0.481 ± 0.053	0.109 ± 0.106	1.796	-0.001	88.54	0.98	4.097 ± 3.406	70.32 ± 57.33
2.4	12.611 ± 0.026	0.02 ± 0.315	0.616 ± 0.045	0.037 ± 0.195	2.302	0	84.63	1.28	1.941 ± 2.121	33.66 ± 36.44
2.6	10.961 ± 0.016	0.021 ± 0.244	0.782 ± 0.026	0.034 ± 0.125	2.92	0	88.30	1.40	1.283 ± 1.242	22.32 ± 21.46
2.8	9.299 ± 0.020	0.018 ± 0.207	0.791 ± 0.037	0.027 ± 0.137	2.955	0	83.10	1.93	1.574 ± 1.089	27.33 ± 18.77
3	6.655 ± 0.020	0.019 ± 0.290	1.048 ± 0.029	0.015 ± 0.295	3.916	0.001	64.31	1.81	2.382 ± 1.333	41.21 ± 22.81
3.3	5.809 ± 0.010	0.018 ± 0.073	3.341 ± 0.015	0.012 ± 0.131	12.511	0	49.78	5.36	2.932 ± 0.451	50.60 ± 7.67
3.6	5.59 ± 0.008	0.02 ± 0.056	4.613 ± 0.014	0.012 ± 0.048	17.295	0.001	48.62	26.88	2.890 ± 0.167	49.88 ± 2.84
3.9	4.794 ± 0.007	0.02 ± 0.034	4.749 ± 0.014	0.008 ± 0.044	17.805	0.001	37.30	31.25	3.025 ± 0.113	52.18 ± 1.92
4.2	3.682 ± 0.012	0.018 ± 0.062	5.024 ± 0.016	0.005 ± 0.091	18.841	0.001	20.36	19.26	2.952 ± 0.141	50.94 ± 2.40
4.5	4.15 ± 0.010	0.017 ± 0.051	4.888 ± 0.015	0.006 ± 0.096	18.331	0	26.27	9.13	3.079 ± 0.178	53.11 ± 3.03

RBI-04-35-3-1 Hornblende

J = 0.009696±0.000012

Laser Power (%)	$^{40}Ar/^{39}Ar$	$^{38}Ar/^{39}Ar$	$^{37}Ar/^{39}Ar$	$^{36}Ar/^{39}Ar$	Ca/K	Cl/K	%^{40}Ar atm	f ^{39}Ar	$^{40}Ar^*/^{39}Ar_K$	Age
2	280.879 ± 0.045	0.209 ± 0.110	1.095 ± 0.058	0.949 ± 0.060	4.174	0.004	98.26	0.42	4.917 ± 11.155	84.02 ± 186.26
2.2	131.802 ± 0.045	0.085 ± 0.468	1.531 ± 0.052	0.452 ± 0.069	5.839	-0.003	99.56	0.27	0.580 ± 7.021	10.13 ± 122.13
2.4	120.314 ± 0.049	0.092 ± 0.292	1.496 ± 0.064	0.391 ± 0.072	5.703	0.001	94.38	0.43	6.792 ± 6.115	115.07 ± 100.36
2.7	35.617 ± 0.032	0.024 ± 0.275	0.958 ± 0.048	0.112 ± 0.124	3.652	-0.003	91.30	0.86	3.106 ± 4.016	53.54 ± 68.19
3	5.302 ± 0.017	0.016 ± 0.296	1.516 ± 0.024	0.013 ± 0.303	5.782	0	67.16	2.20	1.745 ± 1.168	30.27 ± 20.10
3.3	4.451 ± 0.009	0.019 ± 0.062	2.325 ± 0.015	0.007 ± 0.198	8.873	0.001	35.74	6.79	2.872 ± 0.391	49.55 ± 6.65
3.6	4.282 ± 0.007	0.018 ± 0.092	2.899 ± 0.014	0.006 ± 0.149	11.067	0.001	31.77	8.50	2.935 ± 0.273	50.62 ± 4.64
3.9	3.444 ± 0.011	0.017 ± 0.049	2.952 ± 0.015	0.003 ± 0.064	11.272	0.001	15.41	33.68	2.927 ± 0.071	50.49 ± 1.21
4.2	3.862 ± 0.007	0.017 ± 0.062	2.716 ± 0.013	0.005 ± 0.161	10.37	0	26.42	8.21	2.854 ± 0.235	49.24 ± 3.99
4.5	3.526 ± 0.008	0.016 ± 0.050	2.907 ± 0.015	0.004 ± 0.139	11.1	0	19.57	17.38	2.849 ± 0.160	49.16 ± 2.73
4.9	3.501 ± 0.006	0.016 ± 0.044	3.102 ± 0.013	0.004 ± 0.086	11.847	0	16.78	21.27	2.928 ± 0.094	50.50 ± 1.59

Table 5: $^{40}Ar/^{39}Ar$ results for hornblende and groundmass separates, and a whole rock from the Princeton Group continued

RBI-04-34-2-1 Hornblende

J = 0.009699±0.000012

Laser Power (%)	$^{40}Ar/^{39}Ar$	$^{38}Ar/^{39}Ar$	$^{37}Ar/^{39}Ar$	$^{36}Ar/^{39}Ar$	Ca/K	Cl/K	%^{40}Ar atm	f ^{39}Ar	$^{40}Ar^*/^{39}Ar_K$	Age
2	152.182 ± 0.039	0.124 ± 0.225	1.18 ± 0.069	0.518 ± 0.063	4.409	0.003	98.85	0.37	1.749 ± 7.659	30.34 ± 131.79
2.2	69.331 ± 0.055	-0.004 ± 7.463	1.353 ± 0.066	0.243 ± 0.141	5.056	-0.014	101.88	0.47	-1.318 ± 9.403	-23.20 ± 166.66
2.4	88.412 ± 0.059	0.079 ± 0.296	1.523 ± 0.075	0.307 ± 0.127	5.693	0.002	100.80	0.45	-0.717 ± 10.260	-12.58 ± 180.79
2.6	61.308 ± 0.054	0.055 ± 0.521	1.983 ± 0.075	0.2 ± 0.204	7.416	0.001	94.51	0.47	3.378 ± 11.715	58.17 ± 198.49
2.8	22.455 ± 0.053	0.031 ± 0.731	1.963 ± 0.069	0.077 ± 0.285	7.343	0	98.35	0.54	0.367 ± 6.398	6.41 ± 111.56
3	10.305 ± 0.027	0.018 ± 0.612	2.974 ± 0.031	0.029 ± 0.190	11.135	0	76.46	1.28	2.436 ± 1.599	42.12 ± 27.34
3.2	5.755 ± 0.006	0.02 ± 0.104	3.218 ± 0.014	0.011 ± 0.157	12.29	0.001	48.34	10.03	2.988 ± 0.523	51.54 ± 8.89
3.4	4.423 ± 0.007	0.018 ± 0.052	3.119 ± 0.014	0.007 ± 0.061	11.912	0.001	34.79	25.66	2.899 ± 0.127	50.02 ± 2.16
3.9	3.718 ± 0.006	0.017 ± 0.039	3.409 ± 0.014	0.005 ± 0.127	13.021	0	24.26	29.37	2.831 ± 0.182	48.86 ± 3.10
4.2	3.872 ± 0.007	0.017 ± 0.052	3.308 ± 0.014	0.005 ± 0.076	12.636	0.001	27.52	21.48	2.820 ± 0.122	48.69 ± 2.08
4.5	3.662 ± 0.014	0.018 ± 0.070	3.473 ± 0.018	0.005 ± 0.176	13.268	0.001	27.96	9.88	2.652 ± 0.278	45.81 ± 4.74

RBI-04-16-14-1 Groundmass

J = 009703±0.000012

Laser Power (%)	$^{40}Ar/^{39}Ar$	$^{38}Ar/^{39}Ar$	$^{37}Ar/^{39}Ar$	$^{36}Ar/^{39}Ar$	Ca/K	Cl/K	%^{40}Ar atm	f ^{39}Ar	$^{40}Ar^*/^{39}Ar_K$	Age
2	42.87 ± 0.015	0.042 ± 0.046	0.586 ± 0.024	0.133 ± 0.029	2.232	0.001	90.28	3.64	4.179 ± 1.090	71.71 ± 18.34
2.2	7.761 ± 0.010	0.015 ± 0.065	0.83 ± 0.019	0.015 ± 0.082	3.164	0	55.85	4.83	3.436 ± 0.371	59.17 ± 6.28
2.4	5.878 ± 0.007	0.014 ± 0.040	1.097 ± 0.015	0.008 ± 0.081	4.18	0	34.75	7.44	3.848 ± 0.183	66.13 ± 3.09
2.6	4.356 ± 0.005	0.012 ± 0.038	0.945 ± 0.014	0.004 ± 0.039	3.602	-0.001	21.49	13.12	3.431 ± 0.047	59.07 ± 0.79
2.8	3.574 ± 0.007	0.012 ± 0.053	0.7 ± 0.015	0.002 ± 0.137	2.668	-0.001	10.26	18.12	3.216 ± 0.069	55.44 ± 1.18
3	3.45 ± 0.007	0.013 ± 0.030	0.572 ± 0.016	0.001 ± 0.288	2.18	0	7.74	16.34	3.192 ± 0.105	55.02 ± 1.79
3.2	3.447 ± 0.007	0.013 ± 0.026	0.525 ± 0.016	0.002 ± 0.188	1.998	0	11.54	12.91	3.056 ± 0.094	52.72 ± 1.59
3.4	3.561 ± 0.009	0.013 ± 0.049	0.556 ± 0.018	0.002 ± 0.234	2.117	0	12.81	9.86	3.113 ± 0.131	53.68 ± 2.23
3.6	3.806 ± 0.009	0.013 ± 0.067	0.589 ± 0.021	0.002 ± 0.180	2.246	0	16.02	6.64	3.204 ± 0.131	55.24 ± 2.23
3.8	4.15 ± 0.006	0.014 ± 0.053	0.808 ± 0.014	0.002 ± 0.207	3.077	0	11.02	7.09	3.704 ± 0.124	63.70 ± 2.09

Table 5: $^{40}Ar/^{39}Ar$ results for hornblende and groundmass separates, and a whole rock from the Princeton Group continued

RBI-04-36-1-1 Whole Rock
J =0.009698±0.000012

Laser Power (%)	$^{40}Ar/^{39}Ar$	$^{38}Ar/^{39}Ar$	$^{37}Ar/^{39}Ar$	$^{36}Ar/^{39}Ar$	Ca/K	Cl/K	$\%^{40}Ar$ atm	$f\ ^{39}Ar$	$^{40}Ar^*/^{39}Ar_K$	Age
2	8.476 ± 0.006	0.016 ± 0.031	0.07 ± 0.017	0.019 ± 0.021	0.265	0	64.33	9.11	3.030 ± 0.119	52.24 ± 2.02
2.2	3.945 ± 0.006	0.013 ± 0.035	0.084 ± 0.020	0.004 ± 0.033	0.321	0	25.59	9.47	2.941 ± 0.039	50.73 ± 0.66
2.4	3.711 ± 0.005	0.013 ± 0.030	0.095 ± 0.017	0.003 ± 0.055	0.36	0	21.65	14.07	2.913 ± 0.048	50.26 ± 0.82
2.6	3.396 ± 0.005	0.013 ± 0.031	0.101 ± 0.013	0.002 ± 0.075	0.387	0	14.58	12.67	2.907 ± 0.041	50.15 ± 0.71
2.8	3.434 ± 0.005	0.013 ± 0.020	0.102 ± 0.014	0.002 ± 0.087	0.391	0	15.17	12.48	2.919 ± 0.050	50.36 ± 0.84
3	3.554 ± 0.005	0.013 ± 0.032	0.107 ± 0.017	0.002 ± 0.065	0.41	0	19.69	11.45	2.860 ± 0.050	49.36 ± 0.85
3.2	3.632 ± 0.005	0.013 ± 0.027	0.126 ± 0.014	0.003 ± 0.048	0.483	0	19.97	10.76	2.913 ± 0.040	50.26 ± 0.68
3.4	3.702 ± 0.006	0.013 ± 0.039	0.137 ± 0.017	0.003 ± 0.061	0.525	0	21.83	6.70	2.900 ± 0.054	50.03 ± 0.92
3.6	3.788 ± 0.006	0.013 ± 0.038	0.178 ± 0.019	0.003 ± 0.088	0.684	0	23.93	5.62	2.888 ± 0.086	49.83 ± 1.46
3.8	4.052 ± 0.007	0.014 ± 0.069	0.181 ± 0.018	0.005 ± 0.141	0.695	0	31.93	1.81	2.763 ± 0.190	47.71 ± 3.24
4	4.095 ± 0.005	0.014 ± 0.039	0.212 ± 0.018	0.004 ± 0.180	0.817	0	28.56	2.94	2.932 ± 0.220	50.58 ± 3.75
4.2	4.439 ± 0.007	0.014 ± 0.045	0.281 ± 0.019	0.006 ± 0.187	1.082	0	36.06	1.73	2.844 ± 0.314	49.08 ± 5.34
4.5	4.831 ± 0.007	0.013 ± 0.174	0.362 ± 0.017	0.008 ± 0.132	1.393	-0.001	48.22	1.18	2.507 ± 0.322	43.33 ± 5.49

Note: All uncertainties are at 2σ

APPENDIX TWO:
PHOTOMICROGRAPHS AND PETROGRAPHIC DATA

Table 6: Volume % modal abundances of phenocrysts in volcanic rocks of the Princeton Group

Sample ID	Location	SiO_2	Total	Ol	Plag	Hbl	Bio	Cpx	Opx	Opq	Qtz	Kfs	Ap	Zrc
RBI-04-17-03-1	Agate Mtn	55.4	25	15	-	-	-	10	-	-	-	-	-	-
RBI-04-16-14-1	Agate Mtn	56.7	3	3	-	-	-	-	-	-	-	-	-	-
RBI-04-12-01-1	Agate Mtn	57.4	26	10	-	-	-	15	-	1	-	-	-	-
RBI-04-15-13-1	Agate Mtn	58.7	10	10	-	-	-	-	-	-	-	-	-	-
RBI-04-15-12-1	Agate Mtn	59.0	16	5	-	-	-	10	1	-	-	-	-	-
RBI-04-16-17-1	Agate Mtn	60.8	6	-	-	-	-	5	1	-	-	-	-	-
RBI-04-15-10-1	Agate Mtn	61.1	28	-	8	-	-	10	10	-	-	-	-	-
RBI-04-36-01-1	Boss Lake	72.3	13	-	3	-	1	-	-	-	2	3	-	-
RBI-04-35-03-1	Fig Lake	66.7	15	-	3	10	-	1	-	-	2	-	tr	-
RBI-04-30-02-1	Flat Top/Placer	61.4	9	-	-	1	-	7	1	-	-	-	-	-
RBI-04-21-03-1	Flat Top/Placer	61.8	40	-	5	35	-	-	-	-	-	-	tr	-
RBI-04-19-03-1	Flat Top/Placer	62.6	22	-	-	20	-	1	1	-	-	-	-	-
RBI-04-21-02-1	Flat Top/Placer	63.8	7	-	4	2	-	-	-	-	1	-	-	-
DM-04-18-01-1	Flat Top/Placer	65.8	53	-	30	20	-	-	-	3	-	-	tr	tr
RBI-04-20-03-2	Flat Top/Placer	66.1	41	-	30	1	-	7	3	-	-	-	-	-
RBI-04-31-01-2	Flat Top/Placer	66.4	50	-	25	20	-	-	-	3	2	-	tr	tr
RBI-04-22-01-1	Flat Top/Placer	66.8	42	-	30	10	-	1	1	-	-	-	tr	tr
RBI-04-32-02-1	Flat Top/Placer	67.4	28	-	15	10	-	1	-	1	1	-	-	-
RBI-04-31-01-1	Flat Top/Placer	68.5	12	-	5	2	-	4	-	1	-	-	-	-
RBI-04-34-02-1	Merritt	62.6	50	-	25	20	-	-	-	5	-	-	tr	-
RBI-04-39-01-1	Princeton	65.6	10	-	-	-	-	8	2	-	-	-	-	-
RBI-04-37-08-2	Prospect Creek	56.2	25	10	-	-	-	8	7	-	-	-	-	-
RBI-04-37-05-1	Prospect Creek	61.1	2	-	-	-	-	1	1	-	-	-	-	-
RBI-04-24-06-1	Sunday Creek	63.4	53	-	30	20	-	-	-	3	-	-	tr	tr
RBI-04-23-03-1	Sunday Creek	66.1	18	-	1	10	-	7	-	-	-	-	-	-
RBI-04-25-01-1	Tulameen	60.2	13	3	-	-	-	10	-	-	-	-	-	-

Abbreviations: Ol=Olivine; Plag=Plagioclase; Hbl=Hornblende; Bio=Biotite; Cpx = Clinopyroxene; Opx=Orthopyroxene; Opq = Opaque; Kfs=K-feldspar; Ap=Apatite; Zrc=Zircon; tr=trace; "-"=not noted

Notes: SiO_2 is in wt.%. All other numbers are phenocryst abundances in vol.% of the total rock deterrnined by visual estimation. For most rocks, groundmass assemblages consist of plag+cpx+opq+glass

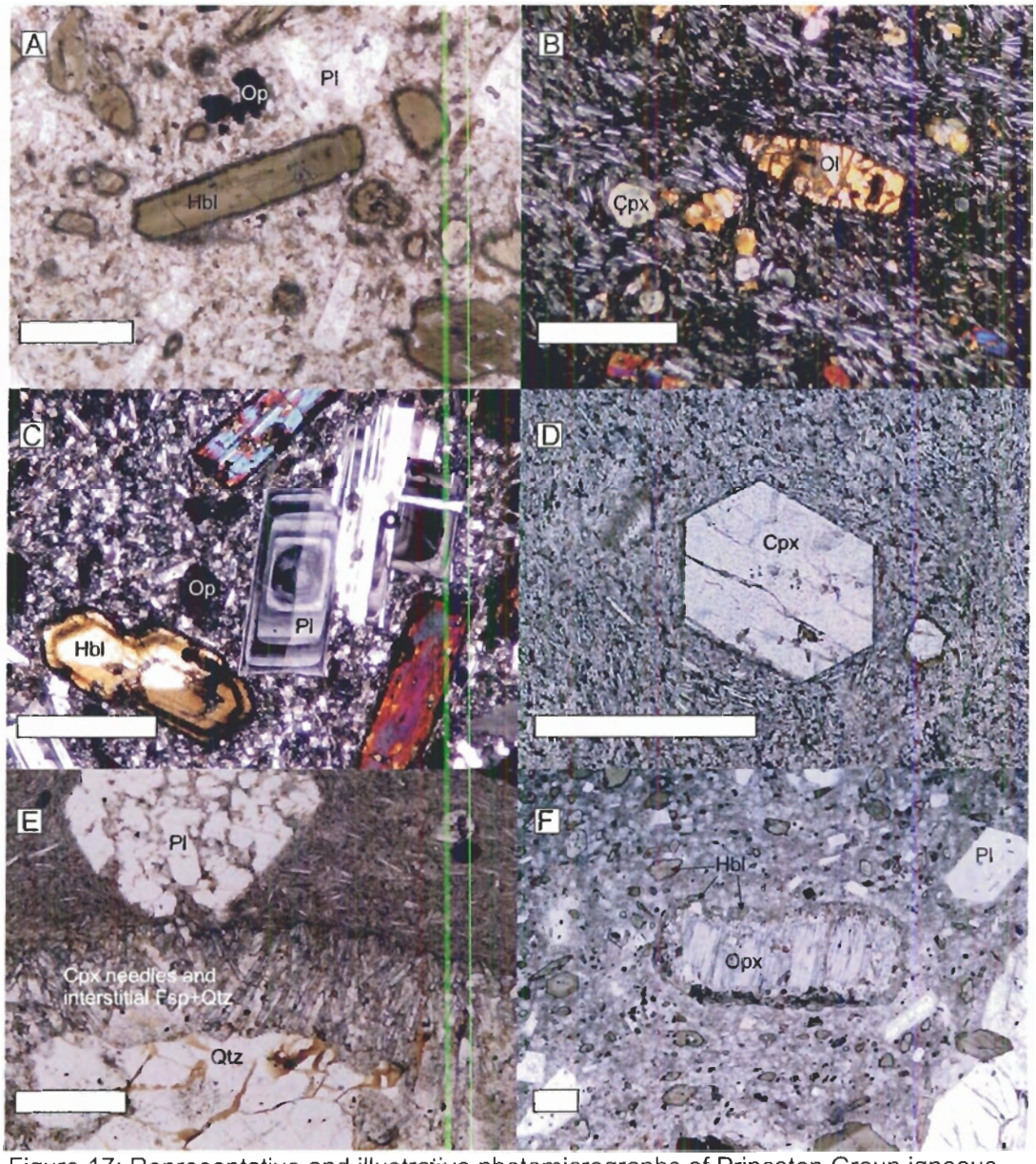

Figure 17: Representative and illustrative photomicrographs of Princeton Group igneous rocks. The scale bar is 0.5 mm for each photomicrograph. A) Representative plagioclase-hornblende porphyritic dacite from Sunday Creek. RBI-04-24-6-1, plane polarized light; B) Representative olivine-clinopyroxene basaltic andesite from near Agate Mountain. There is only one grain of olivine in the field of view. RBI-04-12-1-1, cross polarized light; C) Representative plagioclase-hornblende dacite from Flat Top Mountain. Note the multiple plagioclase and hornblende growth events evident from phenocryst textures. DM-04-18-01-1, cross polarized light; D) Representative sparsely porphyritic clinopyroxene dacite from near the town of Princeton in the Tulameen River valley. RBI-04-39-1-1; plane polarized light. E) Reaction between xenocrystic quartz and groundmass to form clinopyroxene at the margins of the quartz grain in a plagioclase-hornblende porphyritic dacite from Flat Top Mountain. Note sieve-textured plagioclase at the top of the photomicrograph. RBI-04-32-2-1, plane polarized light. F) Growth of hornblende on a possibly xenocrystic grain of orthopyroxene. RBI-04-31-3-1, plane polarized light. Abbreviations: Pl=plagioclase; Hbl=hornblende; Op=opaque mineral; Cpx=clinopyroxene; Opx=orthopyroxene; Qtz=quartz; Fsp=feldspar (undifferentiated);

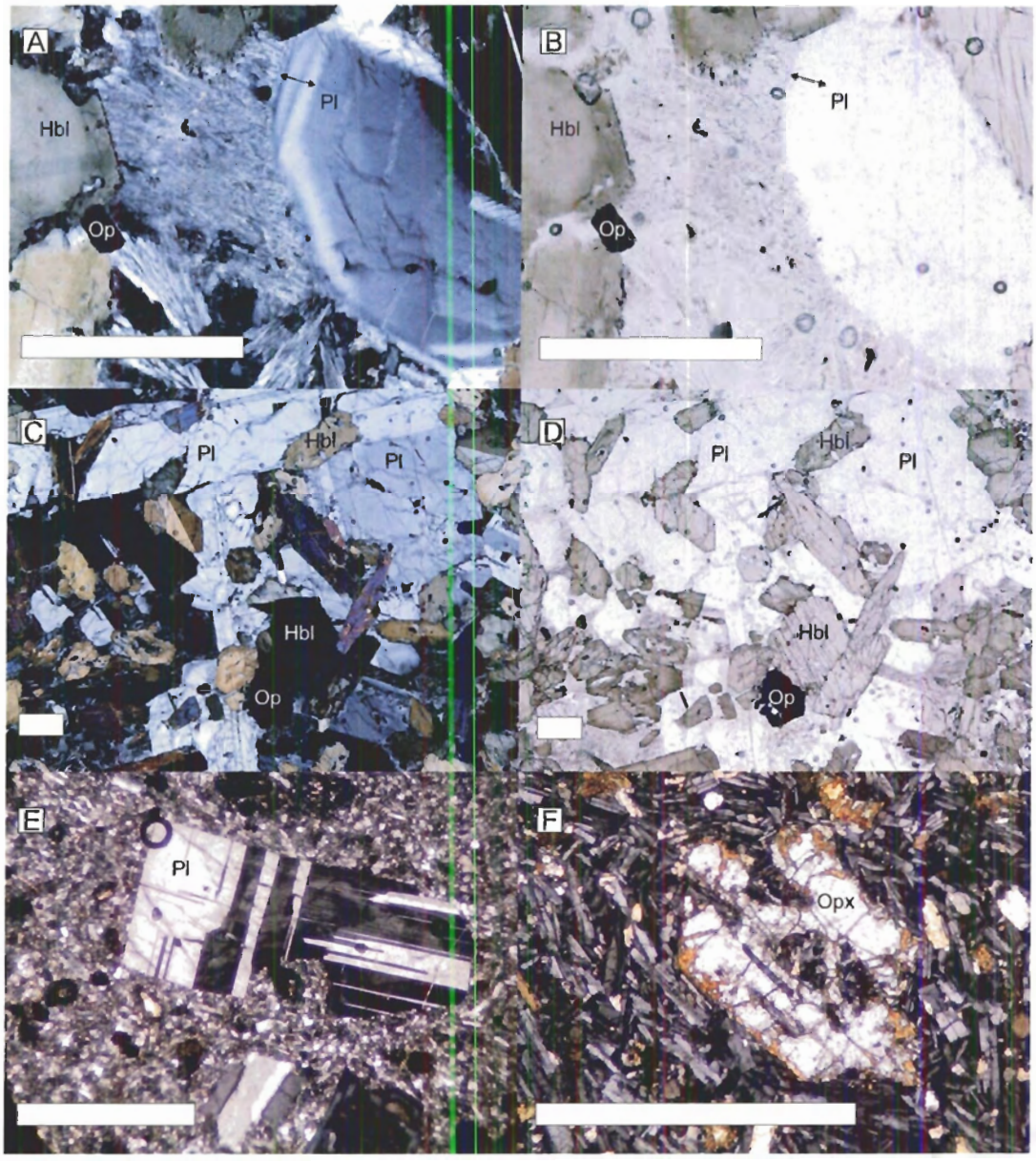

Figure 18: Representative and illustrative photomicrographs of Princeton Group igneous rocks. The scale bar is 0.5 mm for each photomicrograph. A,B) The edge of a hornblende gabbro xenolith from Flat Top Mountain. The arrow denotes area of zoned plagioclase which occurs where it is in contact with the groundmass. A is in cross polarized light, B is in plane polarized light. C,D) A typical hornblende gabbro xenolith (the interior of the xenolith depicted in A and B) from Flat Top Mountain. C is in cross polarized light, D is in plane polarized light. E) An embayed phenocryst of plagioclase from a hornblende plagioclase porphyritic dacite at Flat-Top Mountain. DM-04-18-1-1, cross polarized light. F) A hopper textured phenocryst of orthopyroxene from a highly magnesian (9 wt. % > MgO) basaltic andesite near Prospect Creek. RBI-04-37-8-2, cross polarized light. Abbreviations: Pl=plagioclase; Hbl=hornblende; Op=opaque mineral; Cpx=clinopyroxene; Opx=orthopyroxene.

APPENDIX THREE:
TRACE ELEMENT MODELLING

C_m	Final concentration in melt	ppm	
C_o	Initial concentration in melt	ppm	
f	Ratio of melt mass to total mass		
D_x^y	Mineral/melt partition coefficient of mineral x for element y		
R	Gas constant	kJ/mol·K	0.00814
T	Temperature	K	
X_{An}	Molar fraction of anorthite in plagioclase		
r_y	Ionic radius of ion y	Å	

Batch crystallization and melting is modelled by the equation

$$C_m = \frac{C_o}{f + D_y^x(1-f)}.$$

Mineral-melt partition coefficients are from the literature (Table A2.1). Partition coefficients for Ba, Sr, Th, and the REE+Y in plagioclase were calculated using the predictive models of Wood and Blundy (2003) and Th was assumed to be equivalent to U. The anorthite content of plagioclase was taken at a typical level from experimental work (X_{An} = 0.60) and the temperature was taken to be 950°C. Ionic radii are from Shannon (1976).

$$RT \ln D_{Ba}^{plag} = -38.2(X_{An}) + 10.2$$

$$RT \ln D_{Sr}^{plag} = -26.7(X_{An}) + 26.8$$

$$RT \ln D_{La}^{plag} = -10.8(X_{An}) - 12.4$$

$$RT \ln D_{Th}^{plag} = -48.4(X_{An}) - 7.45$$

$$RT \ln D_{Zr}^{plag} = -90.4(X_{An}) - 15.3$$

$$D_{REE+Y}^{plag} = D_{La}^{plag} \times \exp\left[\frac{-191136\left(\left(z/2\right)\left(r_{La}^2 - r_{REE+Y}^2\right) + \left(1/3\right)\left(r_{REE+Y}^3 - r_{La}^3\right)\right)}{T}\right]$$

$$where \quad z = 1.228 - 0.057(X_{An})$$

Partition coefficients are listed in Table 7 and starting compositions for melting model are listed in Table 9. An analysis of the sensitivity of the melting model to changes in mode is in Fig. 19.

Table 7: Partition coefficients for melting model

	Hornblende	Garnet	Rutile	Clinopyroxene	Plagioclase
D^{Ba}	0.12 B95	0.00041 B02	0.0043 F20	0.073 B02	0.29 WB03
D^{Th}	0.1 GERM	0.0015 K02	0.5 F20	0.082 B02	0.028* WB03
D^{Nb}	0.5 H20	0.0045 B02	102 F20	0.017 B02	0.01 GERM
D^{La}	0.64 H20	0.0041 B02	0.0055 F20	0.0875 B02	0.092 WB03
D^{Sr}	0.5 S94	0.0072 B02	0.06 F20	0.08 B02	2.89 WB03
D^{Zr}	0.5 H20	0.67 B02	4 F20	0.23 B02	0.0011 WB03
D^{Sm}	3.58 H20	0.61 B02	0.001 F20	0.59 B02	0.024 WB03
D^{Gd}	2.2 H20	1.99 B02	0.001 F20	0.861 B02	0.012 WB03
D^{y}	1.3 H20	7.31 B02	0.007 F20	1.17 B02	0.0038 WB03
D^{Yb}	2.2 H20	7.8 B02	0.01 F20	1.31 B02	0.0010 WB03

Abbreviations: B95=Brenan et al. 1995; H2O=Hilyard et al. 2000; S94=Sisson 1994; B02=Barth et al. 2002; K02=Klemme et al. 2002; F20=Foley et al. 2000; WB03 = Blundy and Wood 2003; GERM: estimated from the Earthref database: http://earthref.org

*Assumed equal to D^{U}

Table 8: Partition coefficients for fractional crystallization model

	Plagioclase	Hornblende	Apatite	Zircon	Cpx	Olivine	Magnetite
D^{Th}	0.03	0.1	10	22	0.03	0.01	0.1
D^{Ni}	0.1	9	0.1	0.1	10	20	10

Notes: All partition coefficients are from the Geochemical Earth Reference Model database (http://www.earthref.org/) except for olivine, which is from Bedard (2005)

Table 9: Starting compositions for melting model

	Ba	Th	Nb	La	Sr	Zr	Sm	Gd	Y	Yb
Average Pacific NMORB	8.5	0.12	2.8	3.2	119	107	3.7	5.1	43	3.5
Nicola Group Lava	1127	1.98	5.8	9.6	626	81	4.3	3.7	24	2.6
Spences Bridge Group Lava	289	1.24	6	9.55	580	91	3.59	3.49	15	1.25

Notes: Data from: PetDB (http://www.petdb.org/), Mortimer (1987), Smith and Thorkelson (2002)

Table 10: Trace element model results

	F	Ba	Th	Nb	La	Sr	Zr	Sm	Gd	Y	Yb
Spences Bridge Group	0.15	1597	6.5	5.8	51	3098	162	5.5	2.59	4.0	0.31
Spences Bridge Group	0.25	1042	4.4	5.9	34	2051	148	5.2	2.67	4.4	0.34
EPR MORB	0.15	47	0.6	2.7	17	636	190	5.7	3.80	11.6	0.88
EPR MORB	0.25	31	0.4	2.7	11	421	174	5.4	3.92	12.7	0.97
Nicola Group	0.15	6229	10.5	5.7	51	3344	144	6.6	2.74	6.7	0.65
Nicola Group	0.25	4064	7.0	5.7	34	2213	132	6.2	2.83	7.3	0.72

Notes: F=ratio of melt to solid

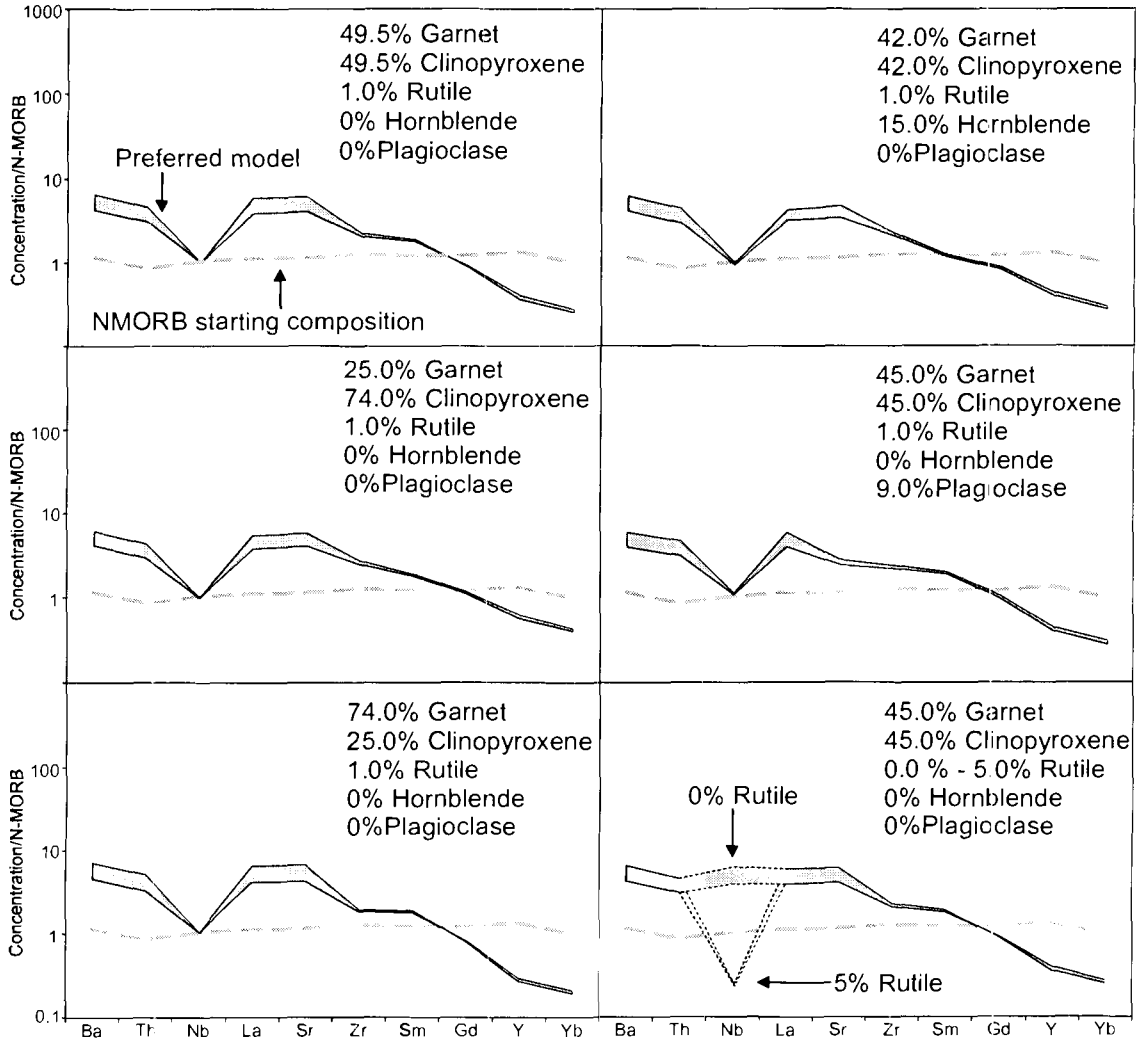

Figure 19: Sensitivity of the partial melting model to different mineral modes. A) The preferred melting model referred to in the main text. B), C), D) Melting models with amounts of garnet, clinopyroxene, and hornblende, note that large changes in the modal amount of garnet and clinopyroxene effect very little change on the model concentrations. E) Melting model with 9% plagioclase. Note the effect that adding plagioclase has on buffering Sr concentrations and fractionating Sr relative to other trace elements, such as La. F) Melting model with more and less rutile than the model depicted in A. The modal amount of rutile has a large effect on the calculated Nb abundances.

APPENDIX FOUR:
EQUATIONS FOR ND ISOTOPIC COMPOSITIONS

Basic Systematics

A total of seven separate whole rock samples were measured for Nd isotopic compositions, and a number of values are derived from these measurements (Table 4). This appendix lists the equations used to calculate these values from the measured $^{143}Nd/^{144}Nd$. The following are some important variables and constants used. The subscript "m" in an isotopic ratio always refers to a present-day ratio either directly measured (as in the case of $^{143}Nd/^{144}Nd_m$) or inferred from another isotopic system and from chemical analyses (as in the case of $^{147}Sm/^{144}Nd_m$). A "t" subscript on an isotopic ratio refers to a ratio which has been recalculated to a time in the past, in this case generally 50 Ma.

$\frac{^{143}Nd}{^{144}Nd_m}$	Measured isotopic ratio	atomic	As measured
Sm	Measured concentration	ppm	As measured
Nd	Measured concentration	ppm	As measured
$at.wt.Sm$	Atomic weight of Sm	g/mol	150.3656
$at.wt.Nd$	Atomic weight of Nd	g/mol	144.2397
^{147}Sm	Fractional abundance of ^{147}Sm relative to total Sm	atomic	0.149957
^{144}Nd	Fractional abundance of ^{144}Nd relative to total Nd	atomic	As defined below
λ	Decay constant for alpha decay of ^{147}Sm to ^{143}Nd	y^{-1}	$6.54 \cdot 10^{-12}$

The calculation of the present day $^{147}Sm/^{144}Nd_m$ from Sm and Nd concentrations and $^{143}Nd/^{144}Nd_m$ is as follows:

$$\frac{^{147}Sm}{^{144}Nd_m} = \left[\frac{Sm \times ^{147}Sm}{at.wt.Sm}\right] \Big/ \left[\frac{Nd \times ^{144}Nd}{at.wt.Nd}\right]$$

where

$$^{144}Nd = \frac{1}{\left(3.69014 + \frac{^{143}Nd}{^{144}Nd_m}\right)}$$

The Sm-Nd isotopic evolution of a closed system through time, and hence calculation of initial $^{143}Nd/^{144}Nd_t$ is given by

$$\frac{^{143}Nd}{^{144}Nd_t} = \frac{^{143}Nd}{^{144}Nd_m} - \frac{^{147}Sm}{^{144}Nd_m}(e^{(\lambda t)} - 1).$$

Similarly, the isotopic evolution of the bulk earth is given by

$$\frac{^{143}Nd}{^{144}Nd_{t,CHUR}} = \frac{^{143}Nd}{^{144}Nd_{m,CHUR}} - \frac{^{147}Sm}{^{144}Nd_{m,CHUR}}(e^{(\lambda t)} - 1)$$

where the subscript CHUR (CHondritic Uniform Reservoir) denotes the values for the bulk earth and have present day values of $^{143}Nd/^{144}Nd_{m,CHUR}$=0.512638 and $^{147}Sm/^{144}Nd_{m,CHUR}$=0.1966 (Jacobsen and Wasserburg 1980; Amelin and Rotenberg 2004).

Initial Nd isotopic ratios are commonly expressed in terms of epsilon notation, which is the variation of an initial $^{143}Nd/^{144}Nd$ from CHUR in parts per 10^4 and is defined as:

$$\varepsilon_{Nd} = 10^4 \left[\left(\frac{\frac{^{143}Nd}{^{144}Nd}_{t}}{\frac{^{143}Nd}{^{144}Nd}_{t,CHUR}} \right) - 1 \right].$$

The fractional variation of the $^{147}Sm/^{144}Nd$ of a sample from CHUR ($f_{Sm/Nd}$) expresses how "fast" it evolves to higher or lower values of ε_{Nd} and is defined as:

$$f_{Sm/Nd} = \left[\frac{^{147}Sm}{^{144}Nd}_{m} \Big/ \frac{^{147}Sm}{^{144}Nd}_{m,CHUR} \right] - 1$$

or

$$f_{Sm/Nd} = \left[\frac{^{147}Sm}{^{144}Nd}_{m} \Big/ 0.1966 \right] - 1$$

The "depleted mantle" is a hypothetical upper mantle reservoir that evolves along a more radiogenic (higher Sm/Nd) trajectory than the bulk earth. There are currently several formulations of the isotopic history of the depleted

mantle, the two most common being phenomenological derivations from compilations of the $^{143}Nd/^{144}Nd_t$ in ancient rocks that are presumed to have a simple history after being extracted from the mantle. These curves are given by De Paolo (1981a) and Goldstein et al. (1984) and a more recent formulation, similar to the Goldstein et al. curve is provided by Nagler and Kramers (1998). These curves are all expressed in epsilon notation and are as follows:

$$\varepsilon_{Nd}^{D81} = \frac{2.5}{10^{19}}t^2 - \frac{3}{10^{-18}}t + 8.5$$

$$\varepsilon_{Nd,DM}^{G84} = \left[\frac{-20}{9\times10^{9}}\right]t + 10$$

$$\varepsilon_{Nd,DM}^{NK98} = \frac{0.164}{10^{27}}t^3 - \frac{0.566}{10^{18}}t^2 - \frac{2.79}{10^{9}}t + 10.4$$

Model ages are calculated by determining the time that a rock would have had the same isotopic composition as a mantle reservoir (usually either the depleted mantle or CHUR), assuming that it has had the same or similar Sm/Nd throughout its history. This can be visualized by plotting a diagram of $^{143}Nd/^{144}Nd$ vs. time (or equivalently εNd vs. time) and determining the time at which the intersection of the DM curve and the curve determined by the evolution of a sample intersect. This provides a first-order constraint on the crustal residence time of a particular igneous rock, although in detail it is much more complex (e.g.

Arndt and Goldstein 1987). Uncertainties on these calculations are typically very large, in part because the intersections of the two curves are very oblique.

Several of the above equations (including one of the DM curves) must be combined to determine the model age of a sample. These combinations form implicit equations and cannot be solved in closed form, therefore they are determined by numerical techniques. First, the ε_{Nd} evolution of a rock sample is equated to the ε_{Nd} evolution of a mantle model, in this case the model of Goldstein et al. (1984) is used:

$$\left[\frac{\frac{^{143}Nd}{^{144}Nd_m} - \frac{^{147}Sm}{^{144}Nd_m}(e^{(\lambda t)}-1)}{\frac{^{143}Nd}{^{144}Nd_{CHUR}} - \frac{^{147}Sm}{^{144}Nd_{CHUR}}(e^{(\lambda t)}-1)}\right]10^4 + 10^4 = \left[\frac{-20}{9\times10^9}\right]t + 10.$$

Rearranging,

$$\left[\frac{\frac{^{143}Nd}{^{144}Nd_m} - \frac{^{147}Sm}{^{144}Nd_m}(e^{(\lambda t)}-1)}{\frac{^{143}Nd}{^{144}Nd_{CHUR}} - \frac{^{147}Sm}{^{144}Nd_{CHUR}}(e^{(\lambda t)}-1)}\right]10^4 + 9990 + \left[\frac{20}{9\times10^9}\right]t = 0$$

Iteratively solving for time using Newton's method by setting the above equation equal to *f(t)*:

$$g^{k+1} = g^k - \frac{f(t)}{f'(t)}$$

Solving for *g* iteratively should lead to a very precise model age in <10 iterations.

The derivative *f'(t)* is as

$$f'(x) = 10^4 \frac{\left[\left(C - De^{(\lambda t)} + D\right)\left(-B\lambda e^{(\lambda t)}\right)\right] - \left[\left(A - Be^{(\lambda t)} + B\right)\left(-D\lambda e^{(\lambda t)}\right)\right]}{\left(C - De^{(\lambda t)} + D\right)^2} + \left(\frac{20}{9\times 10^9}\right)$$

where

$$A \equiv \frac{^{143}Nd}{^{144}Nd_m}$$

$$B \equiv \frac{^{147}Sm}{^{144}Nd_m}$$

$$C \equiv \frac{^{143}Nd}{^{144}Nd_{m,CHUR}}$$

$$D \equiv \frac{^{147}Sm}{^{144}Nd_{m,CHUR}}$$

A somewhat simpler technique (not used here) can be employed to determine model ages by assuming $e^{\lambda t}-1 \approx \lambda t$.

Propagation of Error in Isotopic Data

Propagating the standard deviation, σ, through a linear function *f(x,y,z...)* is:

$$\sigma_f = \sqrt{\left(\frac{\partial f}{\partial x}\right)^2 \sigma_x^2 + \left(\frac{\partial f}{\partial y}\right)^2 \sigma_y^2 + \left(\frac{\partial f}{\partial z}\right)^2 \sigma_z^2 \ldots}$$

Propagation of error in $^{147}Sm/^{144}Nd_m$, $\sigma^{147}{}_{Sm/}{}^{144}{}_{Nd}$, from $^{143}Nd/^{144}Nd_m$, and Sm/Nd is therefore:

$$\sigma_{^{147}Sm/_{144}Nd} = \sqrt{E + F}$$

where

$$E = \left(\sigma^2_{Sm/Nd}\right)\left(\frac{^{147}Sm \times at.wt.Nd \times \left[3.69014 + \frac{^{143}Nd}{^{144}Nd_m}\right]}{at.wt.Sm}\right) \quad and$$

$$F = \left(\sigma^2_{^{143}Nd/_{144}Nd}\right)\left(\frac{Sm \times ^{147}Sm \times at.wt.Nd}{Nd \times at.wt.Sm}\right)$$

Similarly, the propagation of error into the $^{143}Nd/^{144}Nd_t$ is (assuming $e^{\lambda t}$-1≈λt) is:

$$\sigma_{^{143}Nd/_{144}Ndt} = \sqrt{\sigma^2_{^{143}Nd/_{143}Ndm} + \left(\sigma^2_{^{147}Sm/_{144}Nd}(\lambda t)^2\right)}$$

The propagation of error into the ε_{Nd} notation:

$$\sigma_{\varepsilon Nd} = \sqrt{\left(\sigma^2_{^{143}Nd/_{144}Ndt}\right)\left[10^4 \Big/ \left(\frac{^{143}Nd}{^{144}Nd_{CHUR}}\right)\right]^2}$$

APPENDIX FIVE:
WHOLE ROCK GEOCHEMISTRY TECHNIQUES AND UNCERTAINTIES

Whole Rock Geochemistry Analytical Techniques

Whole rock geochemical analyses for all samples except for RBI-05-02-2-1 were determined at the commercial laboratory *Actlabs* (Ontario, Canada). Major element oxide and select trace element concentrations were analyzed by fusing a small amount of powder with lithium metaborate/lithium tetraborate, and the molten mixture was dissolved in 5% nitric acid. Samples were run on a Thermo Jarrell-Ash Enviro II ICP-OES (inductively coupled plasma optical emission spectrometry). Some trace elements were analyzed by INAA (instrumental neutron activation analysis), by irradiation at the McMaster Nuclear Reactor and after a seven day decay measured on an Ortec high purity Ge detector linked to a Canberra series 95 multichannel. Other trace elements were determined by sample digestion with acid followed by measurement on a Perkin Elmer Optima 3000 ICP-MS (inductively coupled plasma mass spectrometry).

Calculation of Uncertainties

Along with the set of unknown samples sent to *Actlabs* for analysis, several of these samples were sent in duplicate to assess the analytical precision of the data. Either eight or four duplicates were run, depending on the analysis, and the results are presented in Table 10,11,12, and 13. The results from each

duplicate were treated as if they were symmetrically distributed measurements of a "true" value, the mean of the two analyses. The difference between each of the two measured values and the mean of the two values were compiled for each element (resulting in, for example 16 values for 8 duplicates, half positive and half negative). The standard deviation was calculated on these values and is used for an estimate of precision. This is somewhat equivalent to using 16 duplicate analyses of the same rock, although it requires that there be no or very little dependence of error on the absolute concentration of an element.

Table 11: Results of duplicate whole rock major element oxide (wt. %) and trace element (ppm) geochemical analyses.

	SiO2	Al2O3	Fe2O3	MnO	MgO	CaO	Na2O	K2O	TiO2	P2O5	Ba	Sr	Y	Zr	Be	V
RBI-04-15-10-1B (A)	59.70	15.42	5.45	0.069	4.00	6.00	4.33	2.26	0.713	0.33	1468	1731	11	125	2	124
RBI-04-15-10-1B (B)	59.65	15.24	5.40	0.068	3.97	5.94	4.27	2.25	0.711	0.32	1448	1710	10	115	2	120
RBI-04-23-3-1B (A)	63.55	16.69	3.85	0.038	0.81	4.06	4.66	2.14	0.452	0.28	1045	980	10	128	2	61
RBI-04-23-3-1B (B)	63.66	16.72	3.89	0.038	0.80	4.09	4.68	2.10	0.454	0.43	1055	986	10	131	2	64
RBI-04-24-6-1B (A)	60.46	15.54	5.35	0.058	2.94	4.99	3.99	1.71	0.674	0.26	746	588	14	98	1	124
RBI-04-24-6-1B (B)	61.40	15.76	5.45	0.059	2.99	5.06	4.03	1.73	0.684	0.21	759	594	14	96	1	123
CS-04-2-5-1b (A)	52.65	15.66	7.93	0.109	7.69	8.86	3.25	0.73	1.249	0.27	188	560	11	93	2	110
CS-04-2-5-1b (B)	52.79	15.69	7.96	0.109	7.64	8.84	3.28	0.76	1.258	0.28	191	564	11	95	2	113
RF-4-11-1b (A)	49.15	15.03	9.43	0.134	7.39	9.07	3.86	1.76	2.434	0.67	344	1061	16	193	3	180
RF-4-11-1b (B)	49.17	14.98	9.46	0.132	7.31	8.97	3.83	1.77	2.410	0.66	341	1053	16	190	3	182
CS-04-3-1-1b (A)	50.00	16.46	8.71	0.120	5.52	8.44	4.74	2.05	2.338	0.73	330	1127	15	208	3	154
CS-04-3-1-1b (B)	49.99	16.46	8.70	0.119	5.52	8.46	4.74	2.06	2.350	0.73	331	1126	15	206	3	154
CS-04-12-1-1b (A)	49.04	13.96	12.11	0.163	8.63	9.00	3.26	0.87	1.795	0.33	219	461	18	120	2	192
CS-04-12-1-1b (B)	49.14	13.99	12.14	0.164	8.64	9.02	3.26	0.91	1.790	0.33	220	461	18	124	2	193
CS-04-24-1-1b (A)	46.78	14.65	10.96	0.145	6.82	9.62	2.39	0.69	1.608	0.28	361	502	18	102	1	208
CS-04-24-1-1b (B)	46.87	14.70	10.94	0.145	6.81	9.62	2.40	0.68	1.609	0.28	361	504	16	105	1	211

Table 12: Results of duplicate trace element (ppm) geochemical analyses.

	Cu	Ni	Pb
RBI-04-15-10-1B (A)	25	93	24
RBI-04-15-10-1B (B)	25	94	22
RBI-04-24-6-1B (A)	26	12	10
RBI-04-24-6-1B (B)	25	11	9
RBI-04-31-1-2B (A)	31	25	-3
RBI-04-31-1-2B (B)	29	25	7
CS-04-2-26-1b (A)	55	79	5
CS-04-2-26-1b (B)	54	77	9
CS-04-3-1-1b (A)	48	51	6
CS-04-3-1-1b (B)	46	53	7
CS-04-8-4-1b (A)	48	214	-3
CS-04-8-4-1b (B)	49	215	4
CS-04-12-1-1b (A)	50	178	5
CS-04-12-1-1b (B)	50	175	6

Table 13: Results of duplicate trace element (ppm) geochemical analyses.

	Co	Cr	Mo	Sc
RBI-04-15-10-1B (A)	21.8	146	15	13.1
RBI-04-15-10-1B (B)	20.8	142	16	12.8
RBI-04-24-6-1B (A)	20.4	35	10	15.2
RBI-04-24-6-1B (B)	18.1	37	-2	15.3
CS-04-3-1-1b (A)	34.9	114	18	15.2
CS-04-3-1-1b (B)	35.1	107	23	14.6
CS-04-12-1-1b (A)	52.7	321	-2	23.6
CS-04-12-1-1b (B)	53.5	321	-2	23.8

Table 14: Results of duplicate trace element (ppm) geochemical analyses.

	Rb	*Zr*	*Nb*	*Cs*	*La*	*Ce*	*Pr*	*Nd*	*Sm*	*Eu*	*Gd*	*Tb*	*Dy*	*Ho*	*Er*	*Tm*	*Yb*	*Lu*	*Hf*	*Ta*	*Th*	*U*
RBI-04-15-10-1B (A)	30	125	3.9	0.5	26.2	55.7	7.35	30.6	6.49	1.65	4.44	0.52	2.34	0.38	1.06	0.151	0.94	0.146	3.5	0.19	4.30	3.27
RBI-04-15-10-1B (B)	31	122	3.6	0.5	25.3	54.8	7.33	30.5	6.20	1.62	4.30	0.52	2.27	0.38	1.06	0.148	0.97	0.138	3.3	0.19	4.21	3.29
RBI-04-23-3-1B (A)	39	126	4.0	0.7	25.9	49.6	5.83	22.1	3.96	1.06	2.75	0.39	1.88	0.34	1.07	0.152	1.10	0.154	3.4	0.25	4.46	1.57
RBI-04-23-3-1B (B)	40	126	3.9	0.7	26.0	48.7	5.75	21.7	3.91	1.07	2.69	0.37	1.84	0.35	0.99	0.155	1.04	0.157	3.4	0.25	4.36	1.56
RBI-04-24-6-1B (A)	29	100	3.3	0.8	15.4	31.8	3.92	16.1	3.60	1.04	3.08	0.50	2.57	0.50	1.59	0.237	1.46	0.214	2.9	0.19	2.74	1.24
RBI-04-24-6-1B (B)	29	97	3.5	0.8	15.7	32.6	3.98	16.7	3.62	1.04	3.01	0.50	2.55	0.48	1.60	0.230	1.49	0.208	2.8	0.21	2.87	1.23
CS-04-2-5-1b (A)	8	92	19.0	0.1	12.4	26.2	3.26	14.0	3.38	1.22	2.95	0.49	2.37	0.39	1.08	0.140	0.85	0.117	2.3	1.18	1.53	0.52
CS-04-2-5-1b (B)	9	92	19.4	0.1	12.6	26.1	3.22	14.1	3.49	1.26	3.06	0.48	2.43	0.41	1.09	0.138	0.88	0.120	2.5	1.20	1.57	0.53
RF-4-11-1b (A)	17	193	48.9	0.2	29.4	61.5	7.51	30.2	7.22	2.37	5.80	0.80	3.73	0.63	1.55	0.190	1.12	0.150	4.5	3.01	2.68	1.05
RF-4-11-1b (B)	18	203	50.6	0.2	28.6	59.5	7.26	29.3	7.01	2.24	5.67	0.80	3.72	0.61	1.49	0.192	1.05	0.149	4.5	3.00	2.63	1.01
CS-04-3-1-1b (A)	20	207	53.1	0.2	32.1	65.9	7.76	30.6	6.82	2.31	5.53	0.73	3.49	0.57	1.40	0.172	0.92	0.137	4.8	3.33	3.06	1.23
CS-04-3-1-1b (B)	20	214	55.0	0.2	32.6	66.0	7.87	31.1	7.11	2.31	5.51	0.76	3.64	0.58	1.42	0.179	1.01	0.134	4.9	3.42	3.11	1.27
CS-04-12-1-1b (A)	13	118	22.3	0.1	16.3	33.9	4.24	17.6	4.67	1.60	4.46	0.70	3.82	0.68	1.88	0.266	1.56	0.229	3.1	1.37	1.77	0.55
CS-04-12-1-1b (B)	12	119	22.0	0.1	15.2	32.1	4.04	17.0	4.54	1.50	4.46	0.69	3.75	0.69	1.91	0.271	1.58	0.220	3.2	1.40	1.87	0.60
CS-04-24-1-1b (A)	12	103	9.8	0.3	13.5	31.1	4.05	17.5	4.62	1.53	4.32	0.65	3.49	0.66	1.80	0.240	1.46	0.207	2.8	0.56	1.46	0.54
CS-04-24-1-1b (B)	12	105	9.6	0.3	13.4	30.3	4.03	17.3	4.69	1.47	4.16	0.64	3.37	0.61	1.75	0.241	1.45	0.209	2.8	0.55	1.49	0.55

APPENDIX SIX:
SAMPLE LOCATIONS

Table 15: Sample locations

			NAD 83		NAD 27			
Sample	Location	ZONE	Easting	Northing	Easting	Northing	Lat	Long
RBI-04-15-10-1B	Agate Mtn	10U	688194	5473307	688200	5473088	N49° 23.0'	W120° 24.4'
RBI-04-15-12-1B	Agate Mtn	10U	688194	5473307	688200	5473088	N49° 23.0'	W120° 24.4'
RBI-04-15-13-1B	Agate Mtn	10U	688194	5473307	688200	5473088	N49° 23.0'	W120° 24.4'
RBI-04-16-14-1B	Agate Mtn	10U	688194	5473307	688200	5473088	N49° 23.0'	W120° 24.4'
RBI-04-16-17-1B	Agate Mtn	10U	688115	5473319	688121	5473100	N49° 23.0'	W120° 24.5'
RBI-04-12-1-1B	Agate Mtn	10U	690764	5473223	690770	5473004	N49° 23.0'	W120° 22.3'
RBI-04-17-3-1B	Agate Mtn	10U	693023	5466414	693029	5466195	N49° 19.2'	W120° 20.6'
RBI-04-36-1-1B	Boss Lake	10U	659096	5529038	659101	5528819	N49° 53.6'	W120° 47.1'
RBI-04-23-3-1B	Sunday Creek	10U	673718	5462027	673724	5461808	N49° 17.2'	W120° 36.7'
RBI-04-24-6-1B	Sunday Creek	10U	676746	5451250	676752	5451031	N49° 11.3'	W120° 34.5'
RBI-04-25-1-1B	Tulameen	10U	661517	5488888	661522	5488669	N49° 31.9'	W120° 46.1'
RBI-04-34-2-1B	Merritt	10U	651195	5557219	651200	5557000	N49° 08.9'	W120° 53.0'
RBI-04-39-1-1B	Princeton	10U	676194	5480219	676200	5480000	N49° 26.9'	W120° 34.1'
RBI-04-37-5-1B	Prospect Creek	10U	633665	5550218	633669	5549999	N49° 05.4'	W120° 07.9'
RBI-04-37-8-2B	Prospect Creek	10U	633275	5548812	633279	5548593	N49° 04.6'	W120° 08.2'
RBI-04-19-3-1B	Flat Top/Placer Mtn	10U	686509	5451715	686515	5451496	N49° 11.4'	W120° 26.4'
RBI-04-20-3-2B	Flat Top/Placer Mtn	10U	687941	5447811	687947	5447592	N49° 09.3'	W120° 25.3'
RBI-04-21-2-1B	Flat Top/Placer Mtn	10U	689777	5448622	689783	5448403	N49° 09.7'	W120° 23.8'
RBI-04-21-3-1B	Flat Top/Placer Mtn	10U	680079	5449259	680085	5449040	N49° 10.2'	W120° 31.8'
RBI-04-22-1-1B	Flat Top/Placer Mtn	10U	689868	5446440	689874	5446221	N49° 08.5'	W120° 23.8'
RBI-04-30-2-1B	Flat Top/Placer Mtn	10U	687241	5439345	687247	5439126	N49° 04.7'	W120° 26.2'
RBI-04-31-1-1B	Flat Top/Placer Mtn	10U	686499	5439182	686505	5438963	N49° 04.6'	W120° 26.8'
RBI-04-31-1-2B	Flat Top/Placer Mtn	10U	686499	5439182	686505	5438963	N49° 04.6'	W120° 26.8'
RBI-04-32-2-1B	Flat Top/Placer Mtn	10U	688077	5441677	688083	5441458	N49° 05.9'	W120° 25.4'
DM-04-18-1-1B	Flat Top/Placer Mtn	10U	689894	5439919	689900	5439700	N49° 05.0'	W120° 24.0'
RBI-05-02-2-1	Flat Top/Placer Mtn	10U	688194	5439319	688200	5439100	N49° 04.7'	W120° 25.4'

APPENDIX SEVEN:
BELT-WIDE GEOCHEMICAL COMPARISON

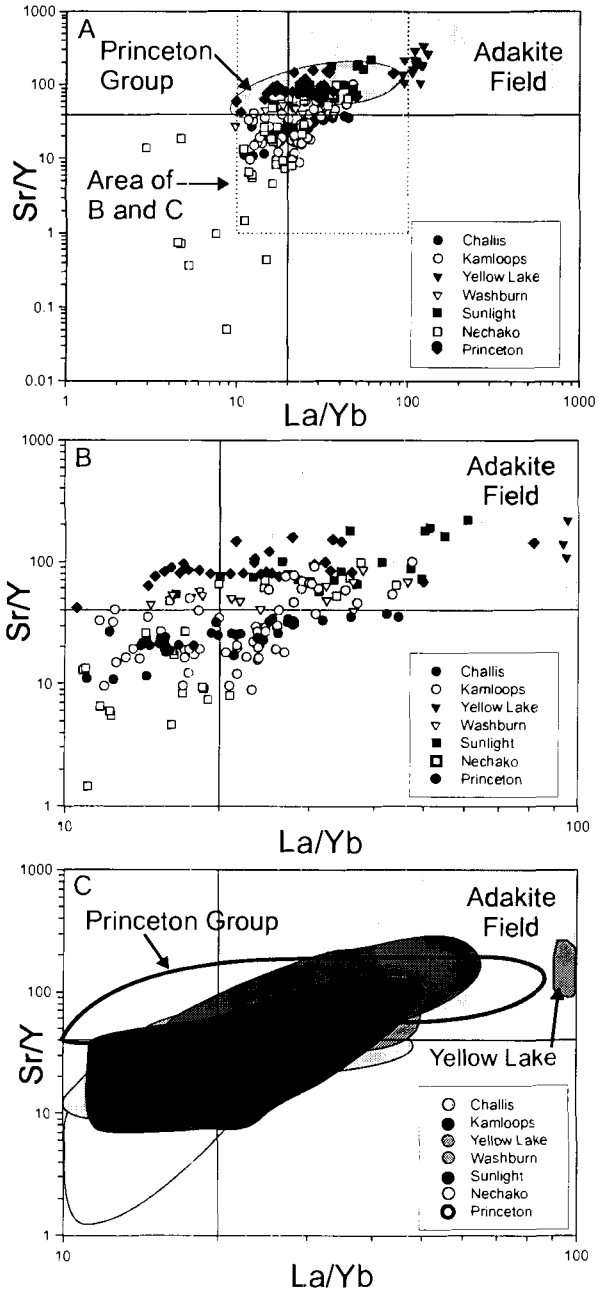

Figure 20: La/Yb vs. Sr/Y for select volcanic fields in the Challis-Kamloops Belt. These plots compare the important adakite "indices" of La/Yb and Sr/Y and suggest that an adakitic trace element signature is present in most volcanic packages in the belt. A) La/Yb vs. Sr/Y with all data plotted, the Princeton Group is enclosed in grey. B) A close up on the high density area of A. C) Same as B, but with fields enclosing each volcanic field. Data sources are as follows. Challis Group, McKervey (1998), Kamloops Group, Breitsprecher (2002), Yellow Lake Member of the Penticton Group, Dostal et al. (2003), Washburn Volcano, Absaroka Volcanic Province, Feeley et al. (2002), Sunlight Volcano, Absaroka Volcanic Province, Feeley and Cosca (2003), Nechako (Ootsa Lake Group), Grainger (2000) and Thorkelson (unpublished)